UNDERSTANDING THE TECTONIC EVOLUTION OF THE EAST ORPHAN BASIN, OFFSHORE CANADA, PORCUPINE BASIN, OFFSHORE IRELAND, AND GALICIA INTERIOR BASIN, OFFSHORE SPAIN.

by © Larry Sandoval

A thesis submitted to the School of Graduate Studies

in partial fulfilment of the requirements for the degree of

Master of Science

Department of Earth Sciences

Memorial University of Newfoundland

March 2019

St. John's Newfoundland and Labrador

ABSTRACT

The East Orphan and the Porcupine basins form two highly promising basins for hydrocarbon exploration along the North Atlantic rifted margins. Despite having formed at conjugate margin positions and similar geological times, the basins appear to have fundamental differences. The objective of this project is to investigate the tectonic evolution of the East Orphan, Porcupine, and Galicia Interior basins. Analysis and interpretation of seismic reflection and well data was integrated with 3D grids of the depth-to-basement and Moho proxy to produce and restore representative geologic cross-sections.

Interpretation of seismo-stratigraphic units across the East Orphan, Porcupine, and Galicia Interior basins reveals similarities in their seismic character. However, structural restoration of the selected lines indicates that basin evolution, sedimentary cover thickness, faulting style, and crustal structure differ significantly. Similarly, kinematic evolution models place Porcupine and Galicia Interior basins forming a continuous basin during Jurassic time.

Based on a comprehensive analysis of the results obtained in this thesis and in the context of published kinematic evolution models, the linkage between the seemingly conjugate East Orphan and Porcupine basins seems implausible. In contrast, a potential connection between the Porcupine Basin and the Galicia Interior Basin is proposed.

ACKNOWLEDGEMENTS

I would like to thank God for guiding me all along the way, and for giving me the necessary patience and perseverance to help me materialise this goal, infinite thanks.

Thanks to my parents who instilled in me the values and principles that have led me to accomplish this achievement. Thank you, this triumph is yours.

To Francis, for always being there, for her unconditional support, words of encouragement, trust, love and respect. We did it...!!!

To my nieces and nephews, for transmitting their joy and enthusiasm, may this achievement serve as a stimulus to achieve all your goals.

To my supervisor Dr J. Kim Welford for giving me the privilege of working alongside her, for her attention, dedication, understanding, and support, and for guiding me in the development of this project.

To Peter Bruce for his infinite support and help through my time at MUN. Thanks a million Peter!

To the Memorial Applied Geophysics for Rift Tectonics (MAGRiT) Group for your constructive comments, suggestions, help and contributions.

To Dr Patrick Shannon and everyone from the Irish Centre for Research in Applied Geosciences (ICRAG) for their support and help.

To the Illustrious Memorial University, which opened its doors to me and gave me the opportunity to grow academically.

I would also like to thank the Department of Communications, Climate Action & Environment of Ireland, TGS-NOPEC Geophysical Company (TGS), the Petroleum Infrastructure Program (PIP), IHS Markit Ltd., Canadian Stratigraphic Services Ltd., the Canada-Newfoundland Offshore Petroleum Board (C-NLOPB), for having provided the data, Innovation NL for the financial support, and Midland Valley and Schlumberger for having provided the software licences.

TABLE OF CONTENTS

LIST OF TABLES

LIST OF FIGURES

LIST OF EQUATIONS

LIST OF ABBREVIATIONS AND SYMBOLS

A34 ---------- Magnetic anomaly 34
AU ---------- Aptian Unconformity
BAP ---------- Biscay Abyssal Plain
CANSTRAT ---------- Canadian Stratigraphic Services Ltd.
CCU ---------- Cenomanian Unconformity
C-NLOPB ---------- Canada-Newfoundland Offshore Petroleum Board
CRS ---------- Coordinate reference system
CU ---------- Cenozoic Unconformity
DSDP ---------- Deep Sea Drilling Project
DT ---------- Sonic log
EOB ---------- East Orphan Basin
FC ---------- Flemish Cap
FP ---------- Flemish Pass Basin
GB ---------- Grand Banks
GIB ---------- Galicia Interior Basin
Hz ---------- Hertz
IAP ---------- Iberia Abyssal Plain
IB ---------- Iberia Peninsula
IODP ---------- Integrated Ocean Drilling Program
IR ---------- Ireland
JdA ---------- Jeanne d'Arc Basin
KB ---------- Kelly Bushing
kHz ---------- kilohertz
km ---------- Kilometre(s)
km^2 ---------- Squared kilometres
Ma ---------- Million years
Moho ---------- Mohorovičić discontinuity
MSL ---------- Mean Sea Level
MTD ---------- Mass Transport Deposits
NL ---------- Newfoundland
ODP ---------- Ocean Drilling Program
OK ---------- Orphan Knoll
PB ---------- Porcupine Basin
PSM ---------- Porto Seamount
PtB ---------- Porto Basin
PH ---------- Porcupine High
RB ---------- Rockall Basin
RC ---------- Reflection coefficient
RH ---------- Rockall High
SDR ---------- Seaward Dipping Reflector
TDR ---------- Time-Depth Relationship

TDVSS ---------- True Vertical Depth Sub-Sea
TU ---------- Tithonian Unconformity
TWT ---------- Two-Way Travel time
UK ---------- United Kingdom
Vp ---------- P-Wave Velocity
VSM ---------- Vigo Seamount
WGS-84 ---------- World Geodetic System 1984
WOB ---------- West Orphan Basin

LIST OF APPENDICES

CHAPTER 1. INTRODUCTION

1.1 Overview

The East Orphan Basin, offshore Newfoundland, and the Porcupine Basin, offshore Ireland, form two of the key basins along the rifted margins of the North Atlantic Ocean (Figure 1.1). These two basins are two of the most promising hydrocarbon basins in the world. After more than fifty years of oil exploration offshore Newfoundland and Labrador, recently acquired data and subsequent studies are revealing the origin and tectonic setting of the East Orphan Basin. On the conjugate Irish margin, similar sedimentary basins like the Rockall Basin and the Porcupine Basin were formed at the same time as the Newfoundland basins; however, there appear to be fundamental differences in their evolution.

From interpretation of seismic and other geophysical data on the Newfoundland and Irish Atlantic margins, previous authors have disagreed about the number and timing of rift phases (Enachescu et al., 2005; Gouiza, Hall, & Welford, 2017; Norton, 2002; Shannon, McDonnell, & Bailey, 2007; Shannon & Naylor, 1998; Sibuet, Srivastava, Enachescu, & Karner, 2007; Skogseid, 2010; Williams, Dehler, Grant, & Oakey, 1999) and the style of rifting (Chian, Reid, & Jackson, 2001; Gouiza et al., 2017; Krawczyk, Reston, Beslier, & Boillot, 1996; Lau, Watremez, Louden, & Nedimović, 2015; Pérez-Gussinyé, Ranero, Reston, & Sawyer, 2003; Reston et al., 2004; Welford, Shannon, O'Reilly, & Hall, 2012) of each basin present on these conjugate passive margins. These theories provide insight into the complex history of these conjugate margins.

An updated, logical, and coherent tectonic evolution of these Atlantic conjugate passive margins is needed. The objective of this project is to reconnect the conjugate margin basins in order to better understand their tectono-stratigraphic evolution.

1.2 Study Area

The study area for this thesis includes the rifted margins of the southern North Atlantic Ocean, with primary focus on the East Orphan Basin on the Newfoundland margin and the Porcupine Basin on the Irish margin, and a secondary focus on the Galicia Interior Basin on the Galicia margin (Figure 1.1).

Orphan Basin is located on the eastern Canadian continental margin, 370 km northeast of St. John's, Newfoundland and Labrador, north of the Grand Banks and southwest of the Orphan Knoll, which is a fragment of continental crust detached from North America during continental rifting (M. J. Keen & Piper, 1990). The basin extends over an area of approximately 150,000 km^2 (Department of Mines and Energy, 2000) of which around 33,000 km^2 correspond to the East Orphan Basin. Water depths vary from west to east from less than 500 m in the west to ~3,000 m in the east in the lower slope near the Orphan Knoll (Enachescu et al., 2005; Gouiza et al., 2017; C. E. Keen, Stockmal, Welsink, Quinlan, & Mudford, 1987).

The Porcupine Basin is a V-shaped basin located offshore Ireland, 320 km southwest of Cork. The basin extends over an area of approximately 44,000 km^2 with water depths ranging from 400 m in the north to 3,000 m in the southwest (Dorschel, Wheeler, Monteys, & Verbruggen, 2010).

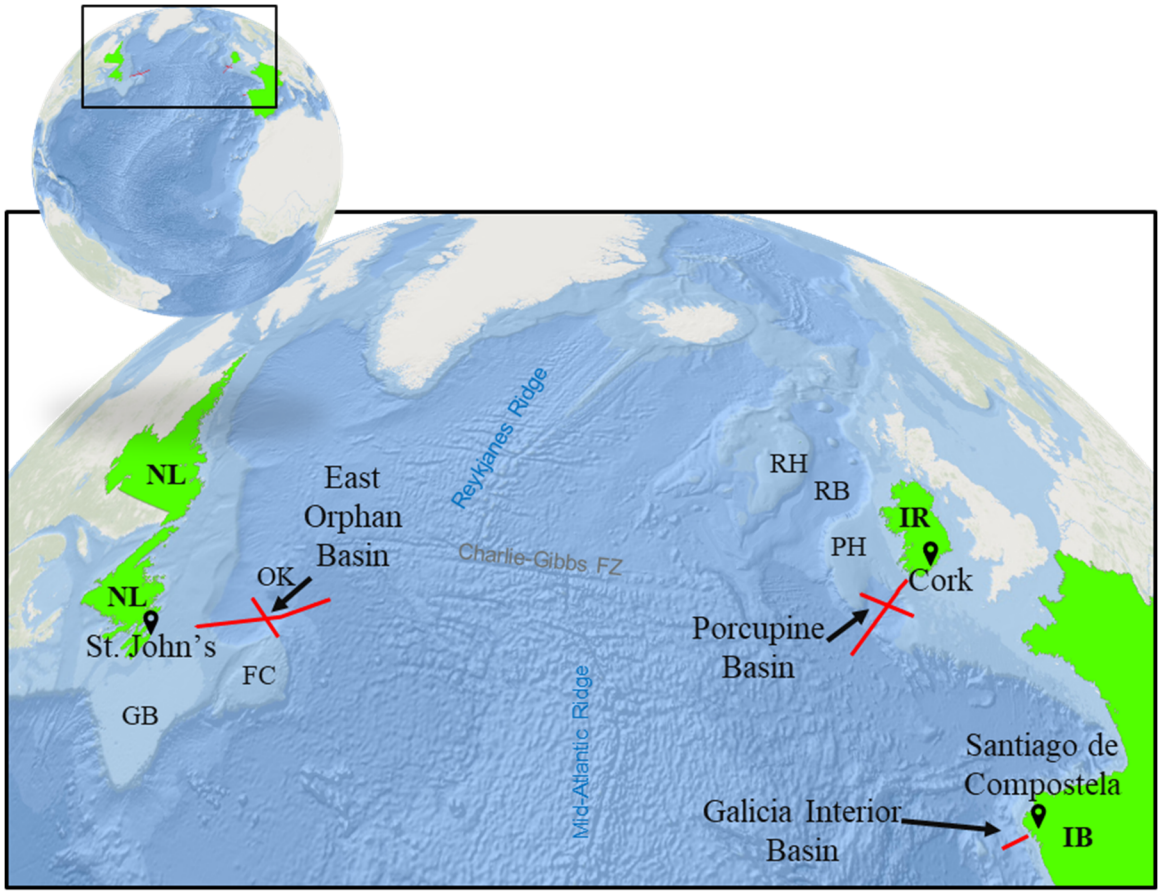

NL=Newfoundland and Labrador FC=Flemish Cap GB=Grand Banks OK=Orphan Knoll
IB=Iberian Peninsula IR= Ireland PH=Porcupine High RB=Rockall Basin RH=Rockall High

Figure 1.1 Location of the study area. Red continuous lines: 2D seismic lines. Bathymetry from Amante & Eakins (2009).

The Galicia Interior Basin, south of the primary focus area of the study, is a U-shaped trough (Murillas et al., 1990) located 100 km offshore Spain, to the west of Santiago de Compostela. Covering an approximate area of 13,000 km^2, the water depths range from 200 m near the shelf to 3000 m in the central part of the basin.

These three basins are associated with the evolution of the triple junction that formed between the classic North American plate, the Eurasian plate, and the African plate, and ultimately resulted in the opening of the modern North Atlantic Ocean (Sibuet & Collette, 1991). Differences in the composition, rheology, temperature, and pre-existing structures

around the triple point are thought to have contributed to the variability in the evolution of each of the basins (Lavier & Manatschal, 2006; Naliboff, Buiter, Péron-Pinvidic, Osmundsen, & Tetreault, 2017).

1.3 History of Exploration

Geological studies offshore eastern Canada began during the 17th century with bathymetric measurements; however, it was not until the late 1950s and early 1960s that airborne magnetometer and seismic refraction surveys showed that the offshore geology was different from onshore (Department of Mines and Energy - Government of Newfoundland and Labrador, 2000). Similarly, exploration offshore Ireland began during the 1960s after several gas field discoveries in the North Sea (Naylor & Shannon, 2009).

The Orphan and Porcupine basins are currently two of the most promising basins in the North Atlantic for hydrocarbon potential. Petroleum exploration offshore Newfoundland and Labrador started in the early 1960s; however, it was not until 1974 that the first well (Bonavista C-99) was drilled in the Orphan Basin. Due to the basin's remote location, deep water setting, poor quality of seismic data, and lack of hydrocarbon discoveries, exploration-drilling ceased and the basin was subsequently abandoned (Hardy, 2007). Although the Orphan Basin was not the subject of a prolific exploration phase, the data acquired, namely gravity, magnetic, seismic profiles, and drilled wells, were the key to the later drilling of two wells in the vicinity of the Flemish Pass Basin during the 1990s and 2000s. The well Mizzen L-11, drilled in 2003 by Petro Canada, was the first to test oil (non-economic) near its boundary with the neighbouring Flemish Pass Basin in Early Cretaceous reservoir rocks and Kimmeridgian source rocks (BeicipFranlab et al., 2016; Enachescu, Fagan, & Smee, 2005).

In 2007, Nalcor Energy, Newfoundland and Labrador's energy company, was created. Later in 2012, Nalcor Energy, with the seismic companies TGS and PGS, acquired a long offset broadband 2D multi-client seismic grid over the Flemish Pass and Orphan Basin area. This grid was later refined in 2014 (BeicipFranlab et al., 2016). In 2015, the acquisition of a 4600 km^2 3D survey over Orphan Basin began and was completed in 2016 (BeicipFranlab et al., 2016).

For the Porcupine Basin, however, the first well (35/13-1x) was drilled in 1977 (Department of Communications, 2010). Similar to the Orphan Basin, due to the economic recession from 1983 to 1993 and the lack of important oil/gas discoveries, the exploration offshore Ireland decreased considerably during that period (Shannon, Corcoran, & Haughton, 2001). After 1993, new seismic data from the Slyne, Erris, and Rockall basins, together with encouraging results offshore UK and Norway, encouraged a new exploration phase (Shannon et al., 2001).

As a result of the advances in technology during the last 15 years (e.g., improvement of seismic acquisition methods), acquisition of new seismic data has taken place, and a better understanding of magma-poor rifted margins has been gained (Chenin et al., 2017; Shannon, 2016). Increased exploration of the Newfoundland-Ireland conjugate offshore basins is ongoing, focusing on the deep and underexplored basins (e.g., East Orphan and Porcupine basins).

1.4 Theoretical framework

1.4.1 Passive Margins

Passive continental margins, are formed by tectonic rifting of continents (Fowler, 2005). In general, their tectonic evolution is dominated by gravity-driven collapse, halokinesis, and growth faulting (Allen & Allen, 2005). They frequently contain thick sedimentary layers, which record the evolution of the rifting episodes and contain a substantial fraction of the world's hydrocarbon resources (Bradley, 2008; Mann, Gahagan, & Gordon, 2003).

1.4.2 Types of passive margins

According to Péron-Pinvidic, Manatschal, & Osmundsen (2013), passive continental margins are subdivided into two end-member types based on the nature of the transitional crust: magma-poor and magma-rich margins (Figure 1.2). These are also classified by Manatschal (2004) and Allen & Allen (2005) as non-volcanic and volcanic margins, respectively. Both are formed during rifting when a continent rifts apart to form a new ocean basin.

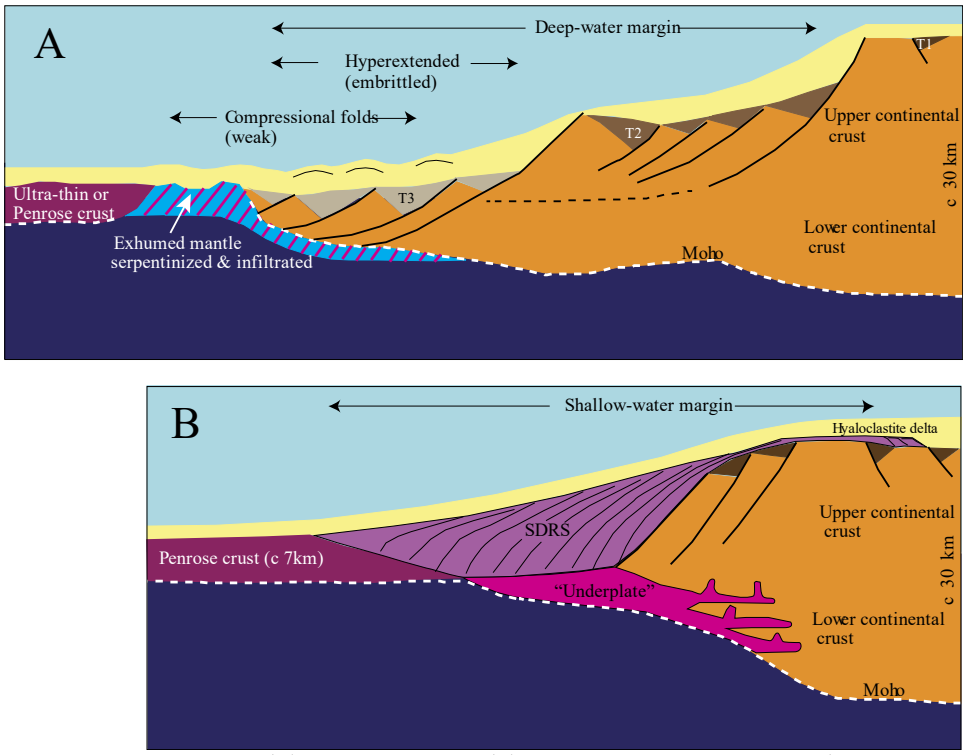

Figure 1.2 Schematic structure of (A) magma-poor and (B) magma-rich passive margins (after Doré & Lundin, 2015).

1.4.2.1 Magma-poor margins

Magma-poor margins (mantle melt ~10%) differ from magma-rich margins principally because of the absence or minor presence of volcanism and a slow extension rate (Anthony G. Doré & Lundin, 2015; Lavier & Manatschal, 2006). Along magma-poor margins, the transitional crust is composed primarily of stretched continental crust and exhumed continental mantle (Sutra & Manatschal, 2012). Several domains based on morphological criteria (Figure 1.3) were distinguised by Péron-Pinvidic et al. (2013), Sutra, Manatschal, Mohn, & Unternehr (2013), and Chenin, Manatschal, Lavier, & Erratt (2015). These domains were better described later by Chenin et al. (2017) as follows:

A) *The proximal domain* is characterised by parallel, roughly flat basement and Moho topographies, and corresponds to unthinned or minimally extended continental crust (30–35 km thick).

B) *The distal domain* records most of the rift-related deformation and is subdivided into several subdomains (Figure 1.3).

   a. *The necking subdomain*, characterised by the abrupt thinning of the continental crust from 30–35 km down to ~10 km, translates into a deepening of the top basement and shallowing of the Moho.

   b. *The hyperextended subdomain* is where continental crust is thinned from ~10 km down to 0 km. The transition between the necking and hyperextended domain corresponds to a sudden decrease in the dip of the Moho on depth-converted seismic sections.

   c. *The exhumation subdomain* may be present along magma-poor rifted margins when lithospheric subcontinental mantle is exhumed at the seafloor. The exhumation of the mantle is associated with serpentinization (to a depth of 4–6 km) and the transition from serpentinised mantle to fresh peridotite translates into a progressive increase in seismic velocity.

C) *The oceanic domain*, consisting of homogeneous oceanic crust (6–7 km thick), exhibits a basement and Moho that are parallel to each other.

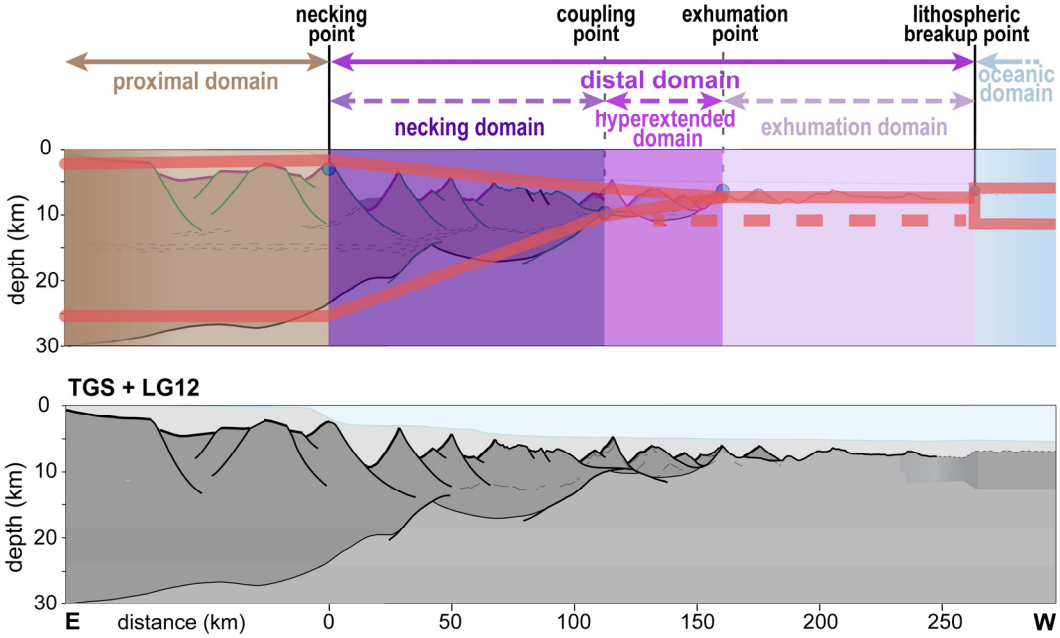

Figure 1.3 Definition of rift domains or subdomains and their simplified morphology (red lines). The red dashed line represents the seismic Moho (after Chenin et al., 2017)

1.4.2.2 Magma-rich margins

Magma-rich margins (Figure 1.2 B) are characterised by extensive extrusive basalts, usually present as Seaward Dipping Reflector (SDR) sequences (Greenroyd, Peirce, Rodger, Watts, & Hobbs, 2007), and igneous underplating with significant surface uplift at the time of break-up (Allen & Allen, 2005).

Two margin end-members are defined as well by Allen & Allen (2005) based on the thickness of sediments (Figure 1.4):

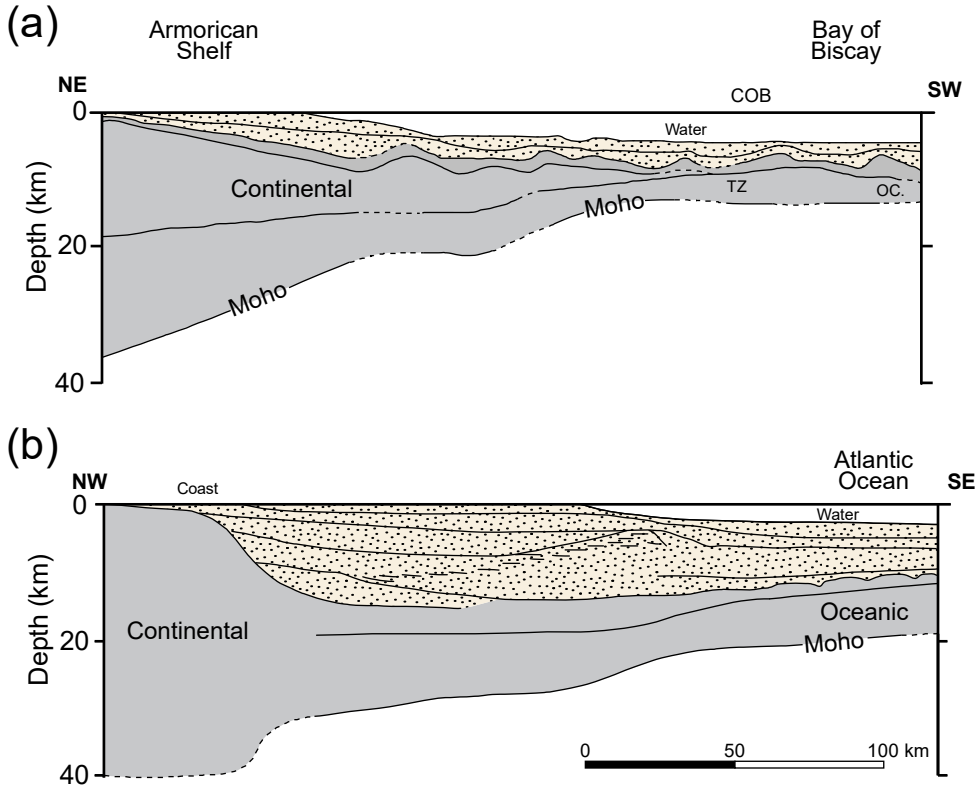

Figure 1.4 Examples of end-member passive margins based on sedimentary thickness. (A) Starved margin, (B) nourished margin (after White & McKenzie, 1989 in Allen & Allen, 2005).

1.4.2.3 Starved margins

Starved margins are characterised by a thin sedimentary layer (2-4 km) covering large areas of rotated syn-rift fault blocks above a subhorizontal detachment (e.g., Bay of Biscay, see Figure 1.4A, and Red Sea).

1.4.2.4 Nourished margins

Nourished margins are characterised by a very thick (<15 km) post-rift sedimentary layer overlying a number of tilted upper crustal fault blocks and a wide region of mid-lower crustal extension (e.g., Baltimore Canyon region of the Eastern Seaboard of North America, see Figure 1.4B, and the Labrador margin)

1.4.3 Fault Systems

Regions affected by extensional tectonics (e.g., rifts) usually exhibit a system of normal faults (Allen & Allen, 2005). While the specific configuration of the system is dictated by the level of complexity of the acting mechanisms (formation model), a generic set of structural features are usually found in areas affected by extensional tectonics such as rifted margins (Allen & Allen, 2005).

The terms used in this thesis are based on the glossary of normal faults proposed by Peacock, Knipe, & Sanderson (2000) and some additional terminology from Gibbs (1984), van der Pluijm & Marshak (2004) and Fossen (2010). Only the main terms are going to be explained in this thesis (see Appendix A). For a wider and detailed explanation of all the terms, see Gibbs (1984), Peacock et al. (2000), van der Pluijm & Marshak (2004), and Fossen (2010).

1.4.4 Rifting

Rifting is defined by van der Pluijm & Marshak (2004) and Fossen (2010) as the process by which continental lithosphere experiences extensional deformation (crust is pulled apart by tectonic forces), through the formation and activation of normal faults. The rifting process depends on several factors that include mantle processes and thermal structure of the mantle and the distribution and orientation of pre-existing weak structures within the crust (Fossen, 2010).

Rifting is commonly discussed in terms of the type of model that produced it (Figure 1.5). Some of these models are:

1.4.4.1 Pure-shear model

In this model (Figure 1.5a), proposed by McKenzie (1978), the contribution of individual faults in the rift creates a symmetric, uniform stretching/thinning of the crust where the horizontal extension is balanced by vertical thinning (Fossen, 2010). A detachment defines the base of the upper-crustal normal faulting zone and it is associated with the brittle–plastic transition in the crust (van der Pluijm & Marshak, 2004).

1.4.4.2 Simple Shear model

Proposed by Wernicke (1985), the simple shear model is controlled by a dipping detachment fault or shear zone that cuts down through the crust, and possibly deeper (Figure 1.5b). The pure shear and simple shear mechanisms are not only geometrically different but also differ in their thermal structure. In the pure shear model, the highest temperature gradient is found in the middle of the basin, while it is offset in the simple shear model (Fossen, 2010; van der Pluijm & Marshak, 2004).

1.4.4.3 Delamination model

According to van der Pluijm & Marshak (2004), the delamination model is considered a variation of the simple shear model, where the region of upper crustal extension does not lie directly over the region of deeper extension. The detachment may be subhorizontal beyond the edge of the rift before bending down (Figure 1.5c).

1.4.4.4 Hybrid model

Combinations of the aforementioned models, which are likely the most common in nature, produce hybrid models that reflect effects of both pure and simple shear models (Figure 1.5d). In this case, according to van der Pluijm & Marshak (2004), the transcrustal shear

zone from the simple-shear model spreads at depth into a band of anastomosing shear zones and disappears in a zone of distributed strain in the lower crust and possibly into the upper mantle.

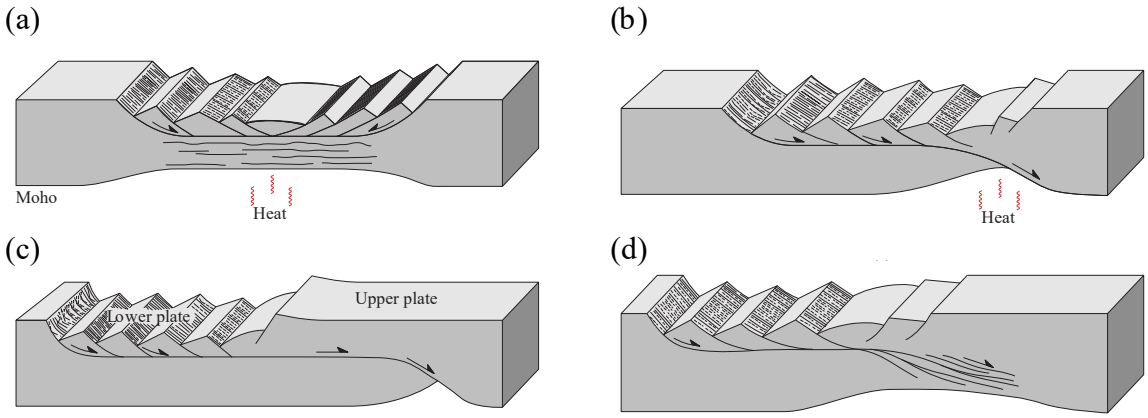

Figure 1.5 Models of rifting at the crustal scale. (a) Pure-shear model; (b) simple-shear model; (c) delamination model; (d) hybrid model. (Adapted from van der Pluijm & Marshak, 2004)

1.4.5 Tectonostratigraphy

The record of tectonic events (e.g., faulting as part of rifting) is typically captured by sediments being deposited concurrently. Fossen (2010) describes three stages of the rift development that could be associated with three different tectonostratigraphic megasequences (Figure 1.6):

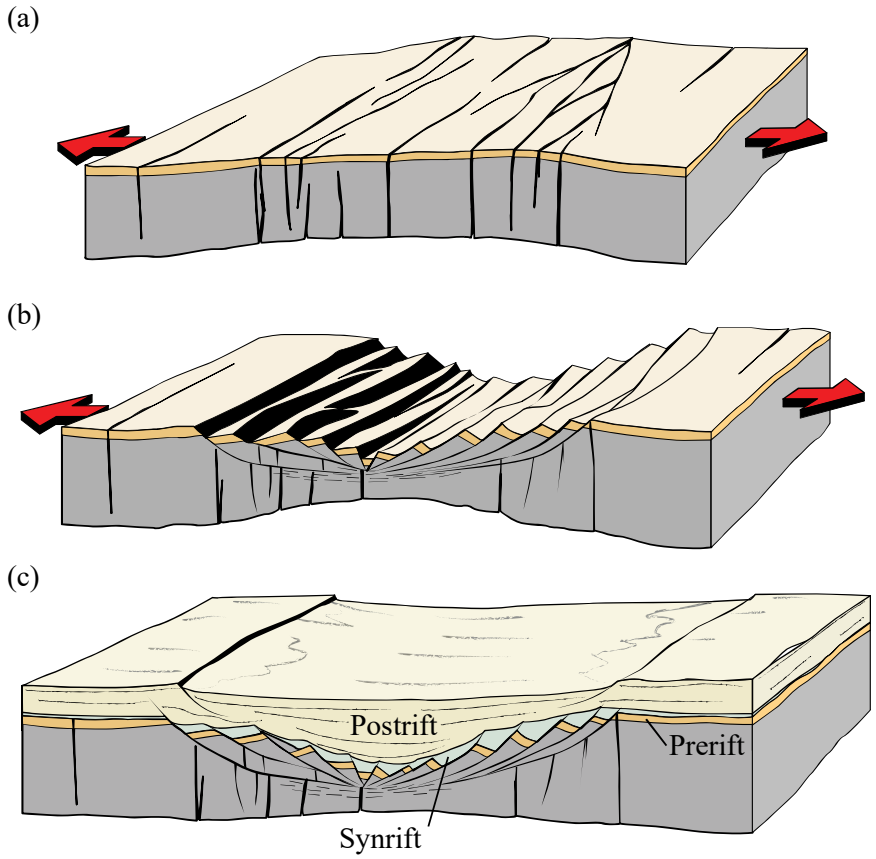

Figure 1.6 Three stages in rift development (after Fossen, 2010). (a) Pre-rift, (b) syn-rift, and (c) post-rift.

1.4.5.1 Pre-rift

Deposited prior to extension, the pre-rift sedimentary sequence is characterised by the lack of thickness changes and sedimentary facies changes across the rift faults.

1.4.5.2 Syn-rift

The syn-rift sequence corresponds to the sediments deposited during the rifting. It is characterised by thickness and facies variations across growth faults, hanging-wall thickening and footwall thinning or non-deposition, and may contain rollovers.

1.4.5.3 Post-rift

The post-rift sequence is controlled by the geometry of fault blocks and thermal subsidence after rifting has finished. This sequence may show thickness and facies changes due to the effects of differential compaction and remnant rift topography.

1.5 Tectonic Framework

Passive continental margins are formed during initial rifting apart of continents to form an ocean (Fowler, 2005). They frequently contain thick sedimentary layers, which record the evolution of the rifting episodes and contain a substantial fraction of the world's hydrocarbon resources (Bradley, 2008; Mann et al., 2003).

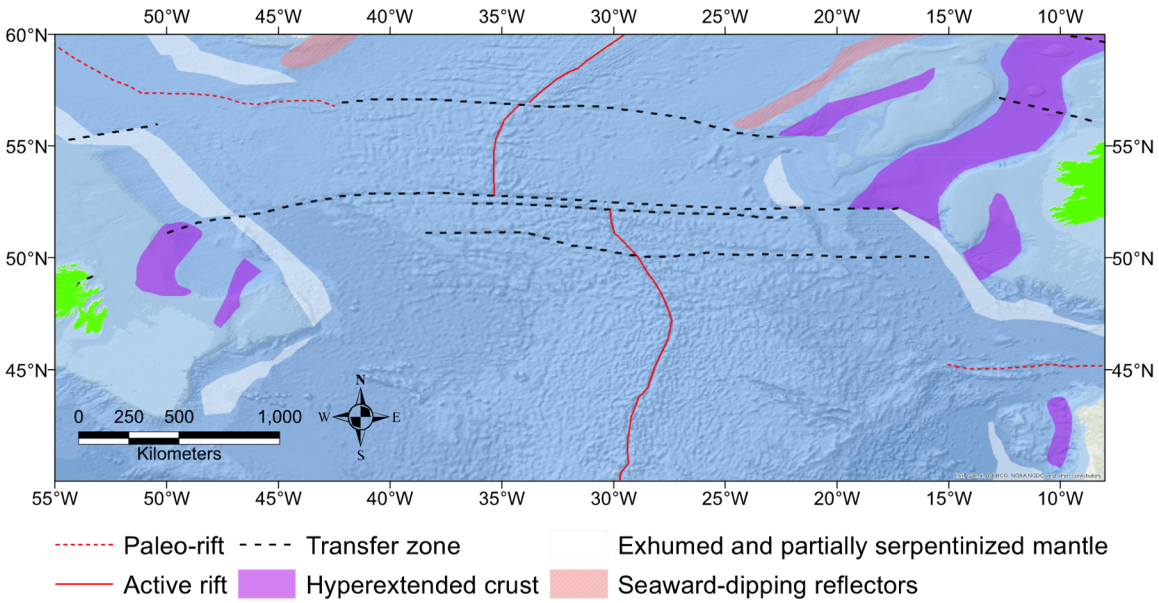

Figure 1.7 Magma-rich and magma-poor margins of the southern North Atlantic (adapted from Lundin & Doré, 2011).

The formation of magma-poor margins is divided into three phases of rifting: the stretching phase, the thinning phase, and the exhumation phase (Lavier & Manatschal, 2006; Manatschal, 2004). Rifting begins with the stretching phase, which is characterised by

distributed listric faulting ahead of propagating rifts. The thinning phase, characterised by localised detachment faulting that first exhumes the middle crustal levels, overprints the previous listric faulting. The exhumation phase follows with the exhumation of serpentinised mantle. Finally, the break-up propagates across the rift sequence and separates the margins, resulting in seafloor spreading (Lavier & Manatschal, 2006; Péron-Pinvidic et al., 2013). The East Orphan Basin and the Porcupine Basin have previously been defined as basins with hyperextended crust and partially serpentinised mantle (Lundin & Doré, 2011; Nirrengarten, Manatschal, Tugend, Kusznir, & Sauter, 2018; Welford, Hall, Sibuet, & Srivastava, 2010; Welford et al., 2012) and therefore as magma-poor margins (Figure 1.7).

1.5.1 East Orphan Basin

The current tectonic framework of Atlantic Canada is the result of multiple ocean opening-closing cycles that started with the formation of the Uranus Ocean in the Neoproterozoic, that led to the formation of the Grenville Orogen (1300-950 Ma), followed by the development of the Iapetus Ocean, to which the Appalachian Orogen (600-300 Ma) is associated, in the Neoproterozoic-Early Paleozoic (Harland & Gayer, 1972; Williams et al., 1999). Based on the rock associations and histories, Williams (1979) divided the Appalachian orogen as it affected Atlantic Canada, into five zones, namely Humber, Dunnage, Gander, Avalon, and Meguma (Figure 1.8). The highly stretched Orphan Basin developed within the Avalon Zone (Williams et al., 1999).

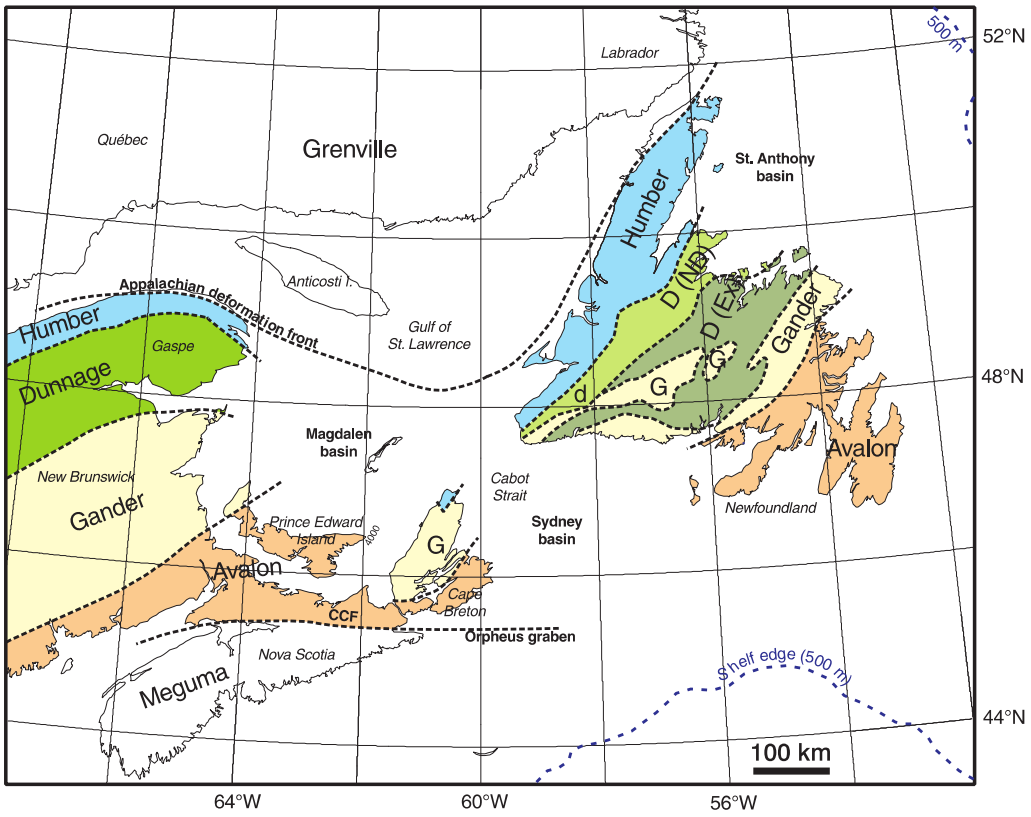

Figure 1.8 Surface geological zones of the Appalachian orogen on the Atlantic borderlands of Canada (adapted from Hall, Marillier, & Dehler, 1998)

The Orphan Basin (Figure 1.9) is bounded to the north by the Dover transfer fault and the Charlie-Gibbs Fracture Zone (C. E. Keen et al., 1987); to the northeast by a high basement ridge that runs between Flemish Cap and the Orphan Knoll; to the south by the Cumberland Belt Transfer Zone (Enachescu, 1987), and to the west by the Bonavista Platform (M. Enachescu et al., 2005; C. E. Keen & Beaumont, 1990; Smee, Nader, Einarsson, Hached, & Enachescu, 2003).

The Orphan Basin, which lies on thinned continental crust (Chian et al., 2001; Lau et al., 2015; Welford & Hall, 2007), is subdivided into the younger shallow-water West Orphan Basin and the older deep-water and hyperextended East Orphan Basin (Welford, Cameron, Carter, & Wright, 2015). These sub-basins are separated by the White Sail complex fault

zone (Enachescu, Kearsey, et al., 2004) that is part of the horst structure described by Gouiza et al., (2015). The basin is characterised by basement ridges and deep sub-basins with an orientation ranging from NE-SW to N-S (Enachescu, Meyer, & Hogg, 2004b, 2004a). Low amplitude magnetic anomalies are associated with high-angle tilted basement blocks (Chian et al., 2001).

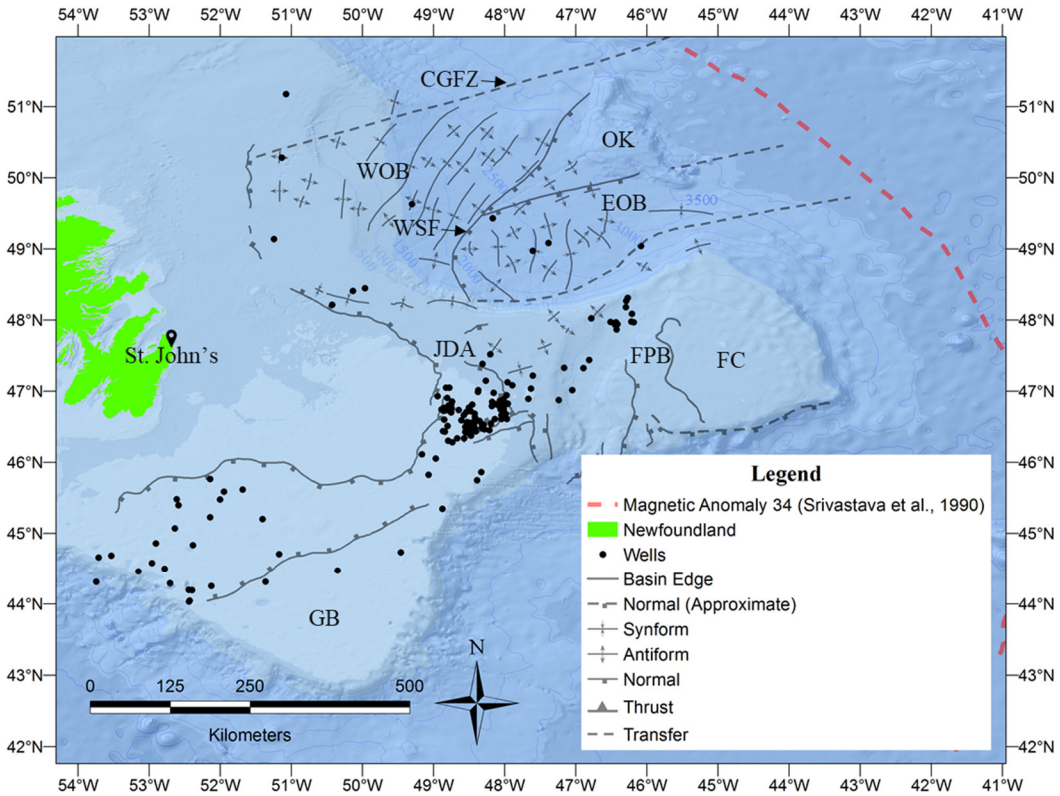

CGFZ= Charlie-Gibbs Fracture Zone FC=Flemish Cap GB=Grand Banks OK=Orphan Knoll JDA=Jeanne d'Arc Basin
FPB=Flemish Pass Basin WSF=White Sail Fault WOB=West Orphan Basin EOB=East Orphan Basin

Figure 1.9. Structural map showing the basins offshore Newfoundland. Adapted from Edwards, Jauer, Moir, & Wielens (2003), Srivastava et al. (1990), and Sibuet et al. (2007)

Different tectonic-stratigraphic evolutionary histories have been proposed for the Orphan Basin (Enachescu, 1987; Enachescu et al., 2005; Enachescu, Meyer, et al., 2004a, 2004b, Gouiza et al., 2015, 2017; C. E. Keen et al., 1987; Sibuet et al., 2007; Skogseid, 2010; Skogseid et al., 2004; Srivastava & Verhoef, 1992). However, in general terms, the first rifting phase

occurred during the Late Triassic-Early Jurassic and is thought to mark the beginning of the formation of the East Orphan Basin (Enachescu et al., 2005; Sibuet et al., 2007; Skogseid et al., 2004; Williams et al., 1999). A second rifting phase from Late Jurassic to Early Cretaceous caused the initiation of the West Orphan Basin and reactivated the movement of basement blocks as well as older sedimentary features in the East Orphan Basin (Enachescu et al., 2005; Gouiza et al., 2017; Sibuet et al., 2007; Skogseid et al., 2004; Williams et al., 1999). A third rifting phase, associated with the opening of the Labrador Sea, took place during the Late Cretaceous, affecting at least the westernmost parts of the West Orphan Basin (Enachescu et al., 2005; Sibuet et al., 2007; Williams et al., 1999). Sibuet et al. (2007) suggest a clockwise rotation (43°) of the Flemish Cap with the East Orphan Basin aligned with the Porcupine Basin and the West Orphan Basin aligned with the Rockall Basin.

According to Gouiza et al. (2015), the Orphan Basin exhibits four distinct domains based on stratigraphic, structural, and crustal characteristics: 1) the shelf domain and 2) the west sub-basin domain, in the West Orphan Basin; 3) the basement high domain, which divides the basin into the West and East Orphan sub-basins; and 4) the east sub-basin domain (Figure 1.10). Normal faulting, bookshelf faults[1], and half-grabens on hyperextended crust are the main characteristics of these domains.

[1] See Appendix A or Peacock et al. (2000) for definition

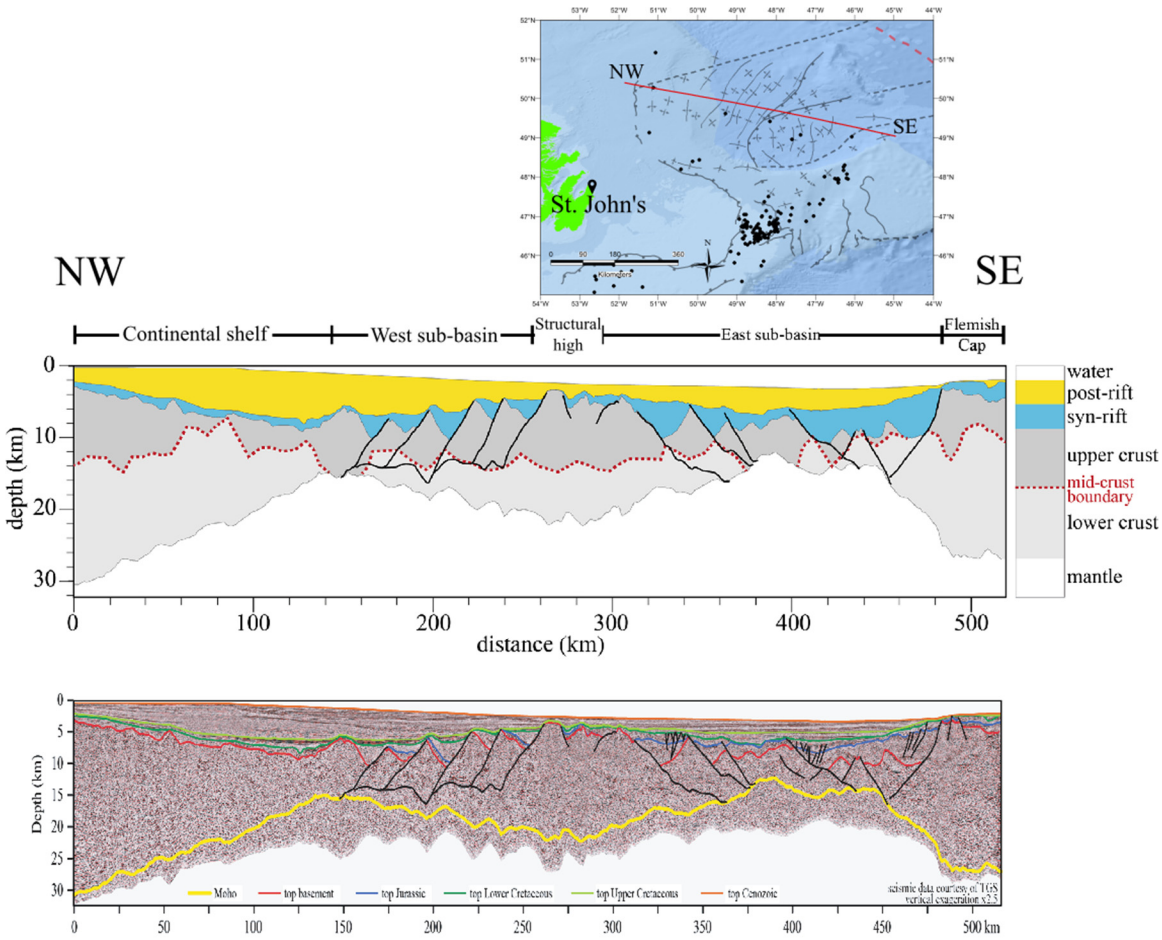

Figure 1.10. Seismic reflection line (after Gouiza et al., 2015; lower plot) and the rift stages proposed by Gouiza et al. (2017; middle plot) showing the crustal architecture of the Orphan Basin. Top plot shows the location map with the seismic line plotted in red.

1.5.2 Porcupine Basin

A set of basins of various shapes, sizes and ages are located on the western Irish Atlantic continental shelf. These include the Porcupine and Rockall basins, that have been the focus of intermittent exploration since the late 1970s (Morewood et al., 2005). The basins are usually elongate, and their orientation is approximately NE–SW, following inherited and reactivated Caledonian structures and fabrics (Naylor & Shannon, 2011).

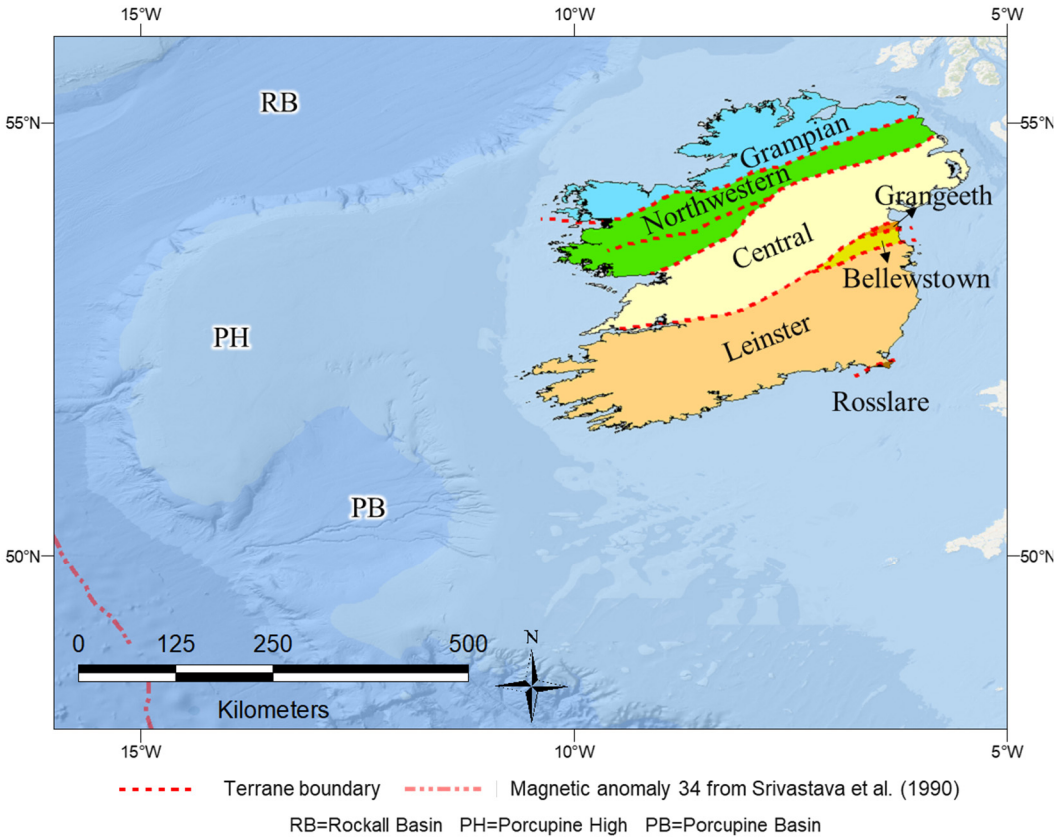

Figure 1.11 Map of terranes of Ireland. Adapted from Murphy et al. (1991).

Similar to the continental shelf of Northwest Europe, offshore Ireland exhibits imprints and structures resulting from Variscan, Caledonian and older orogenic events. The reactivation of some of the basement structures affected the location, orientation and large-scale structures of the sedimentary basins (Naylor & Shannon, 2011). The closure of the Iapetus Ocean in late Silurian to Early Devonian times led to the docking and suturing of distinct basement terranes (Figure 1.11) producing a general N-S orientation on pre-Mesozoic basement in Norway, changing southwards to NE–SW over Scotland and Ireland (Naylor & Shannon, 2011).

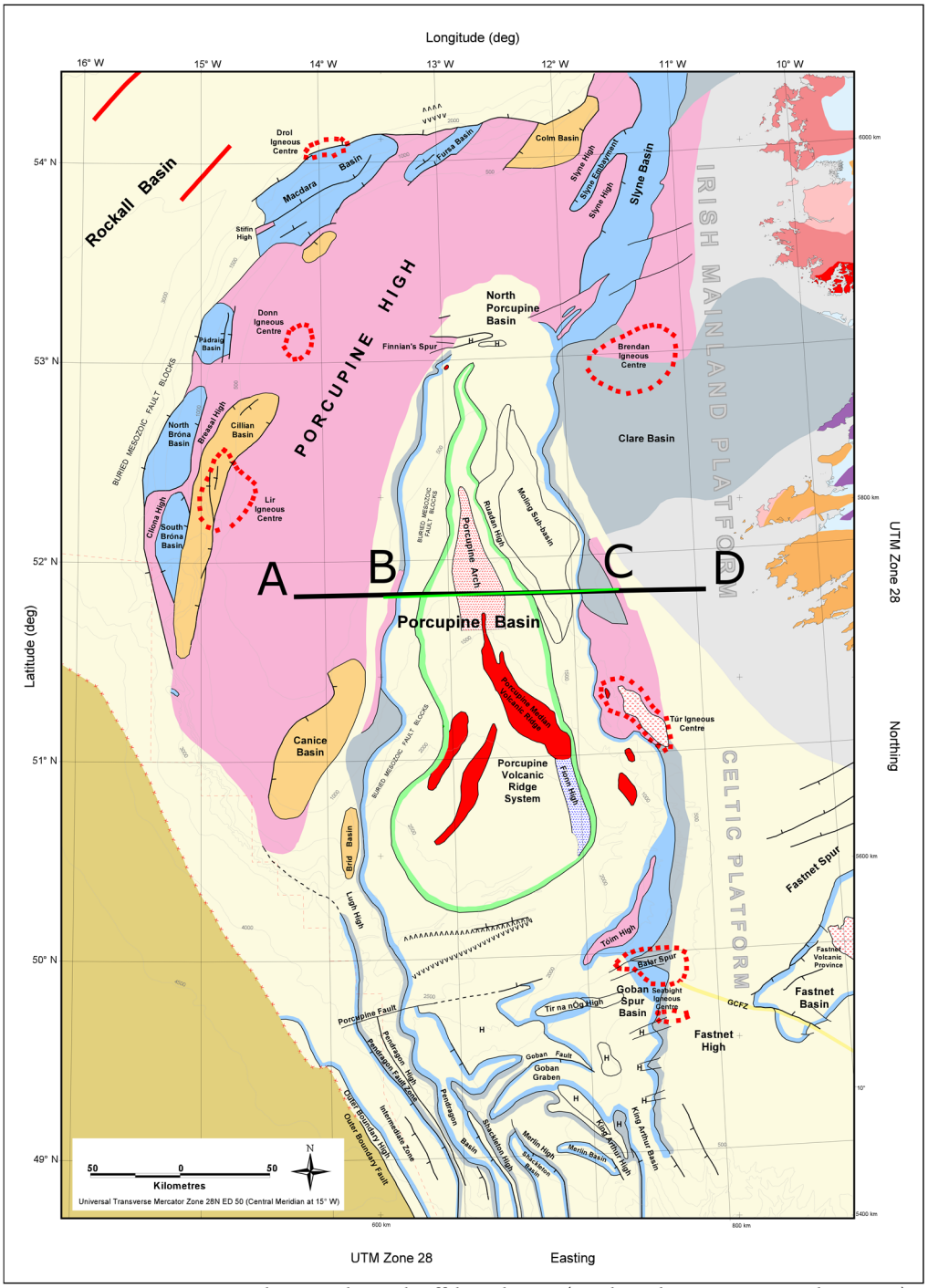

Figure I.12. Location map showing the Irish offshore basins (Naylor, Shannon, & Murphy, 2002). *See Appendix B - Figure B.1 for legend.*

The Porcupine Basin is defined by Naylor, Shannon, & Murphy (2002) as a Mesozoic-early Cenozoic basin with a north-south orientation extending from approximately 50°N,

northwards to Finnian's Spur at the southern margin of the North Porcupine Basin (Figure 1.12). The basin is bounded to the north and west by the North Porcupine Basin and the Porcupine Bank, respectively, and to the south by the Porcupine Fault and the Goban Spur.

The development of the complex Porcupine Basin is associated with the development of the North Atlantic Ocean (Croker & Shannon, 1987). The tectonic framework of the Irish Atlantic Margin, particularly the North Porcupine Basin, was mostly established during the Caledonian orogeny. The ENE-WSW orientation of the Celtic Sea Basins, controlled by the Caledonian and Variscan orogenies, is not apparent in the Porcupine Basin; however, it is seen again in the orientation of the Porcupine Fault and the eastern part of the Goban province (Naylor & Shannon, 2005). According to Stolfová & Shannon (2009), a number of major structural trends on the Northwest European Atlantic margin that were episodically reactivated, exhibit an orientation NE-SW to N-S in the northern region, while in the southern region an E-W strike is shown by the basement structures. The N–S trend seen in the Porcupine Basin (Figure 1.11) is thought to be an inherited orientation of possible Proterozoic origin, similar to the one found offshore Norway (Naylor & Shannon, 2011). Basement structures within the Variscan region are generally E-W to ENE-WSW (Naylor & Shannon, 2011).

The late Palaeozoic and Permian sequence was deposited in an East-West extensional basin, whereas to the south of the Porcupine Basin, Variscan compressional tectonics dominated due to plate collision (Ziegler, 1982). Triassic and Jurassic strata developed in response to the initial break-up of the Pangean super-continent. Changes in extensional directions within Pangea are reflected in a change in rifting direction near the end of the Early Jurassic

(Croker & Shannon, 1987). The thermal sag sequence started with the approximate onset of seafloor spreading in the North Atlantic during the Cretaceous and Cenozoic (Croker & Shannon, 1987).

The Porcupine Basin, similar to the Rockall Basin, developed in response to multi-phase Mesozoic rifting interspersed with compressional events and periods of thermal subsidence (Norton, 2002; Shannon et al., 2007; Shannon & Naylor, 1998). Three rifting phases occurred during the Permo-Triassic, Late Jurassic-Early Cretaceous, and three compressional episodes (Figure 1.16), during the Early Cretaceous, early Cenozoic, and middle Cenozoic, are recognised (Norton, 2002; Shannon et al., 2007; Shannon & Naylor, 1998).

The north and central parts of the Porcupine Basin are characterised by the presence of a deeply buried structural arch (Porcupine Arch) and the Porcupine Volcanic Ridge System, respectively (Naylor et al., 2002). The former is defined by Johnson et al. (2001) and Naylor et al. (2002) as a high-amplitude reflector which may mark the top of the crystalline crust and by Gagnevin, Haughton, Whiting, & Saqab (2017) as a mafic igneous intrusion situated below the sedimentary cover that could potentially have fed sills at a shallower level. The latter, on the other hand, is considered by Tate & Dobson (1988) to represent an igneous complex of mainly Cretaceous age, by Reston, Pennell, Stubenrauch, Walker, & Pérez-Gussinyé (2001) and Reston et al. (2004) as a serpentinite-mud volcano or diapir, by O'Sullivan, Jones, & Hardy (2010a, 2010b) as a rotated fault block composed of sedimentary rocks, by Calvès, Torvela, Huuse, & Dinkleman (2012) as a hyaloclastic mound extruded and deposited close to sea level, and by Watremez et al. (2016) as a volcanic feature.

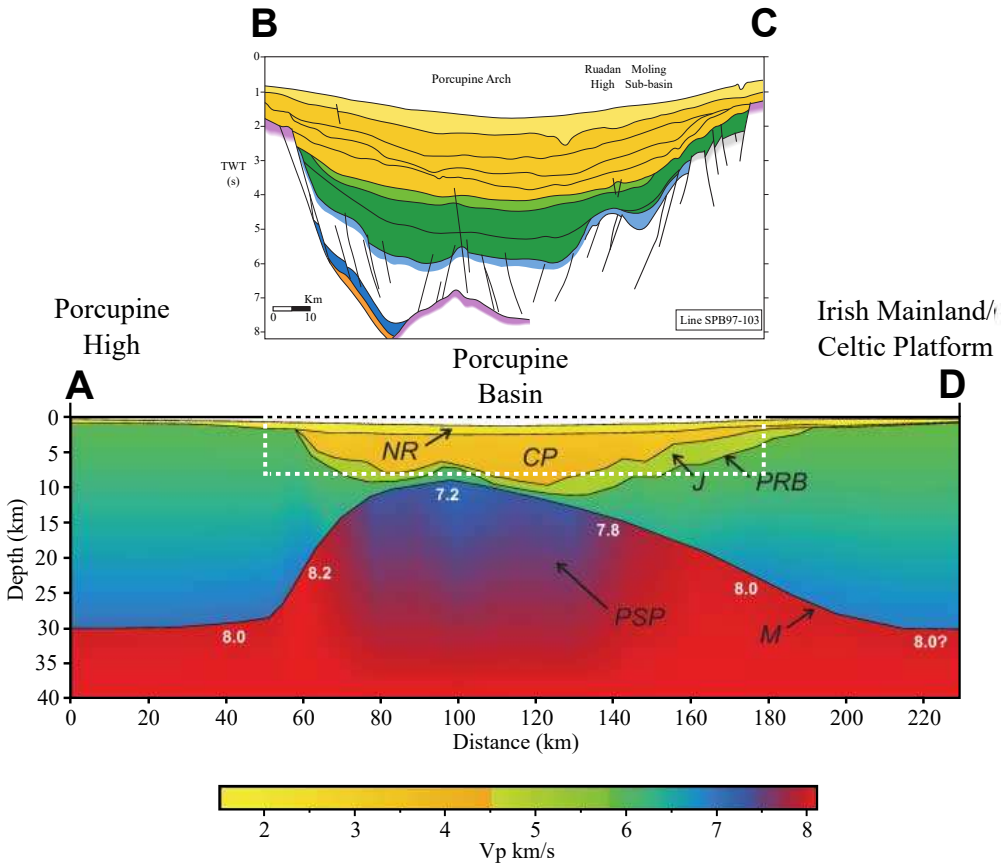

Figure 1.13. Cross section showing the structural setting (B-C; Naylor et al., 2002) and crustal velocity structure (A-D; O'Reilly et al., 2006) *of the Porcupine Basin. See Figure 1.12 for location.*

The continental crust beneath basin-bounding structural highs in the Irish Atlantic margin basins has been interpreted as relatively unstretched continental crust with a thickness of 25-30 km (Morewood et al., 2005; Shannon et al., 1999). Moreover, the continental crust beneath the Porcupine Basin is extremely thin (locally less than 2 km) across the basin centre (Figure 1.13) with partial serpentinization of the upper mantle interpreted below the Porcupine Arch (O'Reilly et al., 2006; Reston et al., 2001).

1.5.3 Galicia Interior Basin

The wide and deep Galicia Interior Basin (GIB), with a N-S to NNW- SSE trend, is bound to the east by the Iberian continental shelf, to the west by the Galicia Bank and the Vigo

Seamount, to the north by the Biscay Abyssal Plain, and to the south by the Aveiro Fault and the Porto Seamount (Montenat, Guery, & Berthou, 1988; Murillas et al., 1990). Its southern onshore equivalent is the Lusitanian Basin (Figure 1.14; Boillot, Auxietre, Dunand, Dupeuble, & Mauffret, 1979; Montenat et al., 1988; Murillas et al., 1990).

According to Murillas et al. (1990), the GIB was a key component in the Triassic rift system that formed between Europe, Africa, and North America, preceding the opening of the Central Atlantic during Bathonian-Callovian times (Klitgord & Schouten, 1986). Similar to some basins in the southern North Atlantic (e.g., Jeanne d'Arc, Orphan, Porcupine, Rockall), the GIB endured different degrees of reactivation with the main extension occurring during Late Jurassic-Early Cretaceous time (Groupe Galice, 1979; Masson & Miles, 1986; Mauffret, Boillot, Auxietre, & Dunand, 1978; Murillas et al., 1990).

Even though the basement of the Iberian Peninsula is related to the Variscan Orogeny, different zones have been defined (Arenas, Martínez-Catalán, & Díaz García, 2004; Farias et al., 1987; Martínez-Catalán, 1990; Matte, 2001; J. B. Murphy, Keppie, Nance, & Dostal, 2010). The Galicia Interior Basin is thought to be the northward continuation of the Ossa-Morena terrain based on samples from the Galicia Bank and velocity analysis (Arenas et al., 2004; Boillot, Mougenot, Girardeau, & Winterer, 1989; Capdevila & Mougenot, 1988; Farias et al., 1987; Martínez-Catalán, 1990; Matte, 2001; J. B. Murphy et al., 2010; Pérez-Gussinyé et al., 2003).

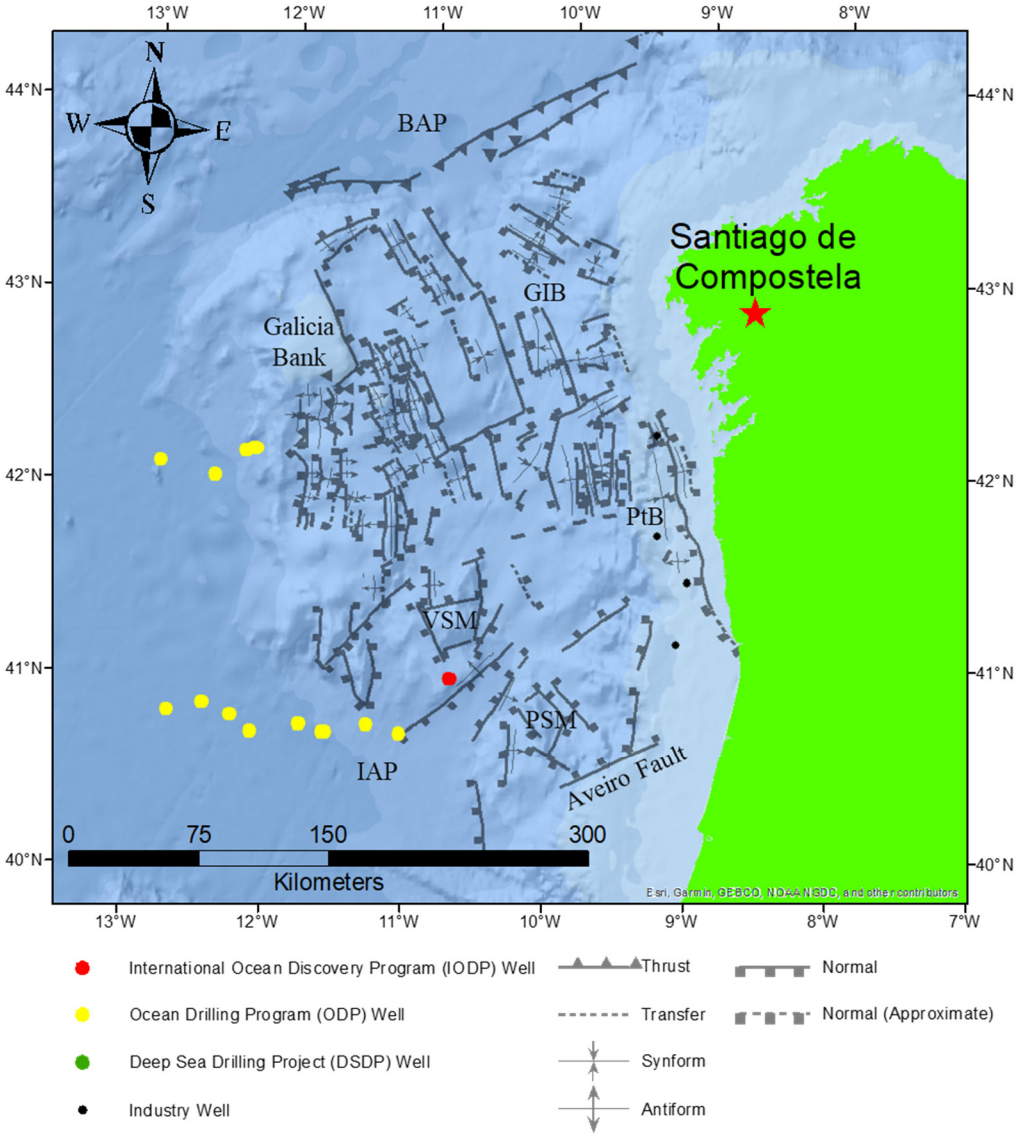

Figure 1.14. Structural map showing the basins offshore the Iberian Peninsula. Adapted from Murillas et al. (1990). IAP: Iberia Abyssal Plain. BAP: Biscay Abyssal Plain. GIB: Galicia Interior Basin. PtB: Porto Basin. VSM: Vigo Seamount. PSM: Porto Seamount.

1.6 Geological Framework

1.6.1 East Orphan Basin

The different lithologies, formations, and structures that characterise the Orphan Basin are depicted in Figure 1.15. The Palaeozoic basement, formed during the Appalachian-

Caledonian orogeny due to the closure of the Iapetus Ocean (Williams, 1995), is composed of low-grade metasedimentary and granitic rocks (Gouiza et al., 2017). Triassic sediments have not been drilled in Orphan Basin but, according to McAlpine (1990), well data in the Jeanne d'Arc Basin suggest that Upper Triassic clastic rocks unconformably lay on the Palaeozoic basement.

The Jurassic sequence, bounded at the top by the Tithonian unconformity, is only visible in some wells in the East Orphan Basin and Flemish Pass and it is composed of the Rankin and Jeanne d'Arc formations (Gouiza et al., 2017). The Lower Cretaceous is bounded at the top by an Aptian–Albian unconformity and at the base by the Tithonian unconformity. It is composed of the Whiterose and Nautilus formations (Gouiza et al., 2017). The Upper Cretaceous, on the other hand, is bounded by the Cenozoic unconformity at the top and the Aptian–Albian unconformity at the base. According to well data, the Upper Cretaceous thickness varies from around 650 m (Baie Verte J-57) on the continental shelf to 10 m (Great Barasway F-66) in the deeper East Orphan Basin (C-NLOPB, 2009; Gouiza et al., 2017).

The Banquereau Formation, bounded at the base by the Cenozoic unconformity, represents the Cenozoic Era in the Orphan Basin. Its thickness varies from 3000-4000 m on the continental shelf in the west to 1500 m in the East Orphan Basin, and 600-1400 m towards the south-east in the Flemish Pass (Gouiza et al., 2017).

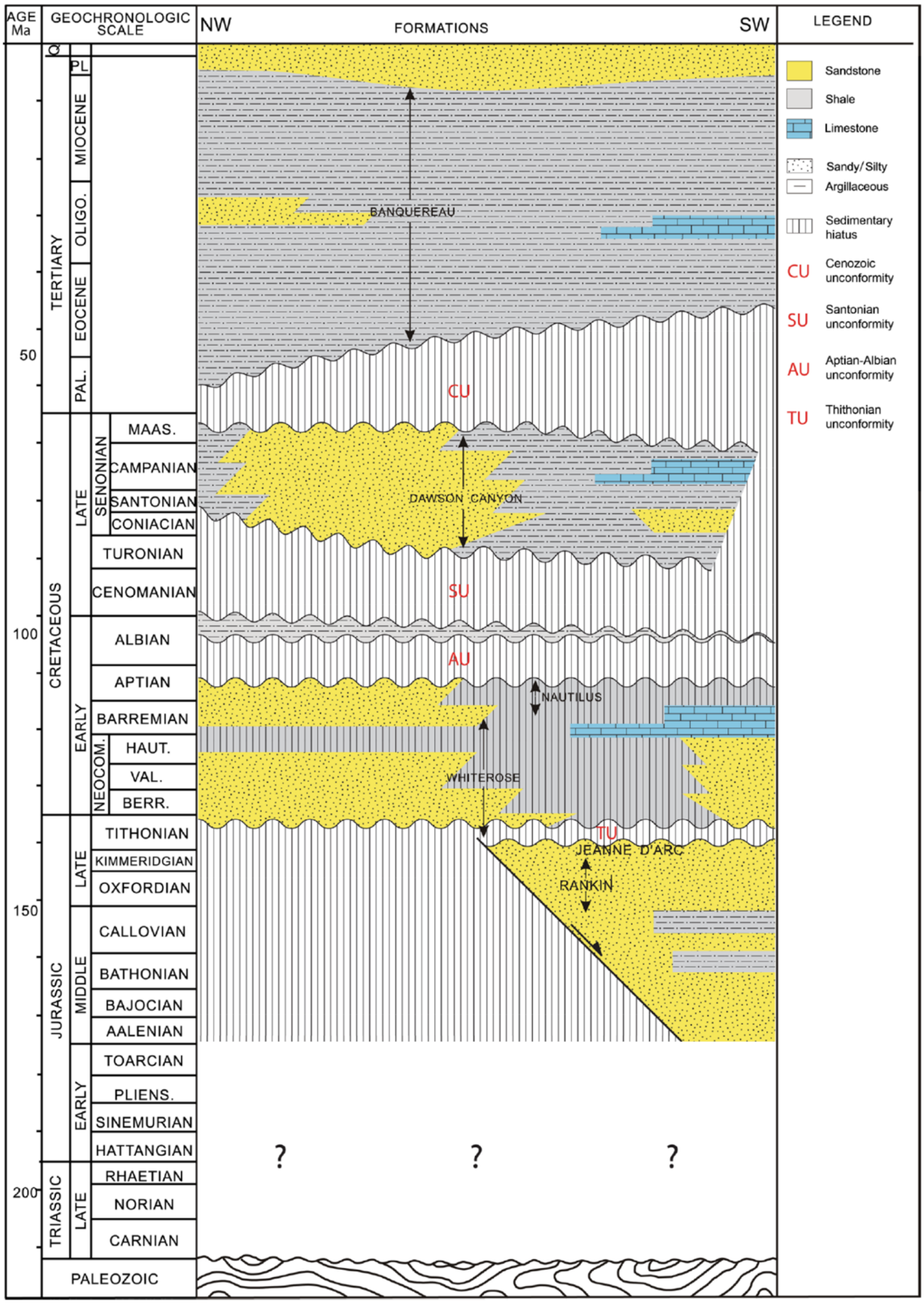

Figure 1.15. Simplified lithostratigraphic chart of Orphan Basin (Gouiza et al., 2017).

1.6.2 Porcupine Basin

The different types of rocks, formations, and structures that characterise the Porcupine Basin are depicted in Figure 1.16. The Porcupine Basin contains up to 10 km of upper Carboniferous to Cenozoic sediments (Croker & Shannon, 1995). The Precambrian is poorly constrained in Ireland; however, Precambrian rocks represent approximately 10% of the surface area of Ireland and are predominantly seen along the west, northwest, and southeast peripheries of Ireland (Daly, 2009; Naylor & Shannon, 2011). No Archaean rocks are known from Ireland; nevertheless, Archaean crustal rocks are suggested to be present to the north of the Anton Dohrn Transfer Fault Zone beneath the northern part of the Rockall Trough within the Laurentian continental terrane (Naylor & Shannon, 2011).

The Palaeozoic (Carbonifeous - Pennsylvanian) rocks are represented by fluvial to deltaic and brackish sandstone, siltstone, mudstone and coal that have been drilled on the eastern margin of the Porcupine Basin (Croker & Shannon, 1987; Robeson, Burnett, & Clayton, 1988). The upper Palaeozoic strata are overlain locally by poorly dated clastic-dominated Devonian-Early Carboniferous, Permo-Triassic shallow-marine sandstones and evaporitic mudstones, and regionally by widespread Middle and Upper Jurassic fluvial to transgressive shallow-marine sandstones, mudstones and thin limestones (Croker & Shannon, 1987).

The Permo-Triassic strata have only been drilled in some wells in the North Porcupine Basin and in a couple of isolated wells in the Porcupine Basin (Naylor & Shannon, 2011). Lower Jurassic limestones and marine mudstones appear to be conformable with the underlying Upper Triassic succession (Croker & Shannon, 1987). The Middle Jurassic strata are represented by sandy braided fluvial deposits, the product of an onset warp phase of

tectonism immediately prior to the onset of the Late Cimmerian rifting (Sinclair, Shannon, Williams, Harker, & Moore, 1994). Upper Jurassic strata within the basin reflect deposition in a syn-rift setting, with the development of a range of lithologies and facies mainly in the Porcupine Basin (Naylor & Shannon, 2011). These facies vary between continental sandstone and shale sequences, interrupted by intercalations of shallow-marine strata (Croker & Shannon, 1987; MacDonald, Allan, & Lovell, 1987). A thick (more than 1000m drilled in wells) Cretaceous succession, composed of mudstones and local marine and deltaic sandstones, overlain by a thick Chalk succession, unconformably overlies the Jurassic succession (Naylor & Shannon, 2011). Up to 2 km of Cenozoic mudstones, sandstones and thin limestones have been drilled in the Porcupine Basin, with upper Paleocene to Eocene deltaic sandstones in the north of the basin (Naylor & Shannon, 2011).

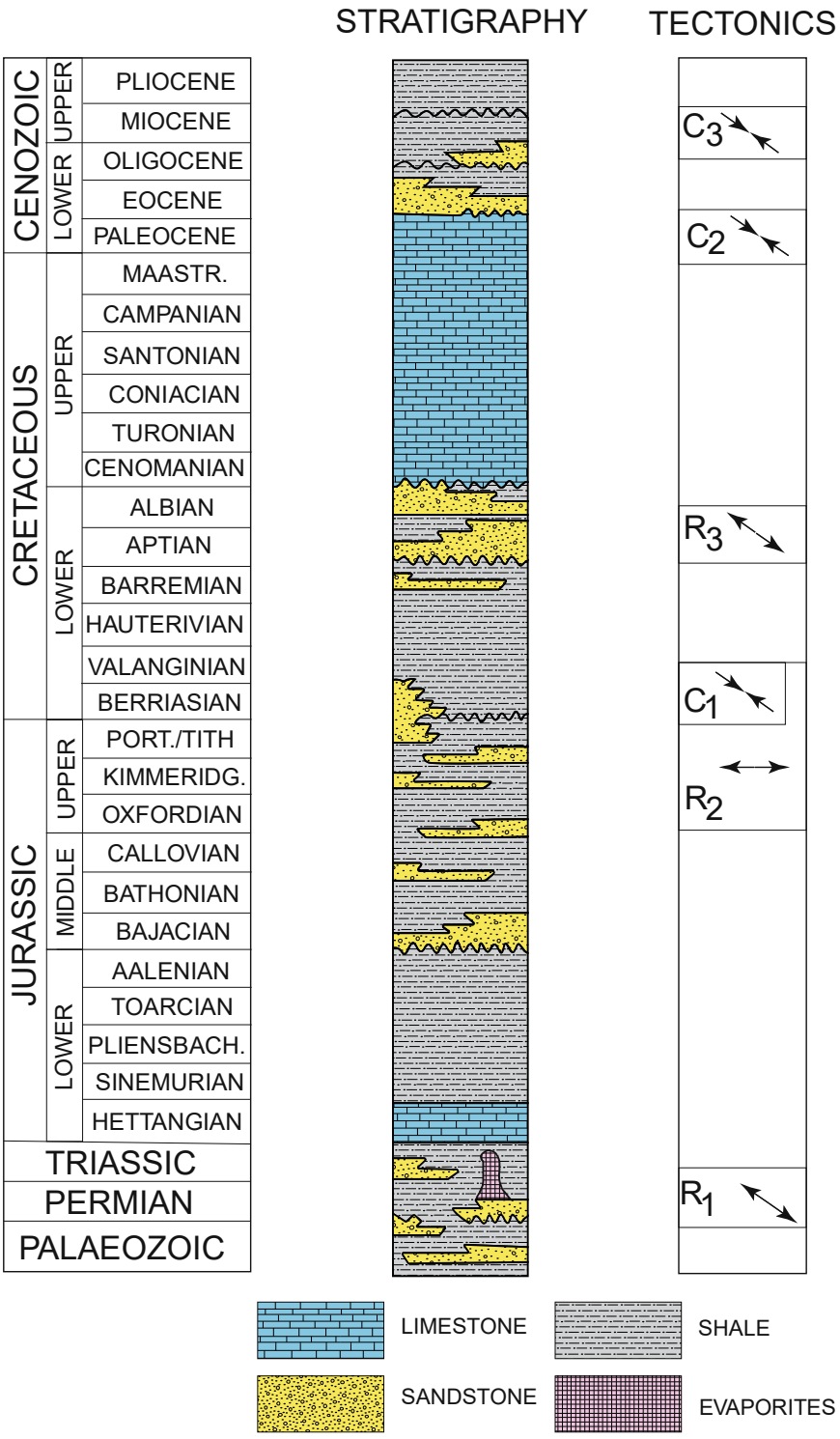

Figure 1.16. Generalised tectonostratigraphic framework of the Rockall and Porcupine region showing the major lithologies, unconformities and tectonic events of the Late Palaeozoic to Cenozoic. R1–3 refer to the major rift phases and C1–3 are compressive phases. The direction of extension and compression is indicated by the arrows (adapted from Shannon, McDonnell, & Bailey, 2007)

1.6.3 Galicia Interior Basin

The GIB consists of a thick sedimentary accumulation of up to 4000 m (Boillot et al., 1979; Groupe Galice, 1979; Mauffret et al., 1978; Montadert, de Charpal, Roberts, Guennoc, & Sibuet, 1979; Montadert, Winnock, Deltiel, & Grau, 1974). Although limited well data are available within the GIB, correlations with wells drilled to the south and west of the GIB (e.g., Lusitanian Basin and Galicia Bank) are used. The Triassic and Lower Jurassic deposits consist of conglomerate, sandstone, and perhaps lagoonal evaporite units that might produce diapirs (Groupe Galice, 1979; Montenat et al., 1988). Argillaceous, oolitic, and pelagic limestones, sometimes with neritic and reefal characteristics, are associated with open marine sedimentation during the Middle and Late Jurassic. Red argillaceous sandstones were deposited at the end of the Late Jurassic. During the Cenomanian, the continental sedimentation is replaced by marine deposits. The southern part of the basin emerged and was covered by volcano-sedimentary layers of uncertain age (Late Cretaceous to Eocene). Alternating transgressive-regressive episodes during Late Cretaceous and Cenozoic time affected the northern part of the basin which progressively subsided (Groupe Galice, 1979; Mena et al., 2018).

1.7 Purpose

The aim of this project is to use existing seismic reflection data, both vintage and newly acquired, on both the Newfoundland and Irish margins (and later the Galicia margin), to attempt to reconnect the conjugate margin basins that were once linked and try to better understand in what ways their subsequent evolution diverged.

1.8 Outline

This thesis is structured as follows:

Chapter 1. Introduction: This chapter contains general information about the study area, the geological and tectonic framework of the main basins included in the study, as well as the purpose of the research.

Chapter 2. Dataset and Methodology: This chapter details the types of data used, the sources of the data, and the different methods applied to carry out the interpretation and analysis.

Chapter 3. Seismic Interpretation: This chapter contains the step by step explanation of how the seismic interpretation was carried out and what constraints were used.

Chapter 4. Structural Restoration: The restoration of the interpreted horizons is detailed in this chapter. The techniques and software that were used to progressively undeform the geological sections and that provide insights into the geometry of earlier stages are documented.

Chapter 5. Kinematic Evolution Models: The reconstructed location through time of the restored lines is described in this chapter. The workflow and software employed to relocate the sections through time, given the possible geometrical constraints of the earlier stages of the basins, are documented.

Chapter 6. Interpretation and Discussion: The findings from the three previous chapters are compiled and integrated into a regional context to subsequently discuss the implications of the results.

Chapter 7. Conclusions: This chapter summarises the conclusions of all of the research work carried out for this thesis project.

CHAPTER 2. DATASET AND METHODOLOGY

In this chapter, the data types and sources are described and the methodologies for interpretation, restoration, and analysis are introduced. A more detailed explanation of the methodology, with accompanying results, is given in Chapter 3 (Seismic Interpretation), Chapter 4 (Structural Restoration), and Chapter 5 (Kinematic Evolution Models). The discussion and analysis of the results are presented in Chapter 6 (Interpretation and Discussion).

2.1 Dataset

The data used in this study include ~22,800 km of 2D pre-stack time migrated (PSTM) seismic reflection profiles, and well logs and lithological data from 22 wells from the East Orphan, Porcupine, and Galicia Interior basins (Figures 2.1, 2.2, and 2.3).

Integration of seismic and well data was performed to define the syn- and post-rift layers and to interpret the regional faults and geological structures across the Orphan Basin, the Porcupine Basin, and later, the Galicia Interior Basin. Although the East Orphan Basin is the focus of this research, seismic interpretation was also carried out over the West Orphan Basin to explore the thickness variations, to get a better understanding of the evolution of the highly complex West and East Orphan basins, and to produce a more coherent regional model.

2.1.1 Well data

2.1.1.1 East Orphan Basin

Well data from the East Orphan Basin were provided by the Canada-Newfoundland Offshore Petroleum Board (C-NLOPB) and from the Basin database of Natural Resources Canada (2017). Twelve wells were used in this study, eleven from the Orphan Basin and one well from the Flemish Pass Basin (Figure 2.1). Paper copies and time-depth data for some logs were provided by the C-NLOPB. Digital logs in .las format (Gamma-Ray, Caliper, Sonic, Density and Spontaneous Potential logs) for several wells, were donated by IHS Markit™. Lithostratigraphic logs were provided by Canadian Stratigraphic Services Ltd (CANSTRAT).

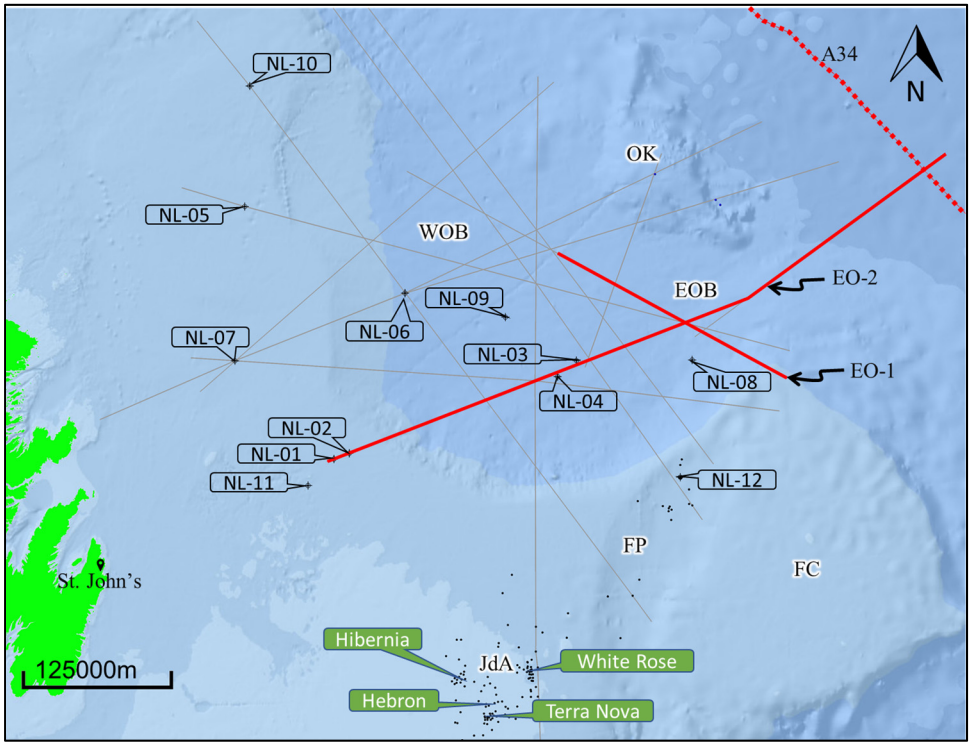

Figure 2.1 Map of the Orphan sub-basins showing wells and 2D seismic data used. FC: Flemish Cap; OK: Orphan Knoll; JdA: Jeanne d'Arc Basin; FP: Flemish Pass Basin; EOB: East Orphan Basin; WOB: West Orphan Basin; A34: magnetic anomaly 34 from Srivastava et al. (1990); grey and red solid lines represent 2D seismic lines, with red ones corresponding to the main focus of this MSc project.

2.1.1.2 Porcupine Basin

For the Irish margin, data from eleven wells (Figure 2.2), one in the Porcupine Basin, one in the Goban Spur Basin, one in the Fastnet Basin, four in the Slyne Basin, one in the Erris Basin, and two in Rockall Basin, were provided by the Department of Communications, Climate Action & Environment of Ireland. These data included well reports, well logs, and lithological data.

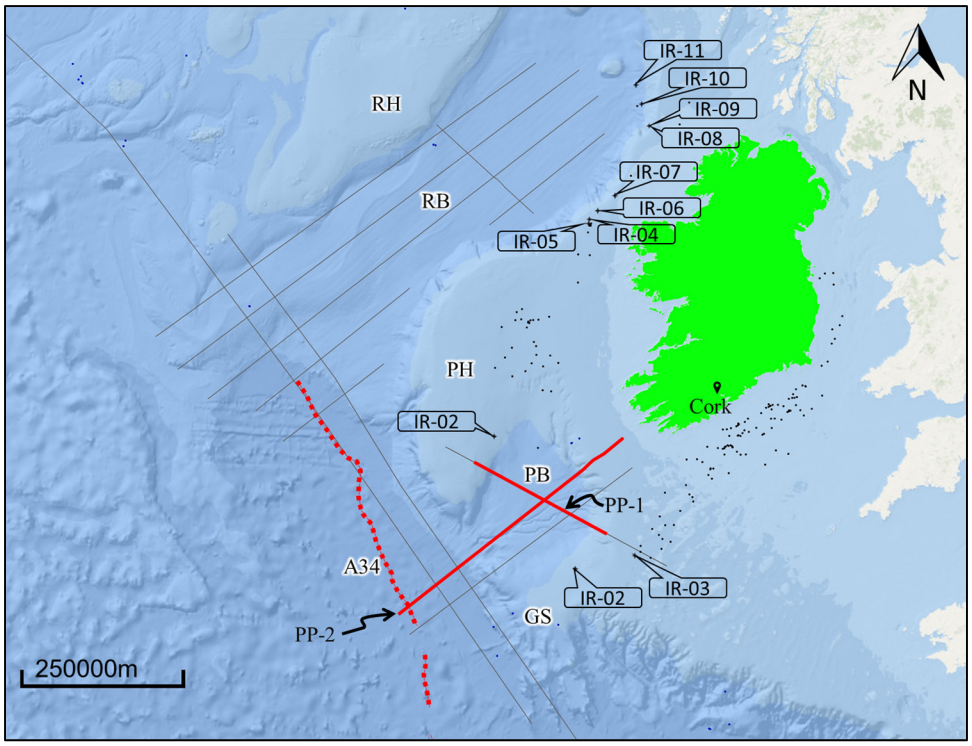

Figure 2.2 Map of the offshore Irish basins showing wells and 2D seismic data used. PB: Porcupine Basin; PH: Porcupine High; RB: Rockall Basin; RH: Rockall High; A34: magnetic anomaly 34 from Srivastava et al. (1990); grey and red solid lines represent 2D seismic lines, with red ones corresponding to the main focus of this MSc project. Magnetic anomaly A34 is shown by the dotted red line.

2.1.1.3 Galicia Interior Basin

No well data for the Galicia Interior Basin are publicly available; however, descriptions and correlations of adjacent wells from the Deep Sea Drilling Project (DSDP), the Ocean Drilling Program (ODP), the Integrated Ocean Drilling Program (IODP), and some industry wells

interpreted by Sibuet et al. (1979), Boillot et al. (1987), Murillas et al. (1990), and Mena et al. (2018) were used (Figure 2.3).

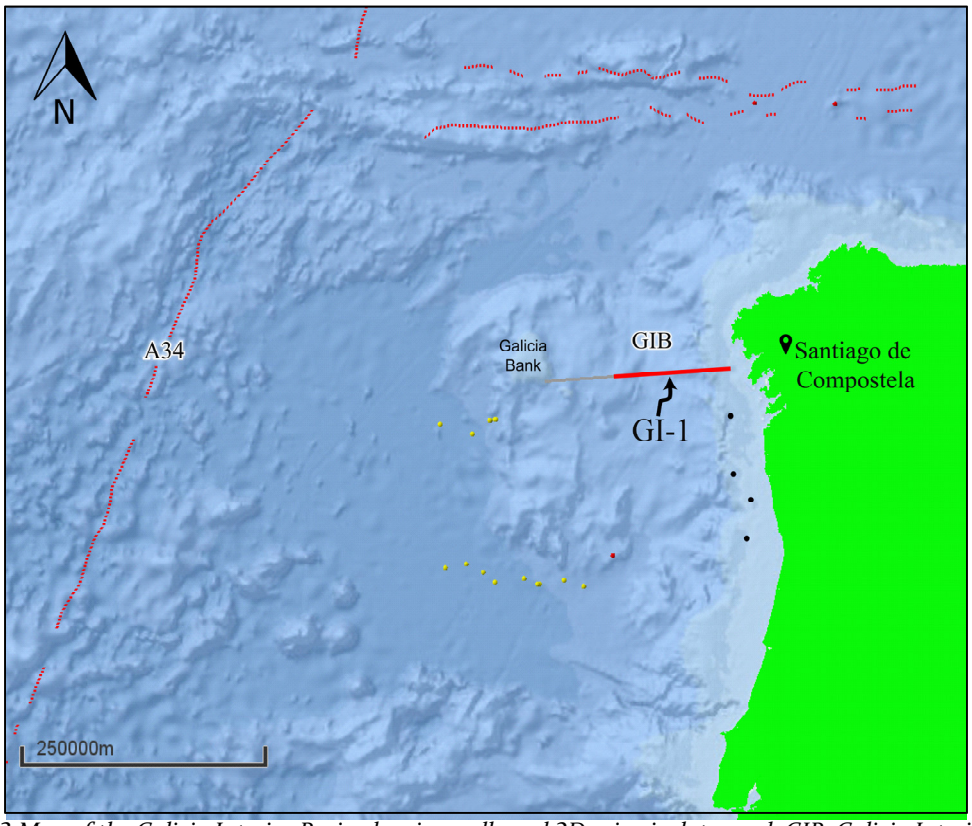

Figure 2.3 Map of the Galicia Interior Basin showing wells and 2D seismic data used. GIB: Galicia Interior Basin; A34: magnetic anomaly 34 from Srivastava et al. (1990); yellow dots: ODP wells; red dots: IODP wells; black dots: industry wells; grey and red solid lines represent 2D seismic lines, with the red one corresponding to the one used in this MSc project.

2.1.2 Seismic data

2.1.2.1 East Orphan Basin

The seismic data for the East and West Orphan basins correspond to eleven 2D Pre-stack Time Migrated (PSTM) seismic lines, along with their corresponding stacking velocities. These lines were acquired in 2002 and have been provided by TGS-NOPEC Geophysical Company (TGS). Two additional 2D seismic lines acquired in 1984 and 1987 as part of the Geological Survey of Canada's Frontier Geoscience Project were also included in this study

(Figure 2.1). Together, the seismic lines cover a combined length of around 6,400 km over the East and West Orphan basins.

2.1.2.2 Porcupine Basin

Fourteen 2D PSTM seismic lines acquired between 2013 and 2014 over the Porcupine and Rockall basins were provided by the Department of Communications, Climate Action & Environment of Ireland. Five of these lines cross the Porcupine Basin while the rest are located mainly in the Rockall Basin (Figure 2.2). The fourteen lines cover a combined length of around 8,200 km.

2.1.2.3 Galicia Interior Basin

A 2D seismic line acquired in 1997, processed, and depth-converted by Pérez-Gussinyé et al. (2003), was digitised and converted into a segy file to be used in this thesis project (Figure 2.3). The seismic line GI-1 crosses the Galicia Interior Basin from west to east with an approximate length of 120 km.

2.2 Methodology

This research project was developed based on the following methodology which consists of five (5) major phases (Figure 2.4).

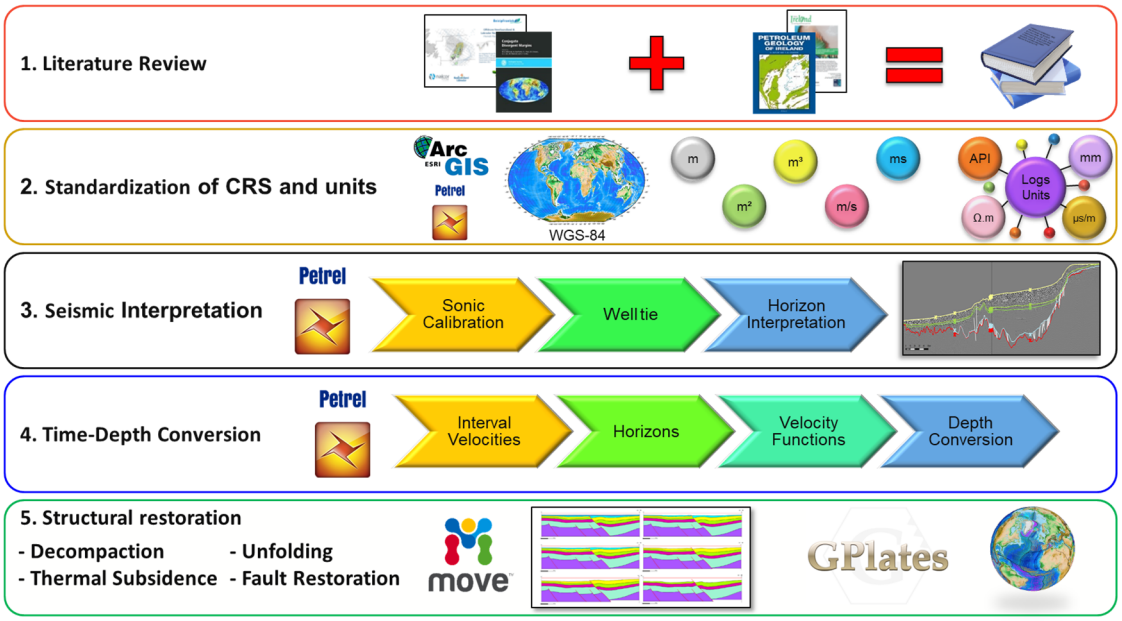

Figure 2.4 Methodological scheme

2.2.1 Literature Review

The research work began with a compilation and review of the peer-reviewed literature in order to understand the geological and tectonic framework of the conjugate margins of Canada and Ireland.

2.2.2 Standardization of coordinate reference systems (CRS) and units

Due to the fact that the CRSs and units used in Canada (North American Datum and Metric system) and Ireland (European Datum and Field units) differ from one another, a standardization of both was carried out to correctly compare and analyse the data from the conjugate margins. The CRS used for this project was the World Geodetic System 1984 (WGS-84) along with the Metric system. For the seismic data, the positive standard polarity (Sheriff & Geldart, 1995) was used. Conversions and transformations were performed using ArcGIS® and Petrel E&P software.

2.2.3 Seismic Interpretation

To carry out the seismic interpretation, seismic well ties were built to tie the lithological information from the wells to the seismic data (Figure 2.5). First, the check-shot data went through a quality control process using a cross-plot of the True Vertical Depth Sub-Sea (TDVSS) and the interval velocity to visualise and remove any abnormal values. Due to the fact that well log data can be affected by changes in hole size (e.g., the density log can show anomalously low values in areas with a washout), a quality control process was also carried out on the sonic and density logs to define areas with higher uncertainty for the well tie process. The sonic logs went through a despiking process with the aim of obtaining a better match with the seismic data by removing the high-frequency variations. The despiking process was also applied to the density logs when abnormal peaks were produced by changes in the drill bit size. Due to the differences in the frequency bands of the sonic logs (5-15 kHz) and the seismic data (15-45 Hz), the sonic logs were corrected by integrating the check-shot information (Sonic calibration process). The replacement velocities used were: 330m/s for the section between the Kelly Bushing (KB) and the Mean Sea Level (MSL) and 1482m/s for the section between the MSL and the water bottom. From the sonic calibration process two curves were generated, a corrected sonic log and a Time-Depth Relationship (TDR).

Using the previously generated TDR and the despiked velocity log, the well tie process was performed. First, the reflection coefficient (RC) series, computed from the sonic and density logs (Equation 2.1), is convolved with a statistical wavelet, in which phase and length of the wavelet are supplied and the amplitude spectrum is predefined from the seismic traces

(Schlumberger, 2018), to produce a synthetic seismogram. Where sections of the density log were missing, the RC was estimated from the velocity log (Vp) using the density (ρ) derived from Gardner's equation (Gardner, Gardner, & Gregory, 1974; Equation 2.2; α and β are constants that depend on the geology). The estimated synthetic seismogram was then compared with the real seismic data. Stretching and squeezing was then applied to obtain a better match between the well tops and the seismic reflectors. This process involves an adjustment of the interval velocities to obtain a better fit. Finally, an integrated TDR was calculated and applied to the corresponding well.

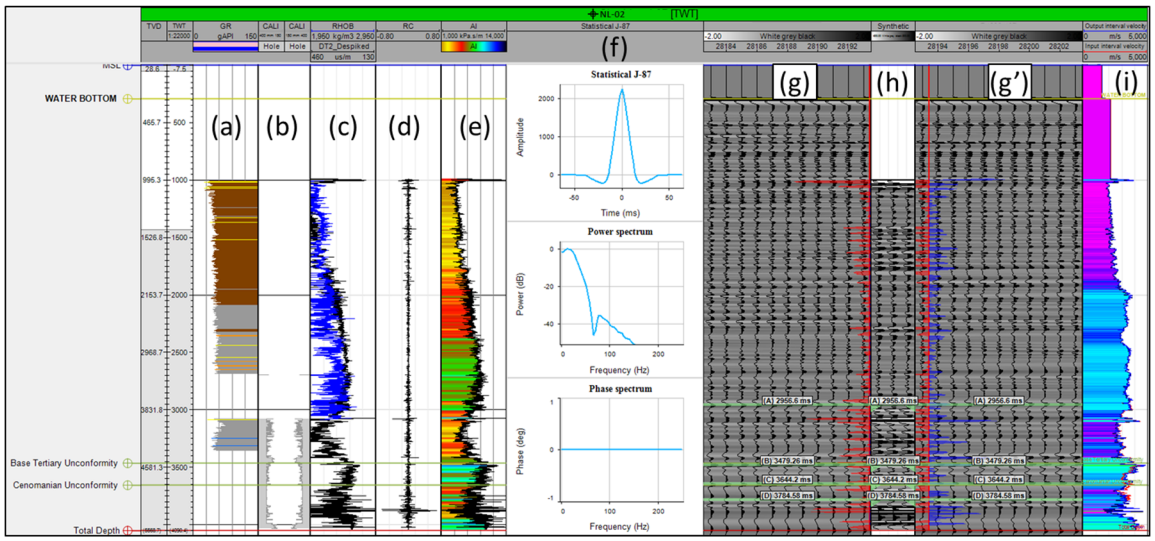

Figure 2.5 Example of a seismic well tie of the well NL-02. The different tracks show (a) Gamma ray log filled with lithological description of the cuttings from CANSTRAT. (b) Caliper log. (c) Blue: Density log; Black Sonic log. (d) Reflection coefficient. (e) Calculated Acoustic Impedance. (f) Statistical wavelet. (g and g') Traces from 2D seismic line. (h) Synthetic seismic trace. (i) Red: Input interval velocity; Blue: Output interval velocity.

Equation 2.1 Reflection coefficient equation (Yilmaz, 2008)

$$RC = \frac{\rho_2 v_2 - \rho_1 v_1}{\rho_2 v_2 + \rho_1 v_1}$$

where:
RC: reflection coefficient
ρ_1 and ρ_2: densities of the layers
v_1 and v_2: velocities of the layers

Equation 2.2 Gardner's equation (Gardner et al., 1974).

$$\rho = \alpha V_p^{\beta}$$

where:
ρ: bulk density
V_p: P-wave velocity
α and β: empirically derived constants that depend on the geology
(α=309.545 and β=0.25 to obtain density in kg/m^3).

Having identified the seismic events near the wells, seismic interpretation was performed over the East Orphan and Porcupine basins, by identifying five horizons (Cenozoic, Upper Cretaceous, Lower Cretaceous, Jurassic, and Basement; Figure 2.6) and defining, based on the character of each layer (Fossen, 2010; Mitchum, Vail, & Sangree, 1977), three tectonostratigraphic megasequences (post-rift, syn-rift, and pre-rift). Interpretation was also perfomed across the West Orphan, Rockall, and Galicia Interior basins to get a better understanding of these complex and underexplored nearby basins. The seismic interpretation was carried out using Petrel E&P software.

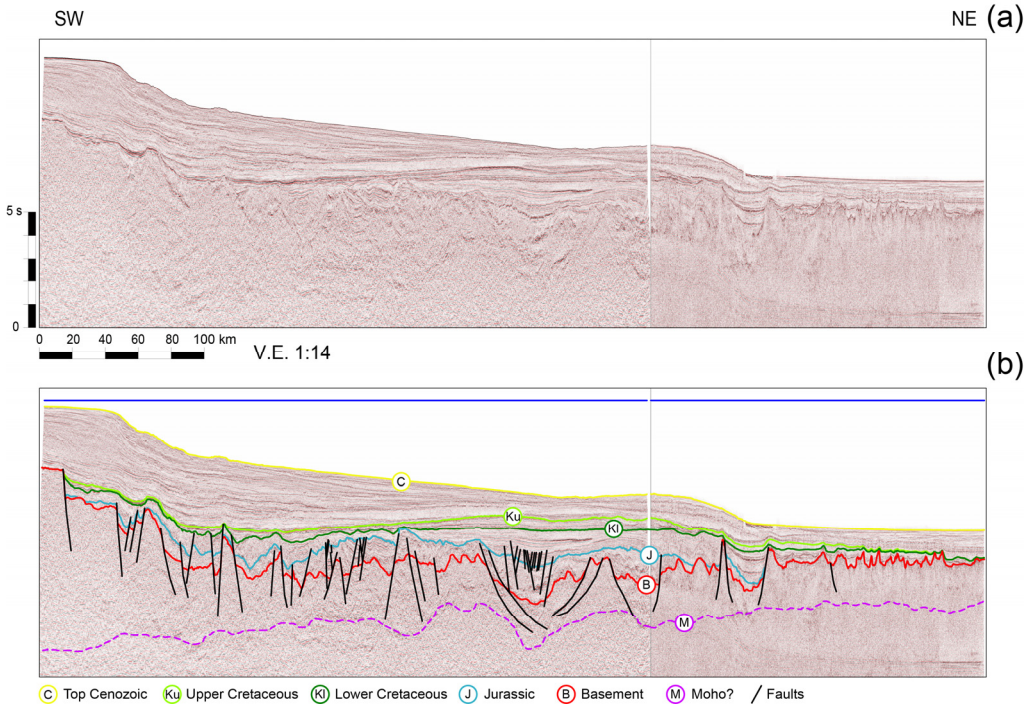

Figure 2.6 Example of a seismic line. (a) Uninterpreted; (b) interpreted.

2.2.4 Time-to-Depth Conversion

Due to the fact that the structural restoration must be done in the depth domain, time-to-depth conversion was performed on the interpreted seismic lines to be restored. The time-to-depth conversion was performed in Petrel E&P software using the stacking velocities for the Orphan lines (Figure 2.7). The stacking velocities were converted to interval velocities using the Dix equation (Dix, 1955; Equation 2.3). Using the horizons previously interpreted in time, velocity intervals were defined and interval velocities were extracted for each layer. For the Porcupine Basin, due to the lack of available stacking velocities, the average interval velocities obtained from the Orphan lines were used to perform the time-to-depth conversion (Table 2.1). These average interval velocities agree with the velocities previously modelled for the Porcupine Basin by Readman, O'Reilly, Shannon, & Naylor (2005) and O'Reilly et al. (2006). An example of a depth-converted line is shown in Figure 2.8.

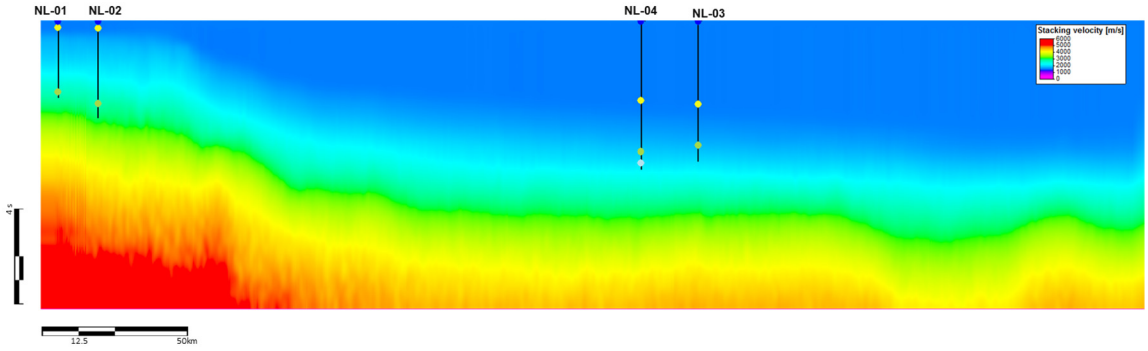

Figure 2.7 Example of the stacking velocities for the Orphan lines

Equation 2.3 Dix equation (Dix, 1955)

$$V_{n-layer}^{int} = \left(\frac{V_n^2 t_n - V_{n-1}^2 t_{n-1}}{t_n - t_{n-1}}\right)^{\frac{1}{2}}$$

where:
V_{n-1} and V_n: stacking velocities from the datum to reflectors above and below the layer
t_{n-1} and t_n: reflection arrival times

Table 2.1 Average interval velocities used for the time-to-depth conversion

Water: 1450 m/s
Cenozoic: 2285 m/s
Upper K: 3238 m/s
Lower K: 3896 m/s
Jurassic: 4718 m/s
Basement: 6000-6900 m/s
Moho: 7200-8000 m/s

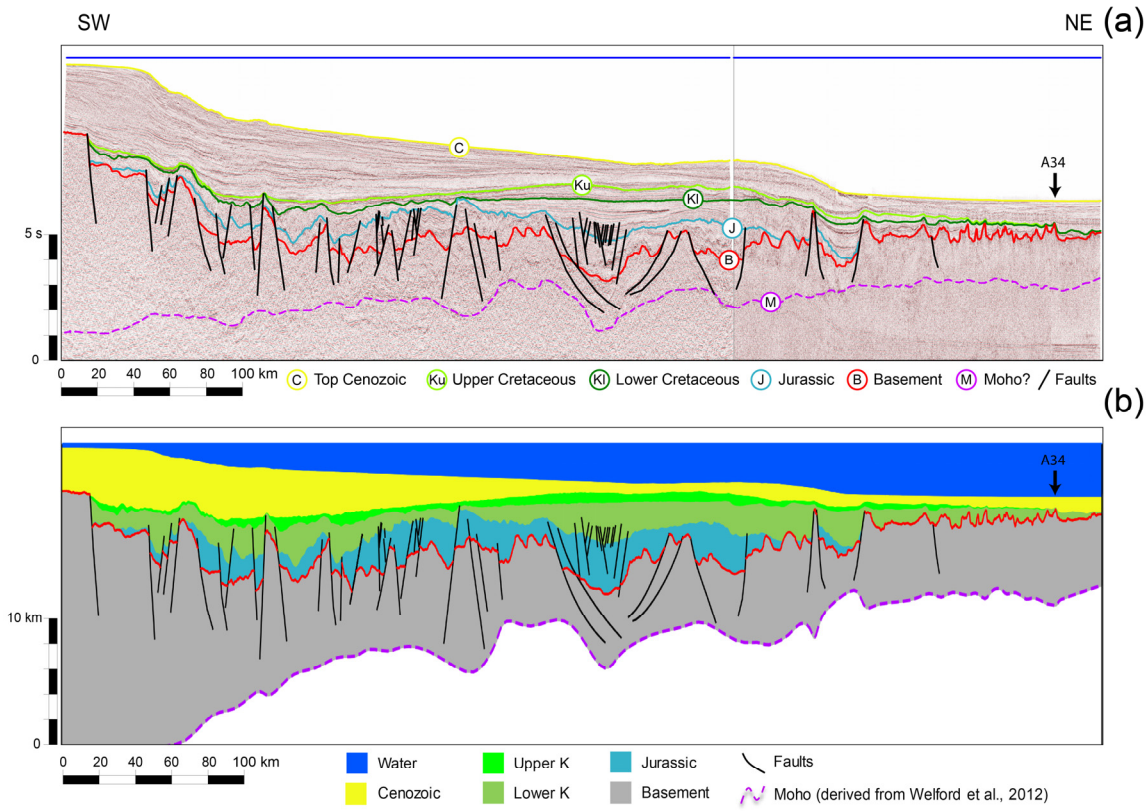

Figure 2.8 Example of the depth-converted line, (a) seismic line in time domain, (b) depth-converted interpretation.

2.2.5 Structural restoration

Before starting the structural restoration, the seismic lines to be restored were chosen using the depth to basement map from Welford et al. (2012) and the structural elements from Edwards et al. (2003), and Sibuet et al. (2007), for the Orphan Basin (Figure 2.3), and Naylor et al. (2002), for the Porcupine Basin (Figure 2.4). Two transects were selected for each

basin, trying to be as close to the dipping direction of the general fault trends as possible (Woodward, Boyer, & Suppe, 1989) but also covering the known extents of both basins.

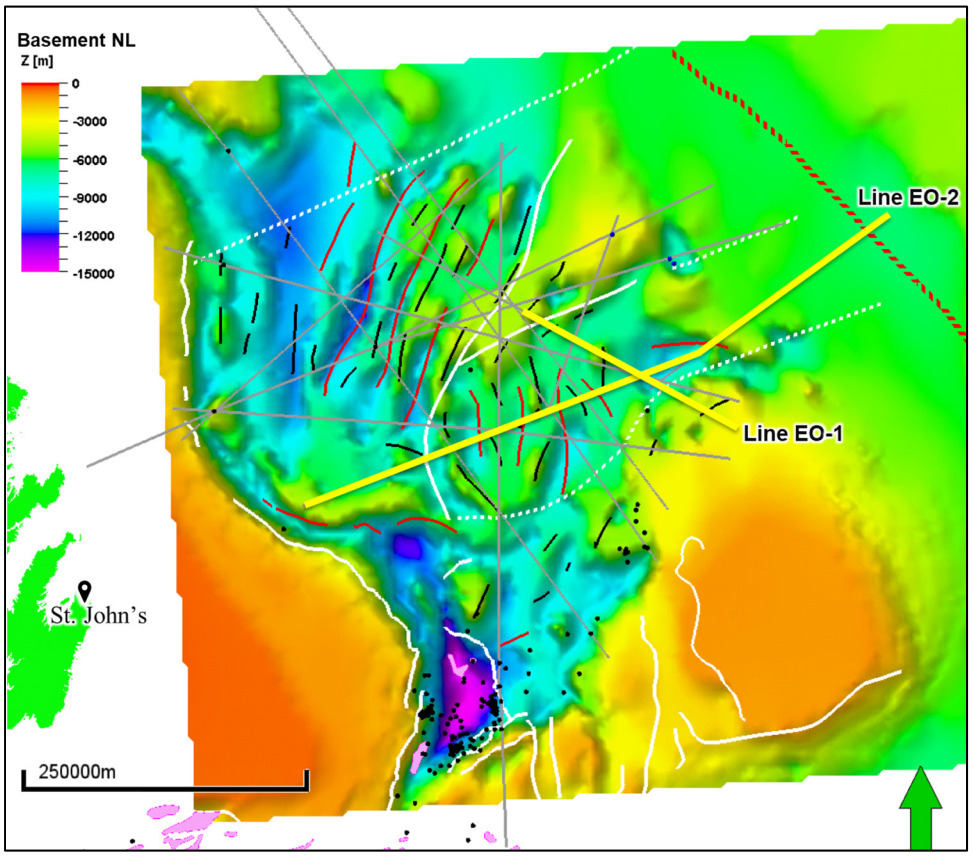

Figure 2.9 Depth to basement map from Welford et al. (2012) with the structural elements of the West and East Orphan basins adapted from Edwards, Jauer, Moir, & Wielens (2003), Srivastava et al. (1990), and Sibuet et al. (2007). Continuous white lines: normal faults/basin edge. Dashed white lines: transfer faults. Black lines: antiform structures. Solid red lines: synform structures. Dotted red line: magnetic anomaly 34 from Srivastava et al. (1990). *Black dots: wells. Gray lines: available seismic lines. Yellow lines: transects restored in this thesis. Pink polygons: salt.*

Similarly, free-air gravity data from Bonvalot et al. (2012) were also used to qualitatively assess if the orientations of the chosen seismic lines were covering the orientations of the main rift features present in the East Orphan (Figure 2.11) and Porcupine (Figure 2.12) basins. For the East Orphan Basin, the lines chosen were EO-1 and EO-2, whereas for the Porcupine Basin, the lines PP-1 and PP-2 were selected (Figures 2.9 and 2.10.).To estimate the depth to the base of the crust, the Mohorovičić discontinuity (Moho) proxy from

Welford et al. (2012) was used. Due to the presence of discontinuous reflections that partially coincide with the Moho proxy for the Moho in the East and West Orphan basins, the Moho proxy estimated for the restorations is a combination of the Moho proxy from Welford et al. (2012) and the Moho interpreted from the seismic lines. For the Porcupine Basin, the Moho depth could not be estimated from seismic data due to the limited depth coverage of the seismic lines across the basin (10-12 s). Therefore, the Moho proxy from Welford et al. (2012) was used.

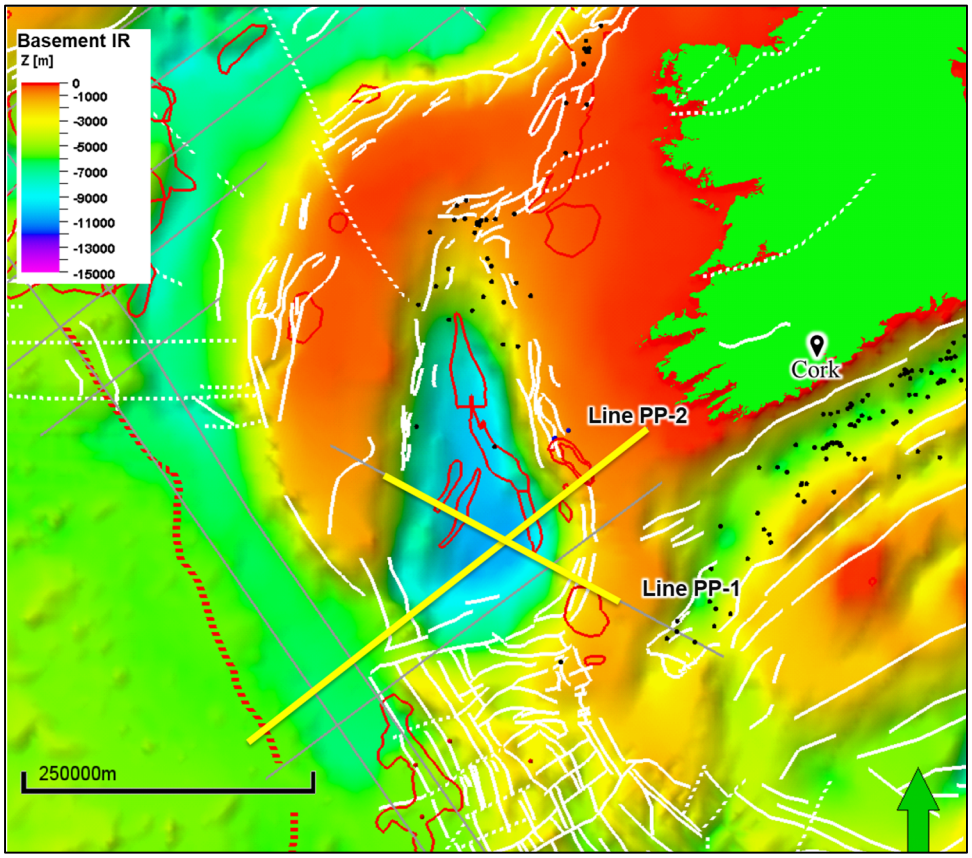

Figure 2.10 Depth to basement map from Welford et al. (2012) with the structural elements of the Porcupine Basin from Naylor et al. (2002). Solid white lines: normal faults/basin edge. Dashed white lines: transfer faults. Solid red polygons: igneous bodies. Dotted red line: magnetic anomaly 34 from Srivastava et al. (1990). Black dots: wells. Gray lines: available seismic lines. Yellow lines: transects restored in this thesis.

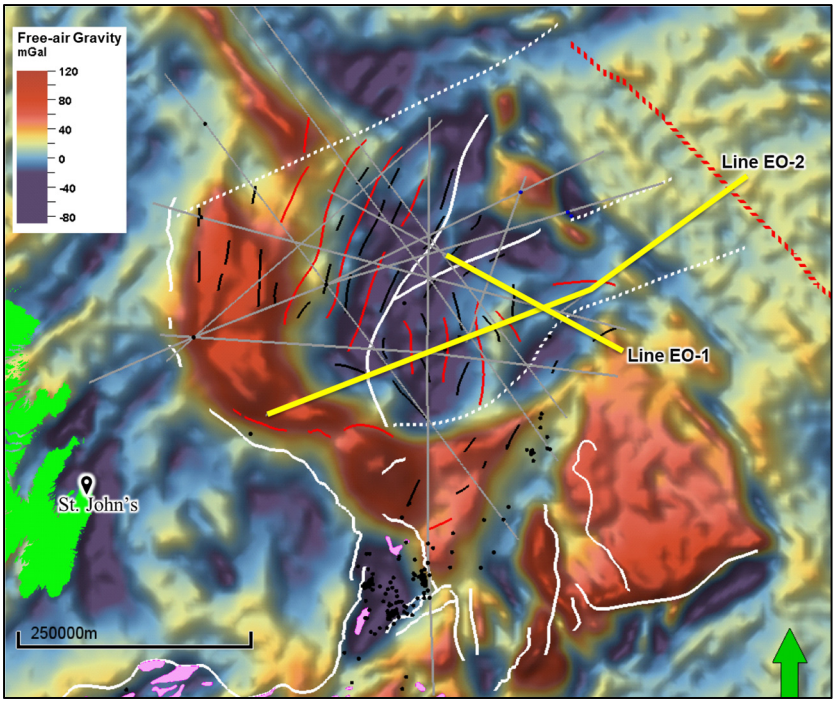

Figure 2.11 Free-air gravity anomaly map from Bonvalot et al. (2012) with the structural elements of the West and East Orphan basins adapted from Edwards, Jauer, Moir, & Wielens (2003), Srivastava et al. (1990), and Sibuet et al. (2007). For legend see Figure 2.9.

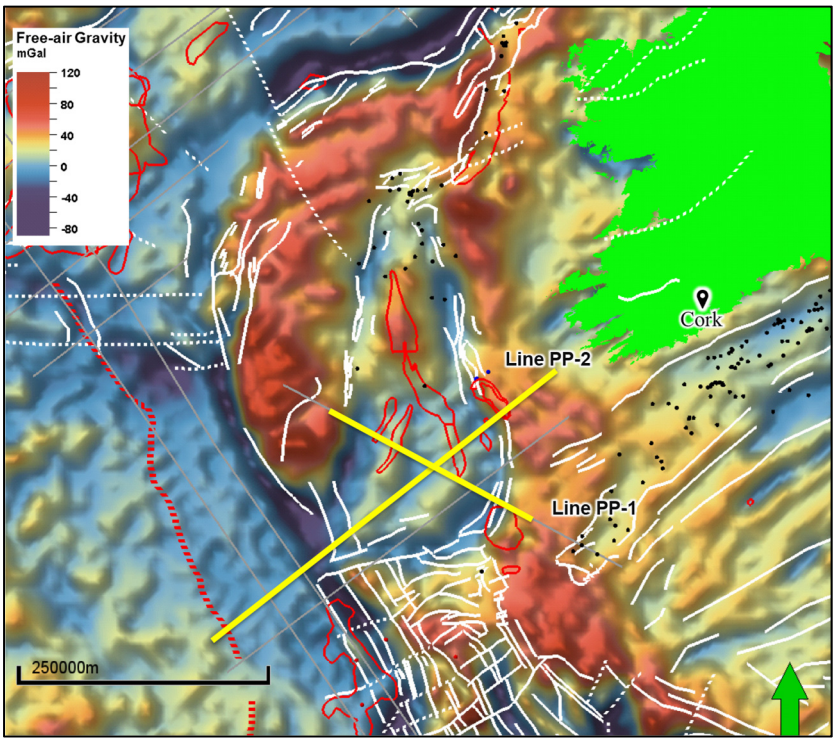

Figure 2.12 Free-air gravity anomaly map from Bonvalot et al. (2012) with the structural elements of the Porcupine Basin from Naylor et al. (2002). *For legend see Figure 2.10.*

Having selected and depth-converted the appropriate seismic lines, the structural restoration was performed. The restoration process involves removal of the effects of thermal subsidence, folding associated with compressional events, fault displacement associated with rifting, and compaction. The structural restoration was performed using Move™ software.

2.2.5.1 Decompaction

The 2D Decompaction workflow in Move™ compensates for the effects of rock volume change due to porosity loss associated with increased burial depth with time. The decompaction and compaction functions in Move™ are based on Sclater & Christie (1980). In the porosity-depth function (Equation 2.4) proposed by Sclater & Christie (1980), it is assumed that porosity decreases with increasing depth (Compaction) and increases with decreasing depth (Decompaction).

Equation 2.4 Porosity-depth function (Sclater & Christie, 1980)

$$f = f_0(e^{-cy})$$

where:
f: Present-day porosity at depth
f_0: Porosity at the surface
c: Porosity-depth coefficient (km^{-1})
y: Depth (m)

Isostatic rebound is also compensated during the decompaction workflow. Isostasy describes buoyancy forces acting on the Earth's crust and mantle. A simple way of explaining isostasy is that the lighter crust floats on the denser underlying mantle at a position of equilibrium such that at some depth the pressure is equal everywhere (Watts, 2001), just as a wood raft floats upon water (Airy, 1855).

The isostatic response to loading or unloading of sediments is important due to its effect on the restored shapes of horizons and faults, palaeo-topographies of restored seafloor surfaces, and absolute heights during restoration.

Two different methods are available in Move™ to account for isostatic relief: Airy isostasy and Flexural Isostasy. The Airy isostasy tool in Move™, based on the work of Airy (1855), assumes that an essentially brittle crust is supported and allowed to move on a fluid layer. The crust is assumed to be of finite strength and cannot support its own weight. When overburden is added or removed, the sediments are isostatically readjusted through compaction or decompaction. An important characteristic of the Airy isostasy method is that the estimated compensation is localised with no lateral flexural effects of loading or unloading. In other words, the material can only move vertically.

In contrast, the flexural isostasy method, based on the equations of Turcotte & Schubert (1982), allows the effects of flexural isostatic deflection of the lithosphere, resulting from extensional and contractional tectonics, to be modelled. The flexural isostasy method does not account for local changes in rigidity and strength of the lithosphere due to contraction, extension or erosion, but rather these changes are distributed regionally. For this project, Airy isostasy was used for both the East Orphan and Porcupine basins to take into account the isostatic response of the lithosphere during decompaction of the sedimentary layers due to the fact that the Airy isostasy compensation is local whereas the flexural isostasy distributes this compensation regionally.

2.2.5.2 Thermal subsidence

According to McKenzie (1978), the total subsidence in an extensional basin is produced by an initial subsidence caused by extension (Equation 2.5) and a subsequent thermal subsidence (Equation 2.6) caused by the cooling and contraction of the lithosphere in order to regain isostatic equilibrium (Allen & Allen, 2005). The former is dependent on the initial thickness of the crust and the amount of stretching (β) whereas the latter is dependent on the amount of stretching alone.

Equation 2.5 Initial subsidence equation (McKenzie, 1978)

$$S_i = \frac{a\left[(\rho_0 - \rho_c)\frac{t_c}{a}\left(1 - \alpha T_1 \frac{t_c}{a}\right) - \frac{\alpha T_1 \rho_0}{2}\right]\left(1 - \frac{1}{\beta}\right)}{\rho_0(1 - \alpha T_1) - \rho_w}$$

where:
S_i: Initial subsidence
a: Thickness of the lithosphere
ρ_0: Mantle density
ρ_c: Continental crust density
ρ_w: Sea water density
α: Thermal expansion co-efficient
T_1: Temperature of the asthenosphere
β: Beta factor (extension factor of the lithosphere)
t_c: Initial thickness of the continental crust

Equation 2.6 Thermal subsidence equation (McKenzie, 1978)

$$e_{(t)} = \frac{a\rho_0\alpha T_1}{\rho_0 - \rho_w}\left\{\frac{4}{\pi^2}\sum_{m=0}^{\infty}\frac{1}{(2m+1)^2}X\left[\frac{\beta}{(2m+1)\pi}\sin\frac{(2m+1)\pi}{\beta}\right]\exp\left(-(2m+1)^2\frac{t}{\tau}\right)\right\}$$

where:
$e_{(t)}$: Elevation change at time t
a: Thickness of the lithosphere
ρ_0: Mantle density
ρ_c: Continental crust density
ρ_w: Sea water density
α: Thermal expansion co-efficient
T_1: Temperature of the asthenosphere
β: Beta factor (extension factor of the lithosphere)
t: time (in million years) since rifting
τ: Lithosphere thermal time constant (Tau)

The thermal subsidence tool in Move™ is based on the work of McKenzie (1978) and it is designed to account for the effects on subsidence of changing temperature. McKenzie's work considers that a sedimentary basin is produced through the stretching of continental

crust, which thins the crust and allows the asthenosphere to rise to fill in the gap. After stretching stops, the crust cools, causing subsidence. This model ignores heat variations produced by radioactivity as only the heat variation from asthenospheric upwelling is considered.

2.2.5.3 Unfolding

In order to obtain a more geologically realistic restored section, a workflow was applied to restore the geological horizons to a pre-deformation stage. Due to the presence of localised inversion structures, a vertical or simple shear process was used to unfold the horizons. The 2D Unfolding tool in Move™ uses a simple shear unfold algorithm, which is the most appropriate for flattening a shallow regional dip that does not dip too steeply. The upper bed is unfolded to a horizontal datum. Vertical vectors, used to restore the Upper Bed, are the same as those used on the Lower Bed (Figure 2.13).

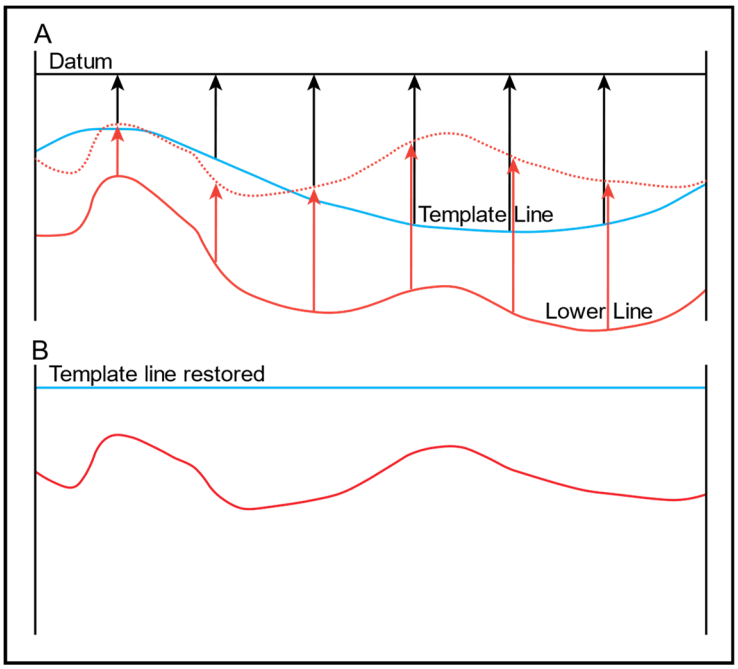

Figure 2.13 A) Example of a section before unfolding. B) Example of a section after unfolding. Black arrows: vertical vectors used to restore upper bed. Red arrows: vertical vectors used to restore lower bed.

2.2.5.4 Fault restoration

The 2D Move-on-Fault workflow in Move™ was applied to those horizons affected or displaced by faults associated with rifting events. The 2D Move-on-Fault workflow can be used to create forward models. These models are used to guide seismic-structural interpretation, to model pre- and syn- tectonic successions and various displacements, to test poorly constrained fault geometries within the stratigraphic framework, and to directly create a balanced interpretation.

Several algorithms can be applied, depending on the fault geometry (Simple Shear, Fault Parallel Flow, Fault Bend Fold, Fault Propagation, Trishear, Detachment Fold, and Elliptical Fault Flow). However, the simple shear algorithm is used for this project as it is the most suitable for extensional tectonic regimes (e.g., East Orphan and Porcupine basins) where non-planar normal faults and rollover structures are usually found. The simple shear algorithm in Move™ maintains the area between beds. To restore the horizons displaced by faults, within the 2D Move-on-Fault workflow, the *Join Beds* movement tool was used to allow the alignment of the horizon segments from the hanging and foot walls. In many cases, the synthetic shear algorithm produces unrealistically steep hanging-wall layers whereas the antithetic shear algorithm produces better results for deformed hanging walls above listric faults (Fossen, 2010). Based on these findings, an antithetic shear angle of ±60° was used.

After restoration, the 2D sections from both margins were compared in order to extract possible similarities and/or discrepancies between them. Additionally, the restored sections were compared with the kinematic evolution model of Nirrengarten et al. (2018) using

GPlates, a plate-tectonic reconstruction open-source software, used to visualise and support the results obtained. The restored sections were then relocated back through geological time and visualised in Move's 3D viewer to carry out the analysis of the results. The interpretation and restoration results are presented in chapters 3, 4, and 5, and discussed in detail in Chapter 6.

CHAPTER 3. SEISMIC INTERPRETATION

The twenty-five PSTM seismic lines (covering a combined length of around 14,600 km) provided by the Department of Communications, Climate Action & Environment of Ireland and TGS, were uploaded into Schlumberger's Petrel software for seismic interpretation along with the available well locations and well logs.

According to Nester & Padgett (1993), seismic interpretation is the science and art of inferring the geology (structure, stratigraphy, and lithology) from processed seismic data. Seismic interpretation may include seismic stratigraphy which is defined by Cross & Lessenger (1988) as "the science of interpreting or modelling stratigraphy, sedimentary facies, and geologic history from seismic reflection data" (p. 319). The four selected megatransects (EO-1, EO-2, PP-1, PP-2) were interpreted in two-way travel time (TWT), defining, describing, and mapping five seismo-stratigraphic units: Basement, Jurassic, Lower Cretaceous, Upper Cretaceous, and Cenozoic, for each basin. Additionally, the line GI-1 that crosses the Galicia Interior Basin was also interpreted. This chapter contains the explanation of how the seismic interpretation was carried out and what constraints were used for each seismo-stratigraphic unit.

3.1 Orphan Basin

Several wells have been drilled in the West and East Orphan basins since 1974 (Bonavista C-99). All of the wells were drilled either in structural highs or near the Bonavista shelf, leaving most of the area of both basins relatively unexplored. With the aim of integrating

the available well data (Figure 3.1), two well ties were integrated with the seismic response of each unit (Figures 3.2 and 3.3).

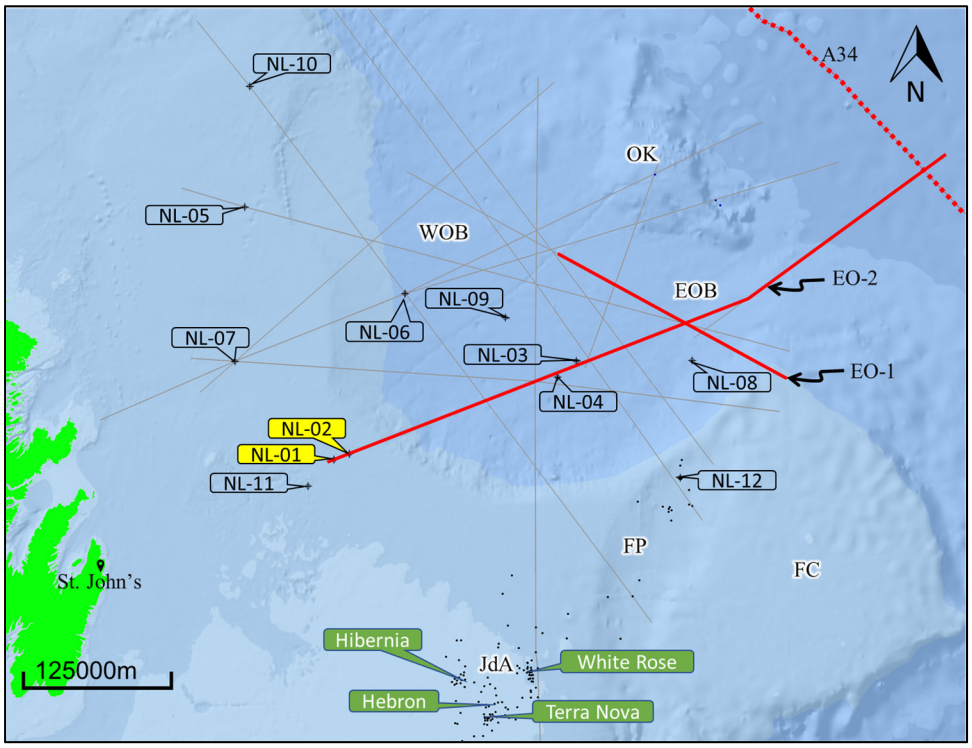

Figure 3.1 Location of wells and seismic lines on the Newfoundland margin. Yellow boxes: well location for which well ties were performed. Empty boxes: wells with not enough information to perform well ties. See Figure 2.1 for legend.

The limitation of this procedure is that there is a lack of penetration into the deeper intervals where different faulting, rifting, and erosional episodes increase the complexity and therefore the uncertainty of the seismic interpretation. Checkshot data from an additional well (NL-03), and the seismic interpretation published by Gouiza et al. (2017) were incorporated into the model of the basin to reduce the uncertainty of seismic interpretation.

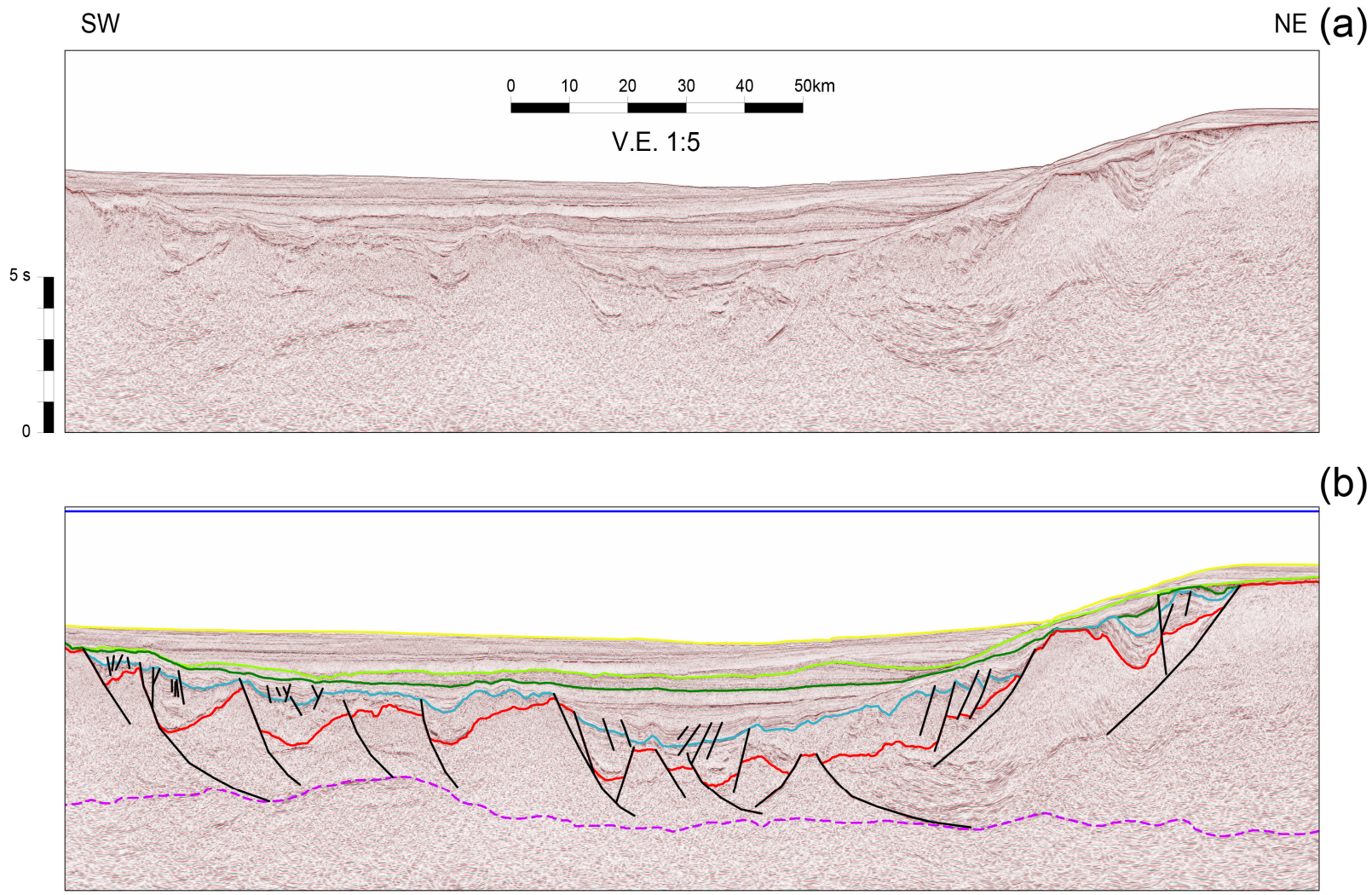

Figure 3.2 Seismic line EO-1 showing the different mapped events, (a) uninterpreted, (b) interpreted. Dark blue line: Mean sea level. Yellow line: sea bed. Light green line: Cenozoic Unconformity. Dark green line: Aptian Unconformity. Light blue line: Tithonian Unconformity. Red lines: basement. Purple line: Moho? (derived from Welford et al., 2012, and seismic interpretation). See Figure 2.1 for location.

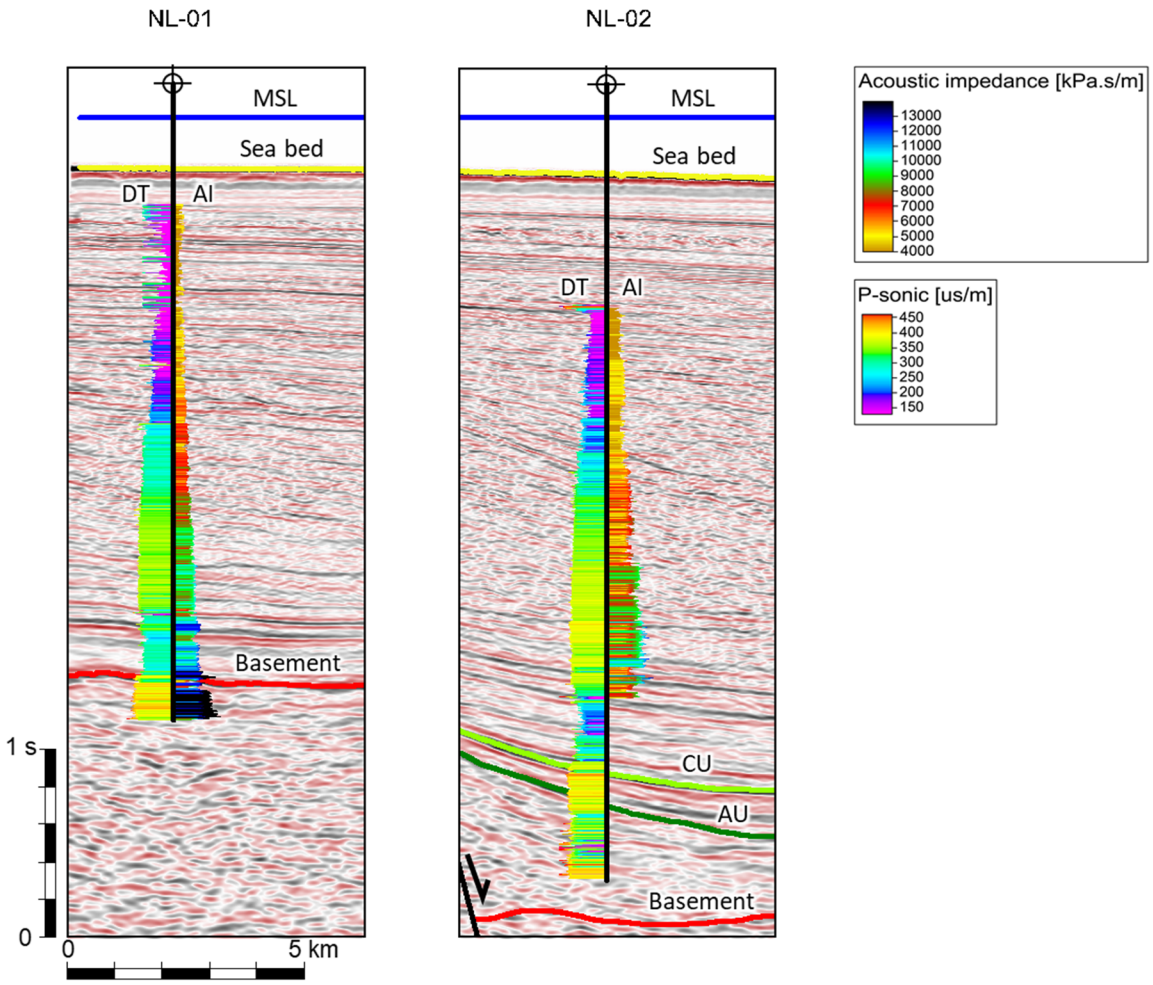

Figure 3.3 Seismic section through the wells used for interpretation in this thesis. DT: sonic log; AI: acoustic impedance log; CU: Cenozoic Unconformity; AU: Aptian Unconformity.

3.1.1 Seismo-stratigraphic units

Five seismo-stratigraphic units were identified:

3.1.1.1 Cenozoic

The Cenozoic Unit is delimited at the top by the seabed reflector and at the base by the top of the Upper Cretaceous unit (Cenozoic Unconformity, CU). It is characterised by a relatively continuous parallel to subparallel, sometimes wavy reflection configuration

(Figure 3.4). Some intervals showed a more hummocky to chaotic character that could be interpreted either as fluvial channelised sediments or as mass transport deposits (MTDs).

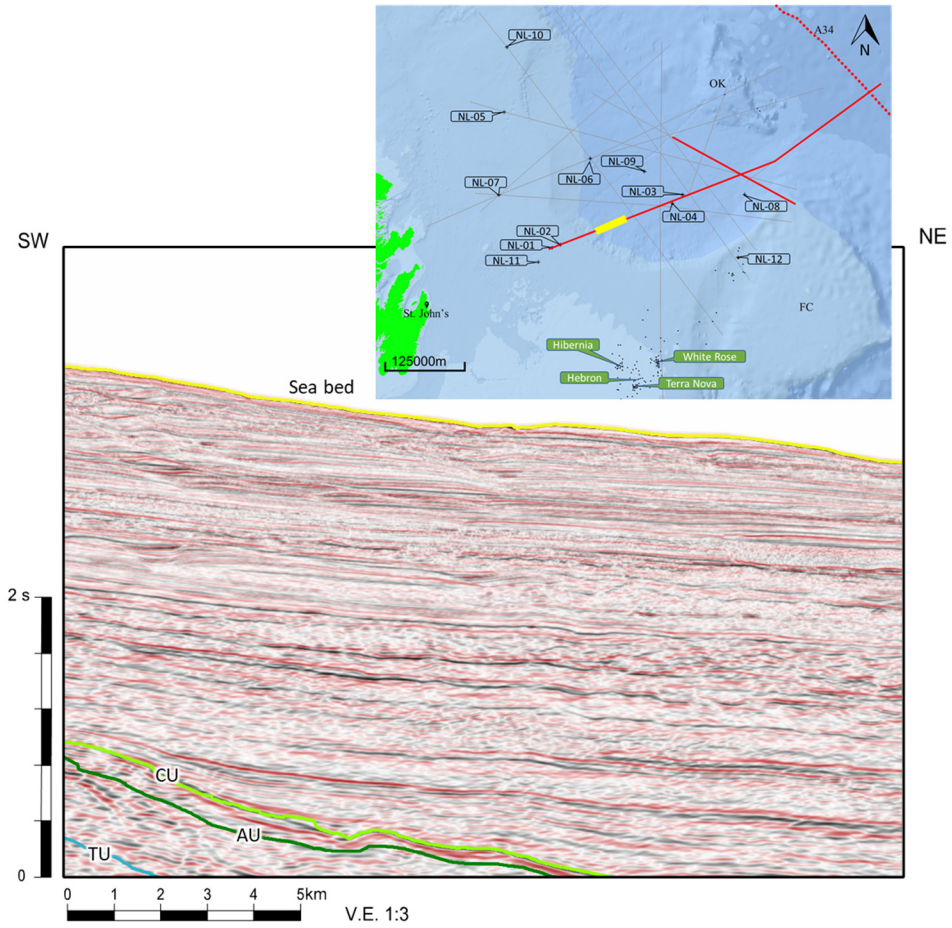

Figure 3.4 Seismic section over EO-2 showing the Cenozoic Unit. Yellow line on map: location of section. CU: Cenozoic Unconformity. AU: Aptian Unconformity. TU: Tithonian Unconformity.

The Cenozoic unit is thicker on the continental slope, gradually thinning towards the eastern part of the basin. This unit is represented by post-rift sediments deposited after cessation of rifting during the Lower Cretaceous. A number of subunits could be defined for a more detailed seismo-stratigraphic analysis. This unit is represented by sandstones and shales equivalent to the Banquereau Formation.

3.1.1.2 Upper Cretaceous

The Upper Cretaceous unit is delimited at the top by the Cenozoic Unconformity, a high amplitude positive reflection, and the Aptian Unconformity (AU) reflection horizon at its base. It exhibits a parallel to subparallel, sometimes discontinuous and wavy, reflection configuration (Figure 3.5). The Upper Cretaceous is a post-rift unit that represents the transition from the proper syn-rift deposition during the Lower Cretaceous into a thermal subsidence phase.

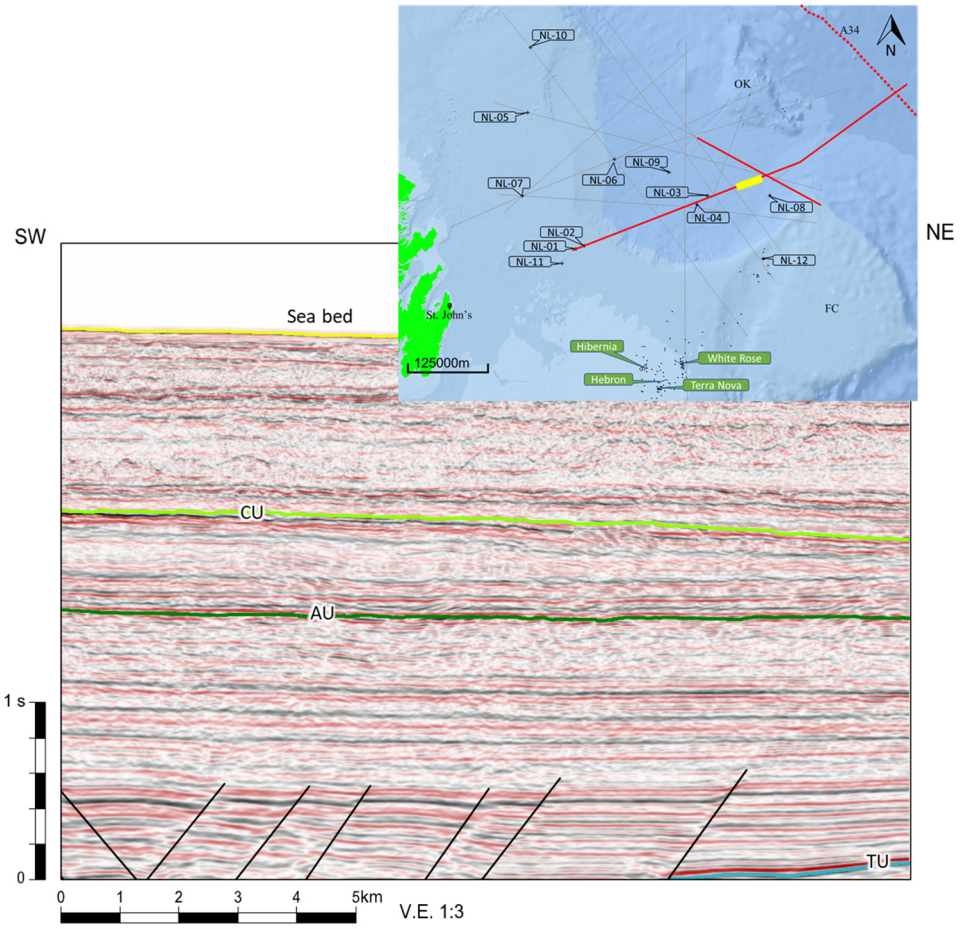

Figure 3.5 Seismic section over EO-2 showing the Upper Cretaceous Unit. Yellow line on map: location of section. CU: Cenozoic Unconformity. AU: Aptian Unconformity. TU: Tithonian Unconformity.

In terms of thickness, the Upper Cretaceous unit exhibits a thin section on the continental slope (near the Bonavista Platform), a thicker section on the central part of the East Orphan

Basin (towards the south of the Orphan Knoll), and a thinner section again towards the eastern-most portion of the East Orphan Basin. The rocks in this unit are represented by sandstones, shales, and carbonates equivalent to the Dawson Canyon Formation.

3.1.1.3 Lower Cretaceous

The top of the Lower Cretaceous unit is represented by the AU, a positive high amplitude reflection that marks a change in the seismic facies, and its base is marked by the Tithonian Unconformity (TU).

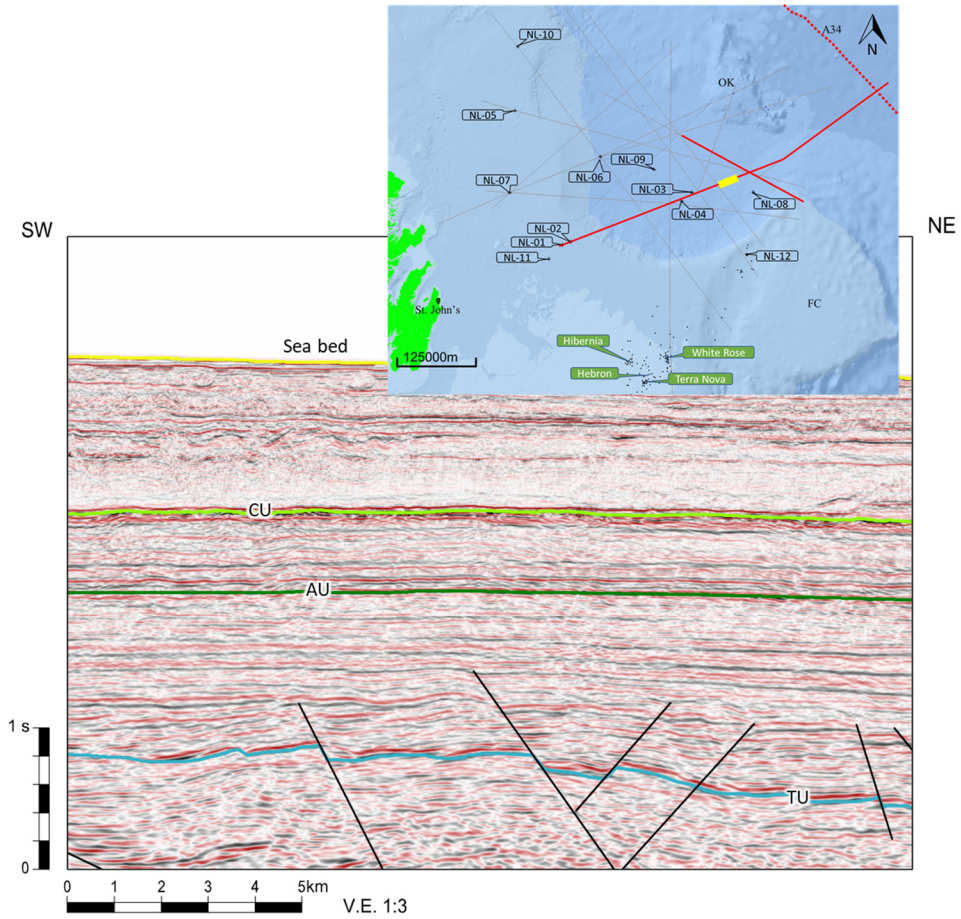

Figure 3.6 Seismic section over EO-2 showing the Lower Cretaceous Unit. Yellow line on map: location of section. CU: Cenozoic Unconformity. AU: Aptian Unconformity. TU: Tithonian Unconformity.

This syn-rift unit is characterised by a laterally continuous, parallel to subparallel, sometimes divergent, reflection character. The section just below the AU, however, exhibits a more wavy to chaotic character. The thickness of this unit varies across the basin with thicker and thinner sections over the local depocenters and basements highs, respectively. The thickest section is observed at the eastern end of the basin to the north of Flemish Cap. Some growth and normal faults are present along with localised inversion structures. This unit is represented by sandstones, shales, and carbonates equivalent to the Nautilus, White Rose, and Hibernia formations.

3.1.1.4 Jurassic

The top of the syn-rift Jurassic unit corresponds to the TU horizon whereas the top of the acoustic basement represents its base. Even though the reflection configuration is highly variable, two main seismic facies were defined. The first corresponds to a fairly continuous, parallel to subparallel wavy reflection configuration, with interleaved high amplitude events. The second dominant seismic facies, on the other hand, is composed of chaotic zones that sometimes show internal subparallel reflections (Figure 3.7). This syn-rift unit is present over the whole basin, except the western-most part of the basin, near the Bonavista platform where this unit seems to be absent. The thickest section of this unit is located in a depocentre in the eastern part of the basin, towards the north of Flemish Cap. The uncertainty in the interpretation of the unit is moderate to high due to limited well data located on structural highs, the potential structural complexity of this unit, and the lower seismic resolution with depth due to signal attenuation. A dense network of normal faults, rollovers, and conjugate faults are characteristic of this unit. This unit is interpreted to be

composed of sandstones, shales, carbonates, and evaporites equivalent to the Rankin, Voyager, Iroquois, and Argo formations.

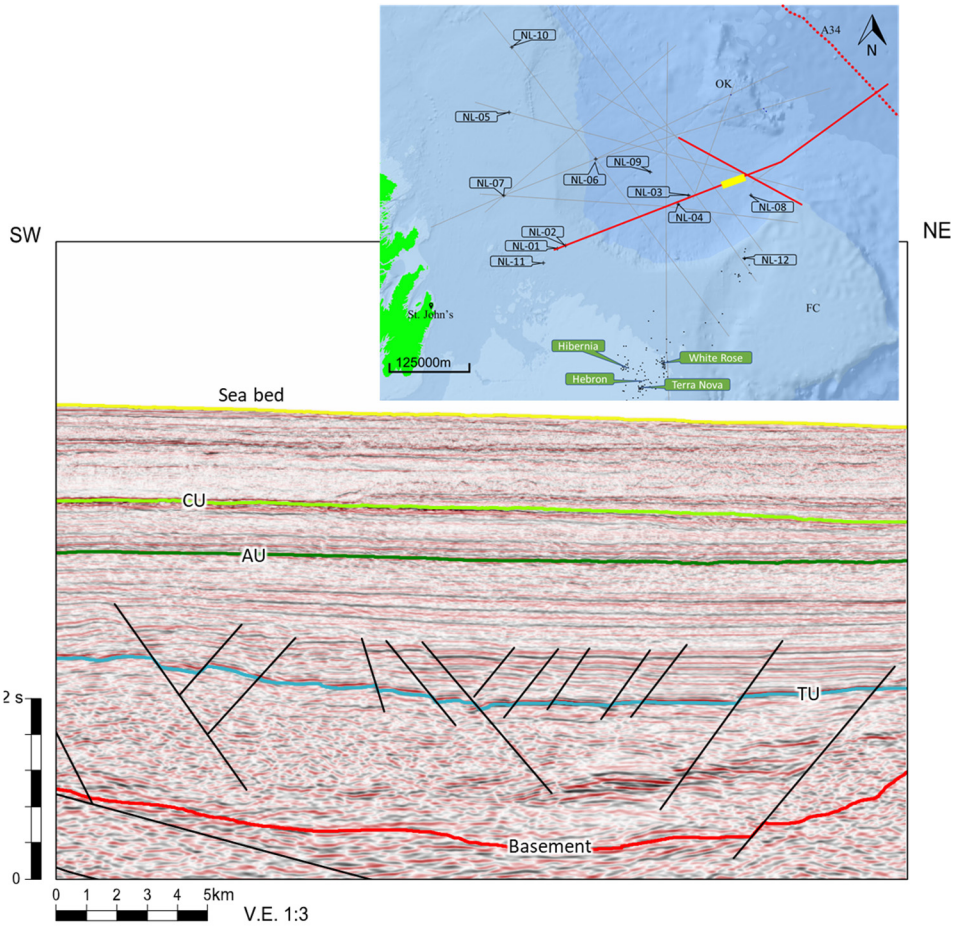

Figure 3.7 Seismic section over EO-2 showing the Jurassic Unit. Yellow line on map: location of section. CU: Cenozoic Unconformity. AU: Aptian Unconformity. TU: Tithonian Unconformity.

3.1.1.5 Basement

The Basement unit is characterised by a chaotic reflection configuration with virtually no primary reflections. Its imaging on seismic reflection profiles is highly affected by multiple reflections. It was affected by numerous normal faults that sole out at depth where some semi-coherent reflections appear (Figure 3.8). This band where the faults disappear and the reflection configuration changes is interpreted as the brittle-ductile transition from the

upper to lower crust. Normal and listric faults, detachments, tilted fault blocks, half grabens, and rotated blocks are present in this unit. This unit is interpreted to consist of Pre-Triassic/Paleozoic rocks.

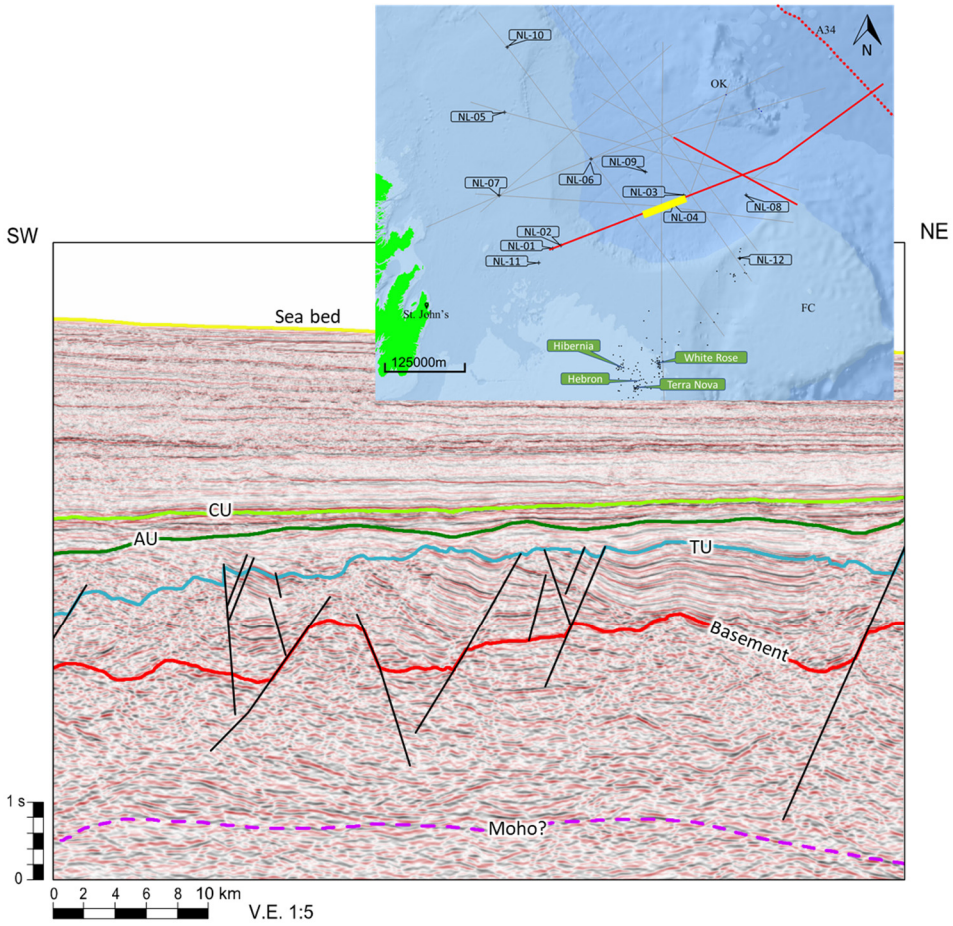

Figure 3.8 Seismic section EO-2 showing the Basement unit. Yellow line on map: location of section. CU: Cenozoic Unconformity. AU: Aptian Unconformity. TU: Tithonian Unconformity. Moho derived from Welford et al.(2012), and seismic interpretation.

3.2 Porcupine Basin

A number of wells have been drilled in the Porcupine and North Porcupine basins since the first well drilled in 1977 (35/13-1x). The majority of those wells have been drilled in the northern part of the basin in shallow to midwater depths (<500m), leaving most of the central and southern area of the Porcupine Basin virtually undrilled. For the identification

of the main seismo-stratigraphic units, and due to the lack of well data near the seismic lines in the study, a geoseismic section published by Naylor et al. (2002) was digitised and loaded into Petrel to be used as a guide during the seismic interpretation stage (Figure 3.9 and Figure 3.10). Similar to the interpretation of the Orphan lines (EO-1 and EO-2), the limitation of this procedure is the lack of penetration into the deeper intervals where different faulting, rifting, and erosional episodes increase the complexity and therefore the uncertainty of the seismic interpretation. More data (3D seismic volumes, more densely spaced seismic lines, sonic and density logs, checkshots, VPSs, etc.) would be required to reduce the uncertainty and better constrain the regional seismic interpretation presented in this thesis.

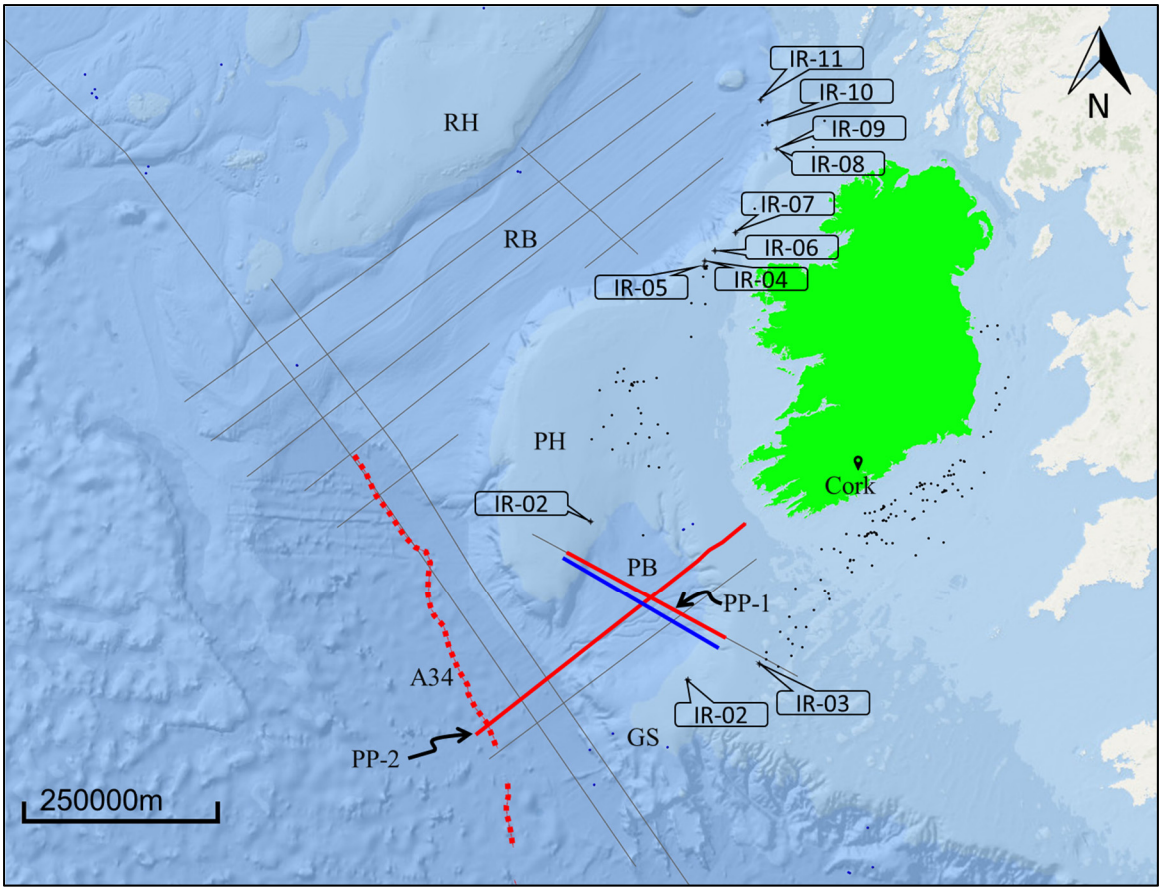

Figure 3.9 Location of wells and seismic lines on the Irish margin. Empty boxes: wells. Blue line: geoseismic section from Naylor et al. (2002). Red solid lines: seismic lines used in this thesis. See Figure 2.2 for legend.

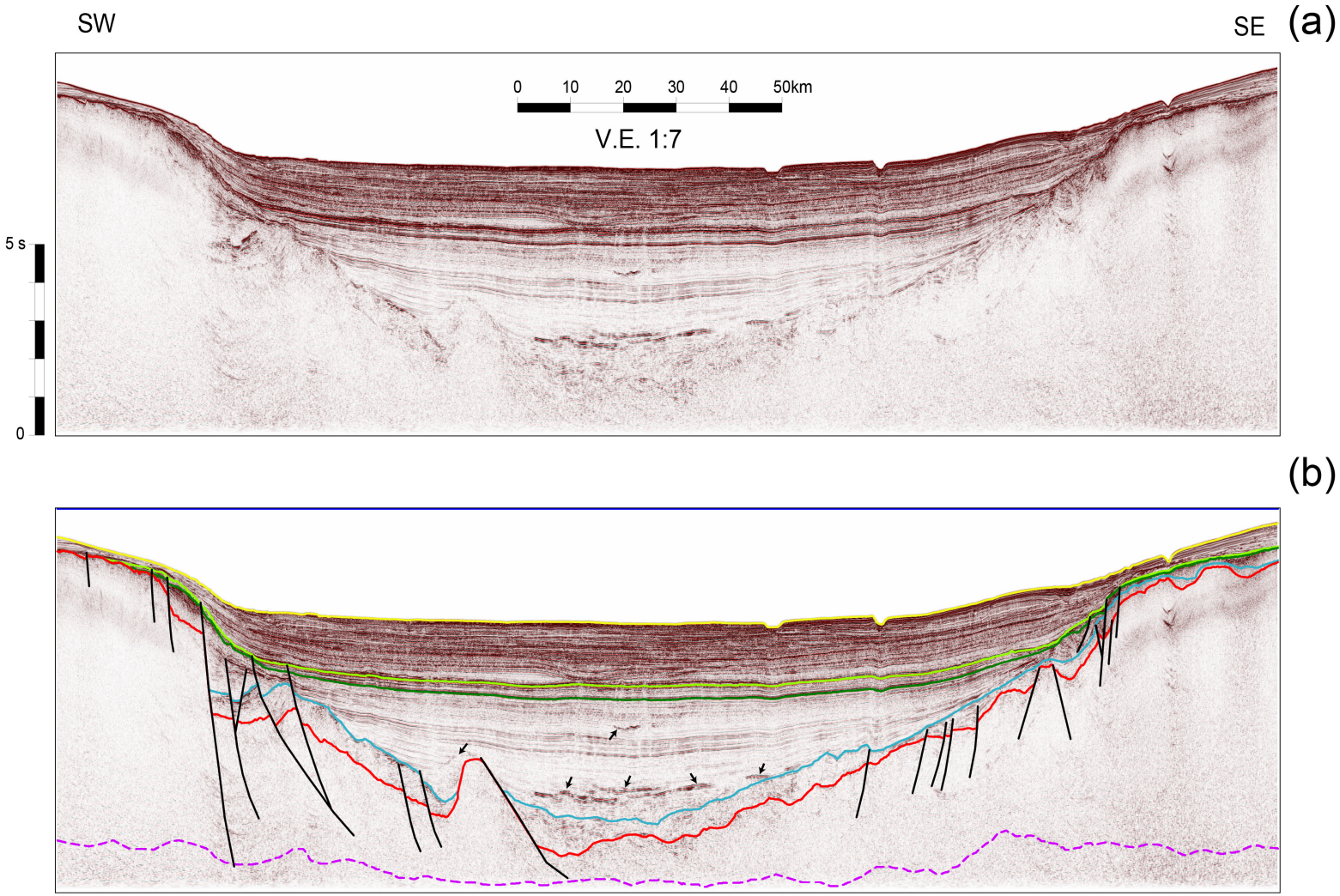

Figure 3.10 Seismic line PP-1 showing the different mapped events, (a) uninterpreted, (b) interpreted. Upper dark blue: Mean sea level. Yellow line: sea bed. Light green line: Base Cenozoic. Dark green line: Cenomanian Unconformity. Light blue line: Tithonian Unconformity. Red line: basement. Purple dashed line: Moho? (derived from Welford et al., 2012). Black arrows: volcanic intrusions. See Figure 2.2 for location.

3.2.1 Seismo-stratigraphic units

Five seismo-stratigraphic units were identified:

3.2.1.1 Cenozoic

The Cenozoic unit is delimited at the top by the seabed reflector that corresponds to the first strong peak (defined by an increase in acoustic impedance). The base is represented by the Base Cenozoic horizon (BC). This unit exhibits a variable reflection configuration going from subparallel, sometimes wavy, to chaotic (Figure 3.11).

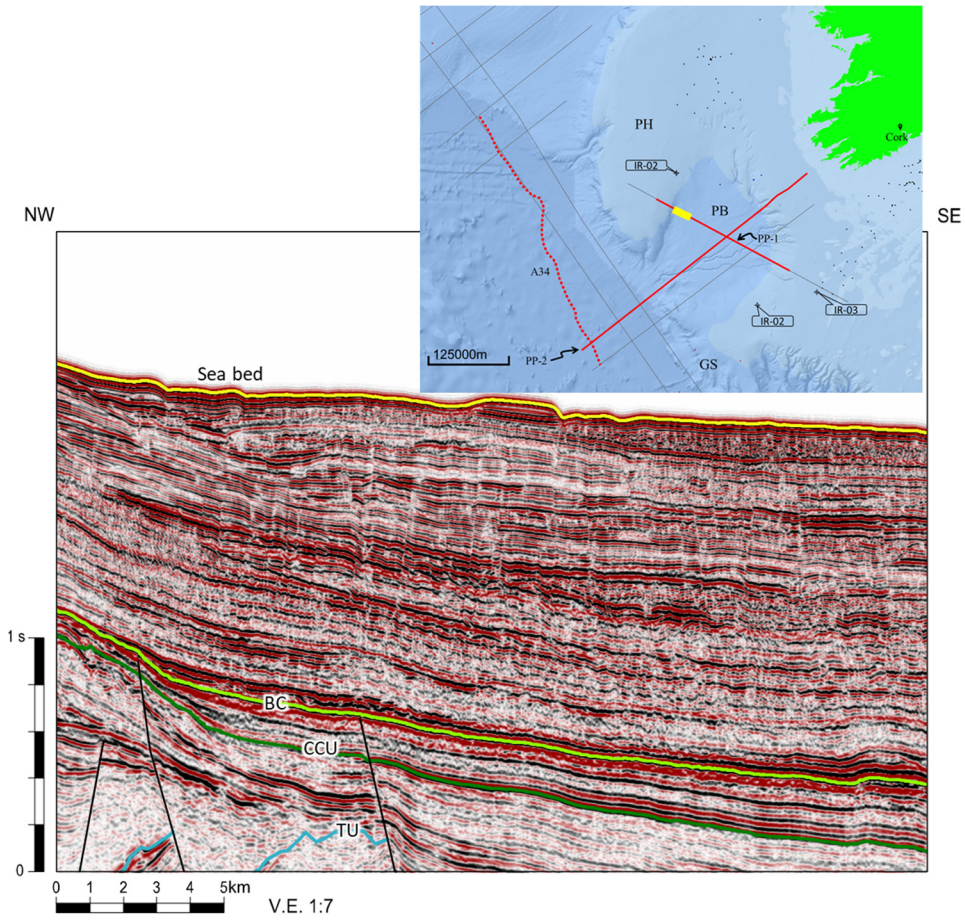

Figure 3.11 Seismic section PP-1 showing the Cenozoic unit. Yellow line on map: location of section. BC: Base Cenozoic. CCU: Cenomanian Unconformity. TU: Tithonian Unconformity.

The intervals with the chaotic character may be interpreted either as fluvial channelised sediments or as mass transport deposits (MTDs). The Cenozoic unit is thicker in the central part of the basin and gets thinner towards the flanks (near the Porcupine High and the Celtic Platform). This unit is composed of post-rift sediments. An apparent inversion structure is identified at the southern limit of the basin indicating that localised uplift occurred during this period. This unit is represented by sandstones, shales, and carbonates equivalent to the deposits found in the North Porcupine Basin.

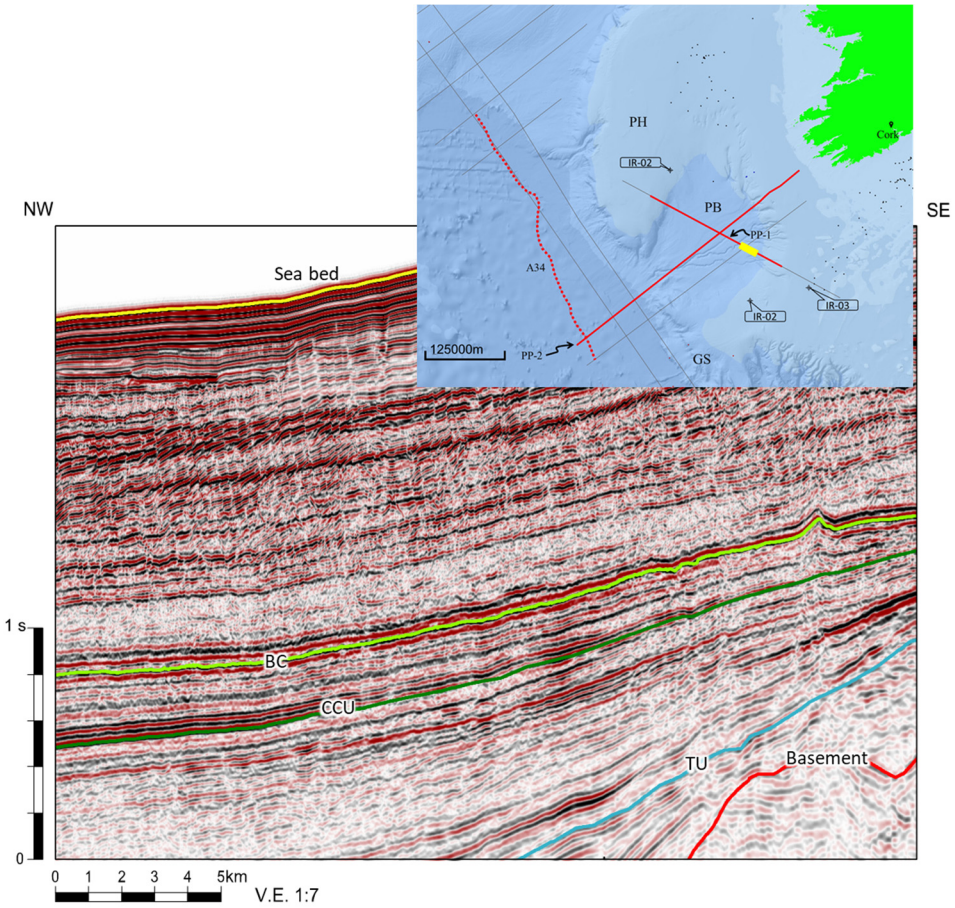

Figure 3.12 Seismic section PP-1 showing the Upper Cretaceous unit. Yellow line on map: location of section. BC: Base Cenozoic. CCU: Cenomanian Unconformity. TU: Tithonian Unconformity.

3.2.1.2 Upper Cretaceous

The top of this unit is represented by the BC that corresponds to a high amplitude positive reflection event. The base corresponds to the Cenomanian Unconformity (CCU). The reflection configuration is mostly parallel to subparallel and becomes chaotic towards the flanks of the basin (Figure 3.12). The Upper Cretaceous post-rift unit is represented by carbonates and sandstones equivalent to the deposits found in the North Porcupine Basin. The thickest section of the unit is located in the central part of the basin and gets thinner towards its flanks.

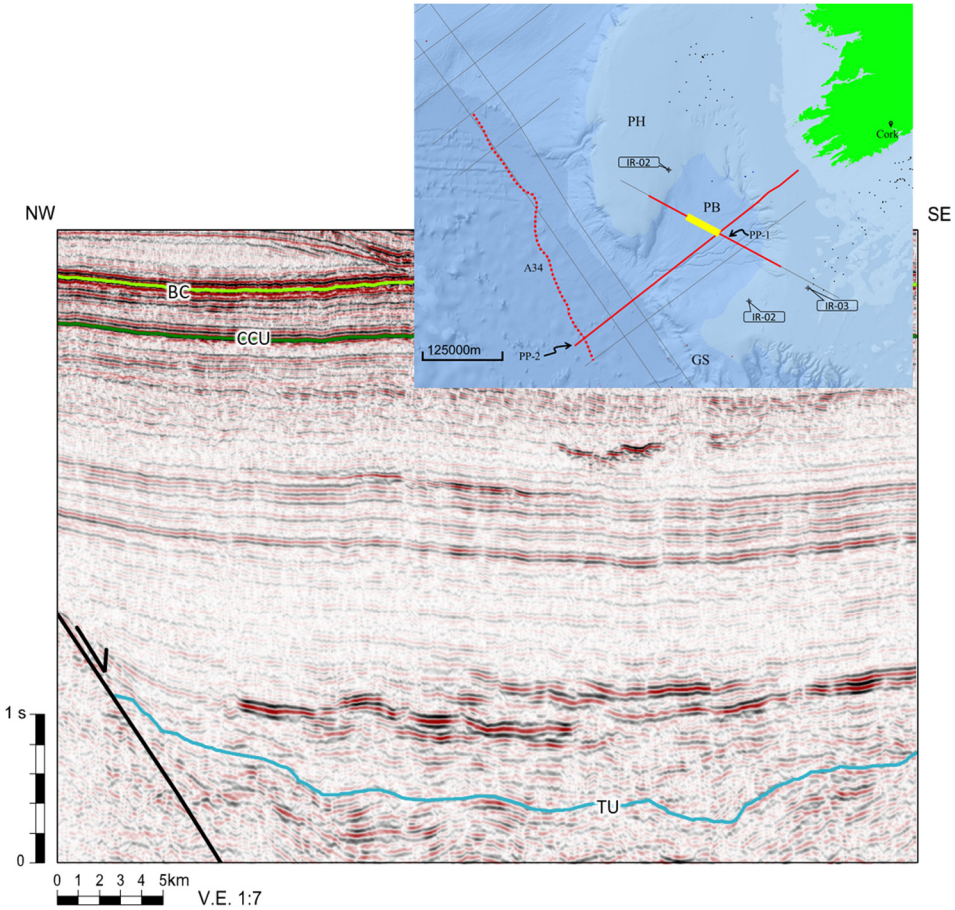

Figure 3.13 Seismic section PP-2 showing the Lower Cretaceous unit. Yellow line on map: location of section. BC: Base Cenozoic. CCU: Cenomanian Unconformity. TU: Tithonian Unconformity.

3.2.1.3 Lower Cretaceous

The top of the Lower Cretaceous unit corresponds to the CCU, a positive high amplitude reflection. The base, on the other hand, is represented by the Tithonian Unconformity (TU). This syn-rift unit is characterised by a variable to wavy subparallel reflection configuration that becomes chaotic on both flanks of the basin (Figure 3.13). Relatively continuous high amplitude reflections stand out in the center of the basin and are interpreted as volcanic intrusions (sills, dykes, or lava flows). This unit is, on average, the thickest compared to the rest of the units. It shows a well-defined depocentre where the thickest section is present. Some growth and normal faults along with localised inversion structures are found in this interval. Sandstones, shales, carbonates, and volcanic rocks make up this unit.

3.2.1.4 Jurassic

The top limit of the Jurassic unit is the TU (a variable amplitude positive reflection) and the top of acoustic basement represents its base. This Jurassic unit is characterised by chaotic reflections with a more subparallel and divergent response on the flanks of the basin (Figure 3.14). The thickest section of this unit is located in the central part of the basin, coinciding with the location of the thickest sections of the rest of the units. The uncertainty associated with the interpretation of this unit is considerably higher than for the other units due to the low quality of the seismic data at this depth and to the fact that seismic quality decreases even more beneath the volcanic intrusions. Normal and growth faults, conjugate faults, and rollovers are common in this unit. The Jurassic unit is interpreted to be composed of sandstones, carbonates and shales.

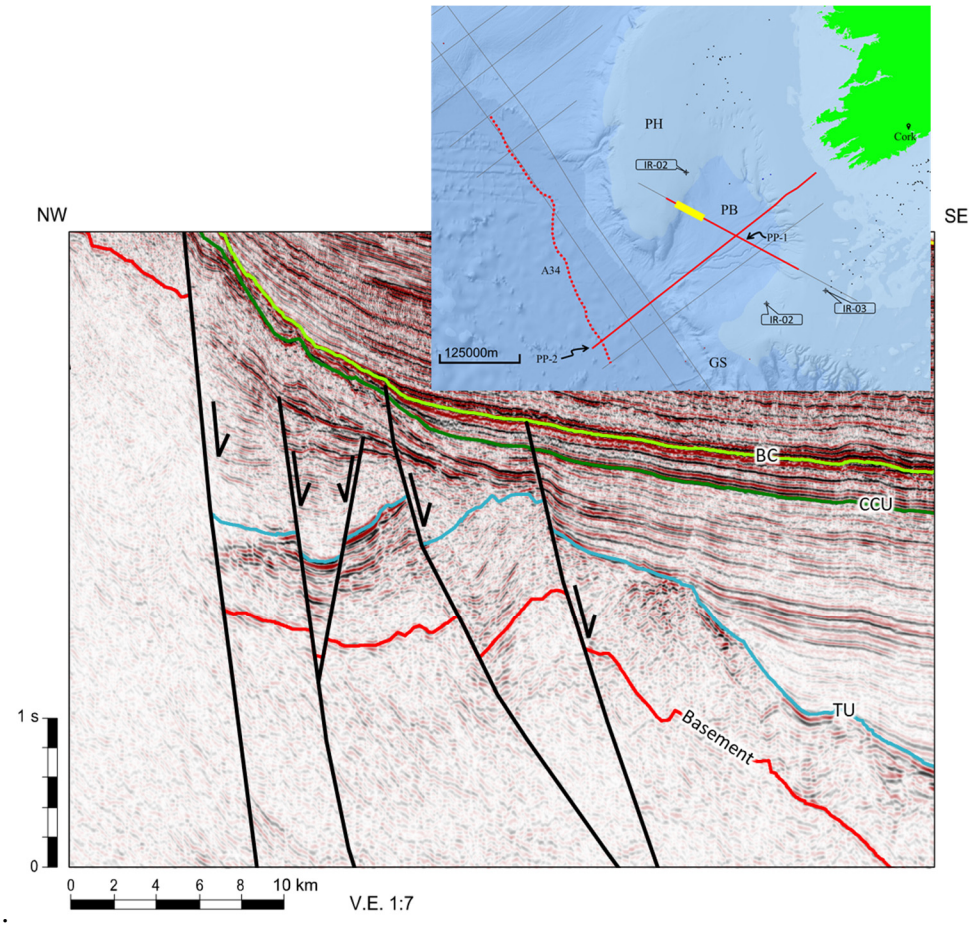

Figure 3.14 Seismic section PP-1 showing the Jurassic unit. Yellow line on map: location of section. BC: Base Cenozoic. CCU: Cenomanian Unconformity. TU: Tithonian Unconformity.

3.2.1.5 Basement

The limit of coherent reflections defines the top of this unit. It is characterised by a chaotic reflection configuration and the presence of seismic reflection multiples. The quality of the seismic image is even lower than for the Jurassic unit. Numerous normal and listric faults, tilted fault blocks, and half-grabens are interpreted to be present within this unit (Figure 3.15). Some of the listric faults sole out at the Moho level. This unit is interpreted to consist of Triassic/Paleozoic rocks.

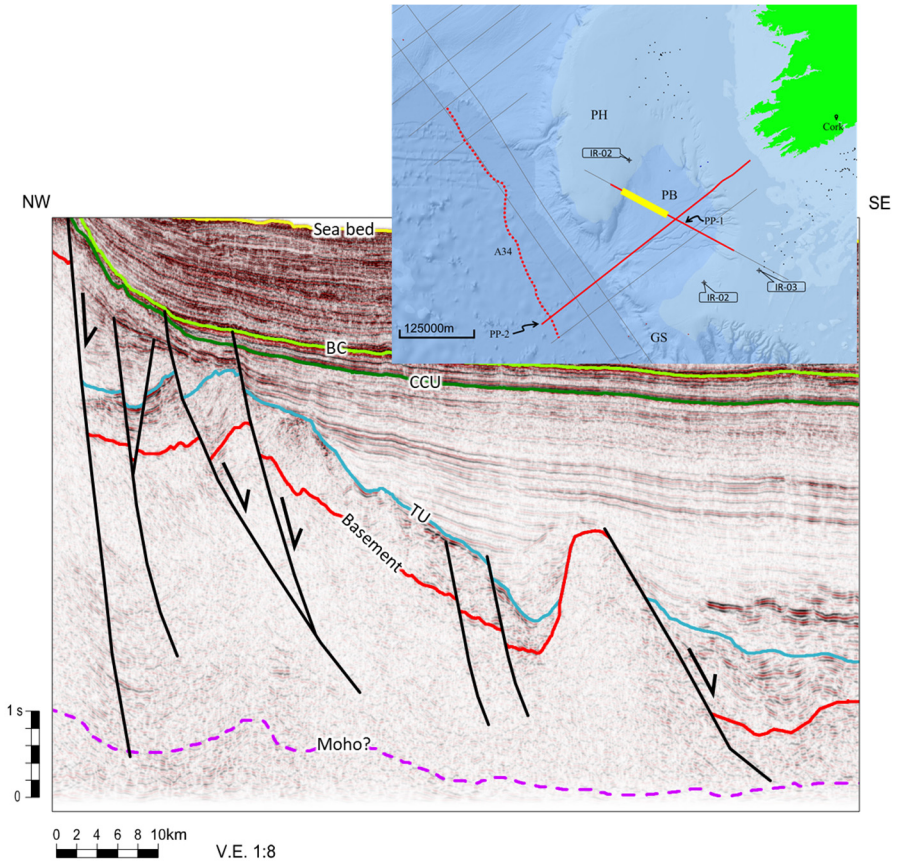

Figure 3.15 Seismic section PP-1 showing the Basement unit. Yellow line on map: location of section. BC: Base Cenozoic. CCU: Cenomanian Unconformity. TU: Tithonian Unconformity. Moho derived from Welford et al. (2012).

3.3 Galicia Interior Basin

No publicly available well data in the Galicia Interior Basin were found. Nevertheless, a number of industry and ODP wells have been drilled in the Porto Basin and the Galicia margin. Due to the lack of available well data close to the seismic line GI-1, the identification of the main seismo-stratigraphic units is based on the work published by Murillas et al. (1990) and Pérez-Gussinyé et al. (2003). Moreover, the seismic section published by Pérez-Gussinyé et al. (2003) was digitised and loaded into Petrel to be used as a guide during the seismic interpretation stage (Figures 3.16 and 3.17). The limitation of this process is the lack

of penetration within the Galicia Interior Basin and the reduction of the seismic quality with depth.

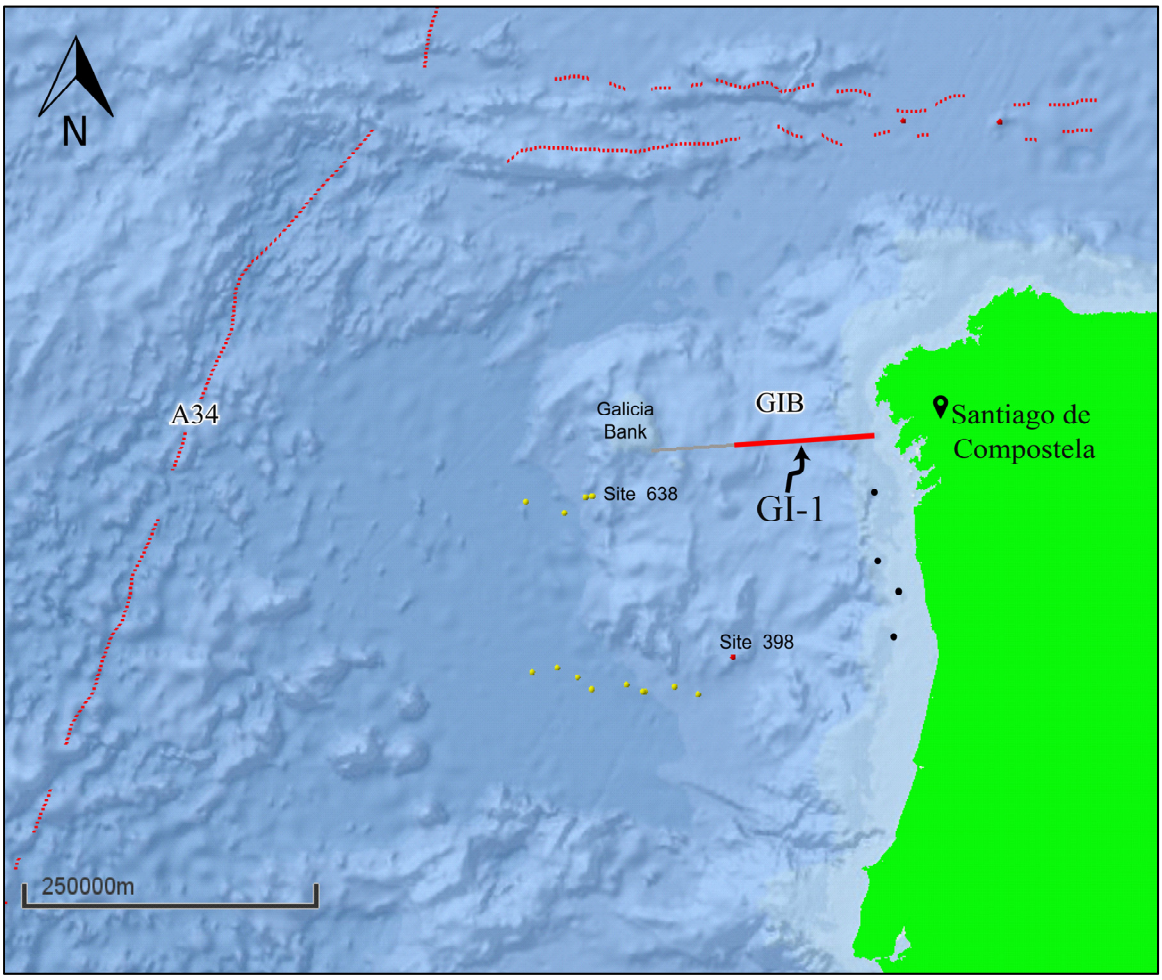

Figure 3.16 Location of wells and seismic line on the Galicia margin. Red solid line: seismic line used in this thesis. See Figure 2.3 for legend.

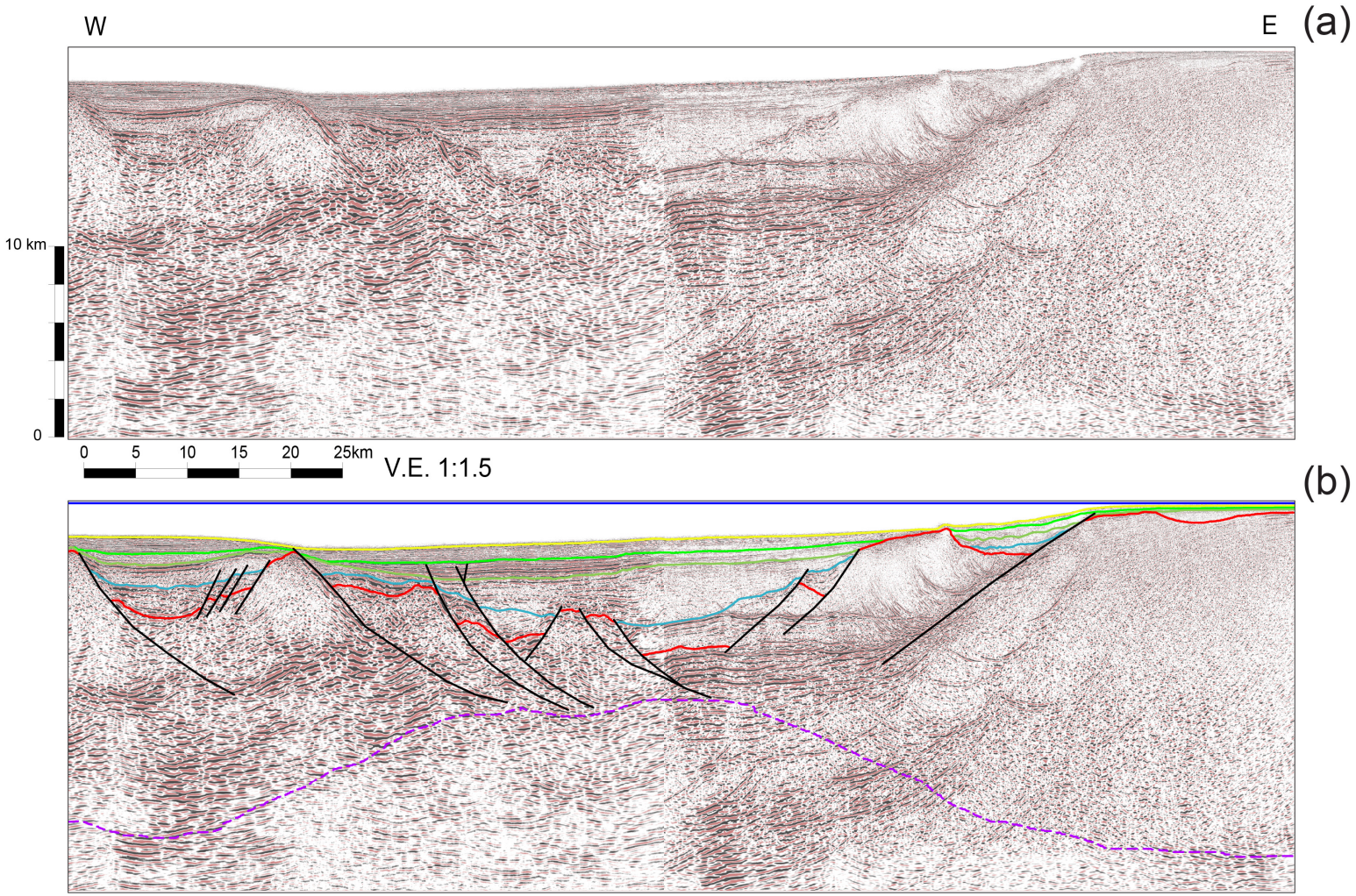

Figure 3.17 Seismic line GI-1 showing the different mapped events, (a) uninterpreted, (b) interpreted. Dark blue line: Mean sea level. Yellow line: seabed. Light green line: Cenozoic Unconformity. Dark green line: Cenomanian Unconformity. Light blue line: Tithonian Unconformity. Red line: basement. Purple dashed line: Moho? (derived from Pérez-Gussinyé et al., 2003). See Figure 2.3 for location.

3.3.1 Seismo-stratigraphic units

Despite the limitations of the seismic quality, five seismo-stratigraphic units were identified:

3.3.1.1 Cenozoic

The Cenozoic unit is delimited at its top by an increase in acoustic impedance (the first strong peak) that represents the seabed. Its base is the top of the Upper Cretaceous unit (Cenozoic Unconformity, CU). The unit is characterised by a variable reflection configuration going from subparallel, sometimes wavy, to chaotic (Figure 3.18). The chaotic character may correspond to MTDs or fluvial channelised sediments. The thickness of this post-rift unit is relatively uniform along the line but gets thinner towards Iberia. An inversion structure is identified at the western end of the seismic line, indicating that localised uplift occurred during the Cenozoic period. It is interpreted that this unit is represented by sandstones, shales, and carbonates similar to the ones described by the Groupe Galice (1979) and Mena et al. (2018).

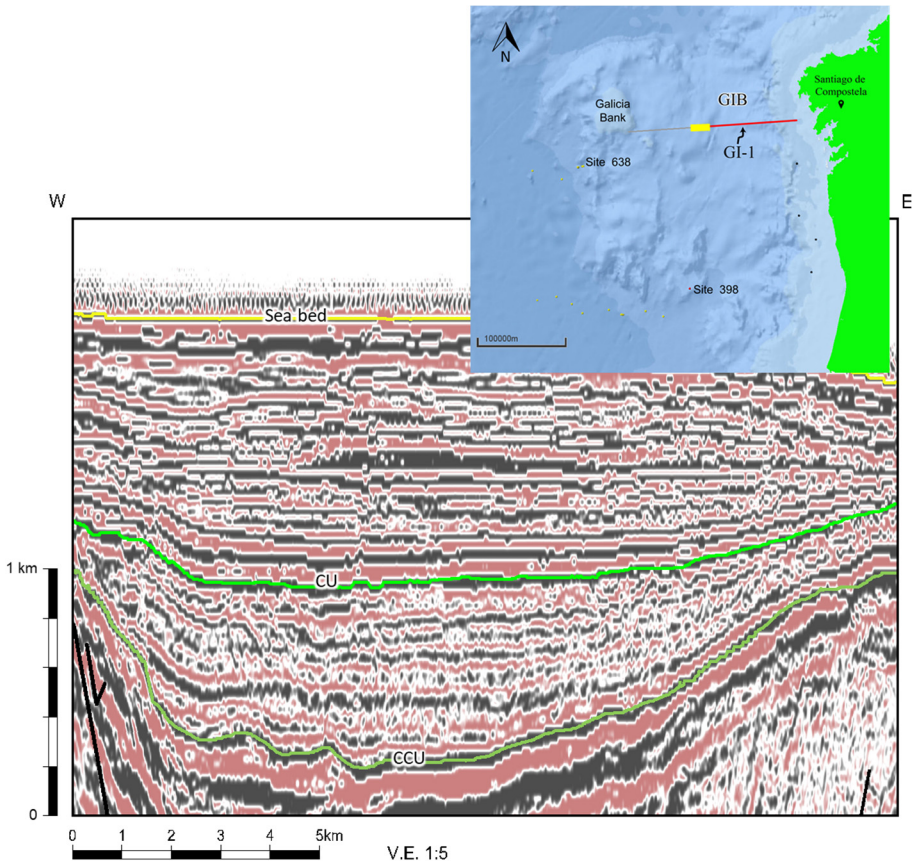

Figure 3.18 Seismic section over GI-1 showing the Cenozoic Unit. Yellow line on map: location of section. CU: Cenozoic Unconformity. CCU: Cenomanian Unconformity.

3.3.1.2 Upper Cretaceous

This unit is delimited at the top by the CU that corresponds to a positive high amplitude reflection, and at its base by the Cenomanian Unconformity (CCU). It exhibits a parallel to subparallel, sometimes discontinuous and wavy, reflection configuration that becomes chaotic towards Iberia (Figure 3.19). This post-rift unit is represented by sandstones, carbonates, and shales possibly similar to the ones found at DSDP Site 398 (Sibuet et al., 1979).

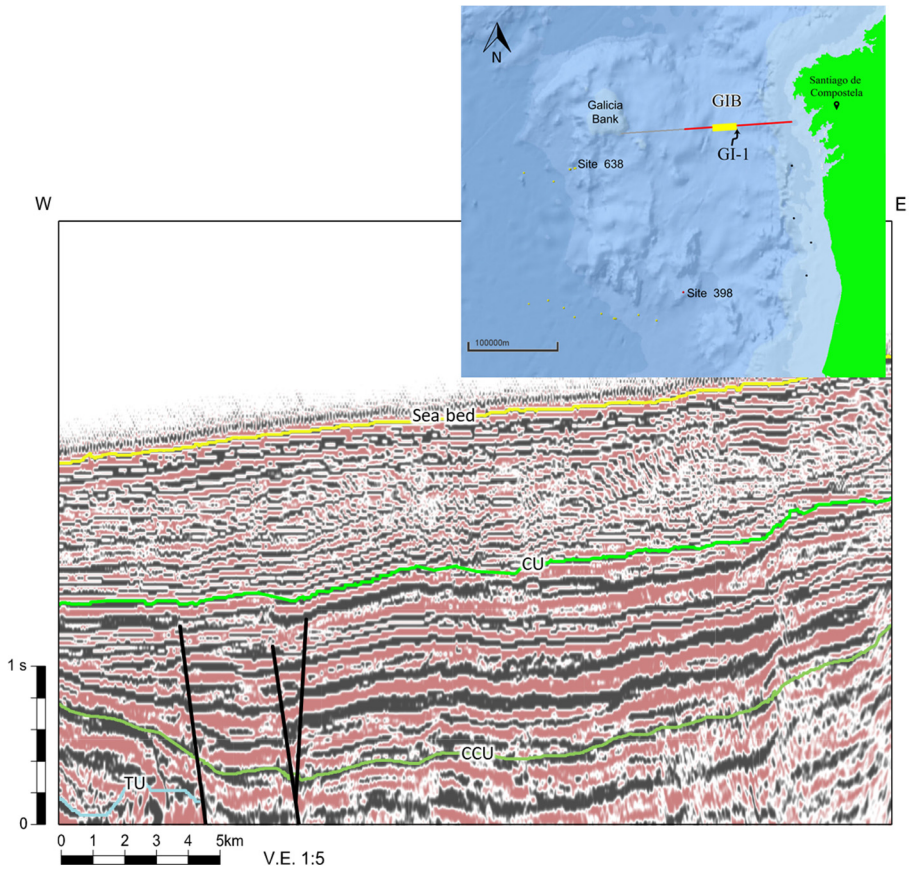

Figure 3.19 Seismic section over GI-1 showing the Upper Cretaceous Unit. Yellow line on map: location of section. CU: Cenozoic Unconformity. CCU: Cenomanian Unconformity. TU: Tithonian Unconformity.

3.3.1.3 Lower Cretaceous

The CCU, a positive high amplitude reflection, represents the top of the Lower Cretaceous unit and the Tithonian Unconformity (TU) is its base. This syn-rift unit exhibits a highly variable to wavy subparallel, sometimes divergent, reflection configuration that becomes chaotic towards the flanks of the basin (Figure 3.20). On average, this unit is the thickest compared to the rest of the units. Some growth faults are present along with an apparent inversion structure that coincides with the main depocentre of the basin during this period. This unit is composed of sandstones and claystones, similar to the ones found at ODP Site 638 (Boillot et al., 1987).

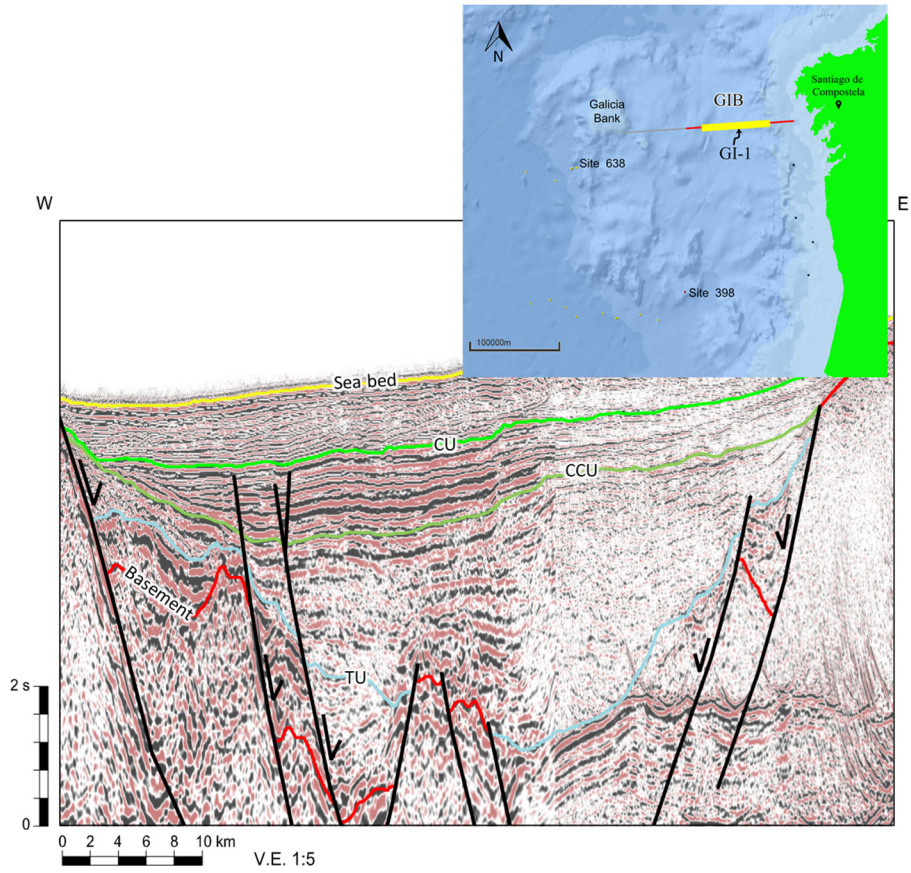

Figure 3.20 Seismic section over GI-1 showing the Lower Cretaceous Unit. Yellow line on map: location of section. CU: Cenozoic Unconformity. CCU: Cenomanian Unconformity. TU: Tithonian Unconformity.

3.3.1.4 Jurassic

The top of the syn-rift Jurassic unit corresponds to a variable amplitude positive reflection and its base corresponds to the top of the acoustic basement. The reflection configuration of this unit is variable and sometimes obscured by multiples. Nevertheless, in general terms, the unit exhibits a chaotic to divergent reflection configuration (Figure 3.21). The main depocentre of this unit is located in the central part of the basin, approximately coinciding with the depocentre of the Lower Cretaceous unit. Normal, growth, and conjugate faults are common in this unit. The uncertainty in the interpretation of this unit is substantially higher than the other units due to the low seismic quality at this depth and the many

multiples that mask the seismic events. This unit is interpreted to consist of sandstones, shales, and carbonates (Boillot et al., 1988).

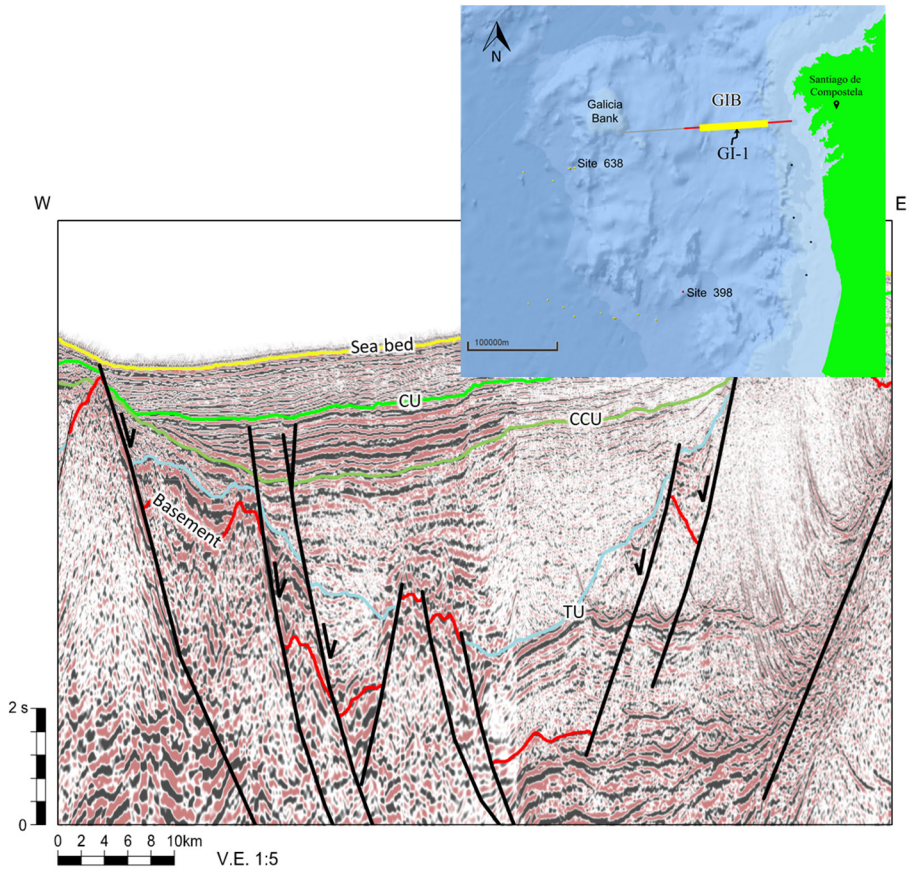

Figure 3.21 Seismic section over GI-1 showing the Jurassic Unit. Yellow line on map: location of section. CU: Cenozoic Unconformity. CCU: Cenomanian Unconformity. TU: Tithonian Unconformity.

3.3.1.5 Basement

This unit is characterised by a chaotic reflection configuration and numerous multiples. The seismic image is negatively affected at this depth by the multiple faults affecting the basement and the overlying units. Normal and listric faults, tilted faults blocks, and half-grabens are identified in this unit (Figure 3.22). Faults soling out at the Moho level are common. Triassic/Paleozoic rocks are interpreted to be represented by this unit.

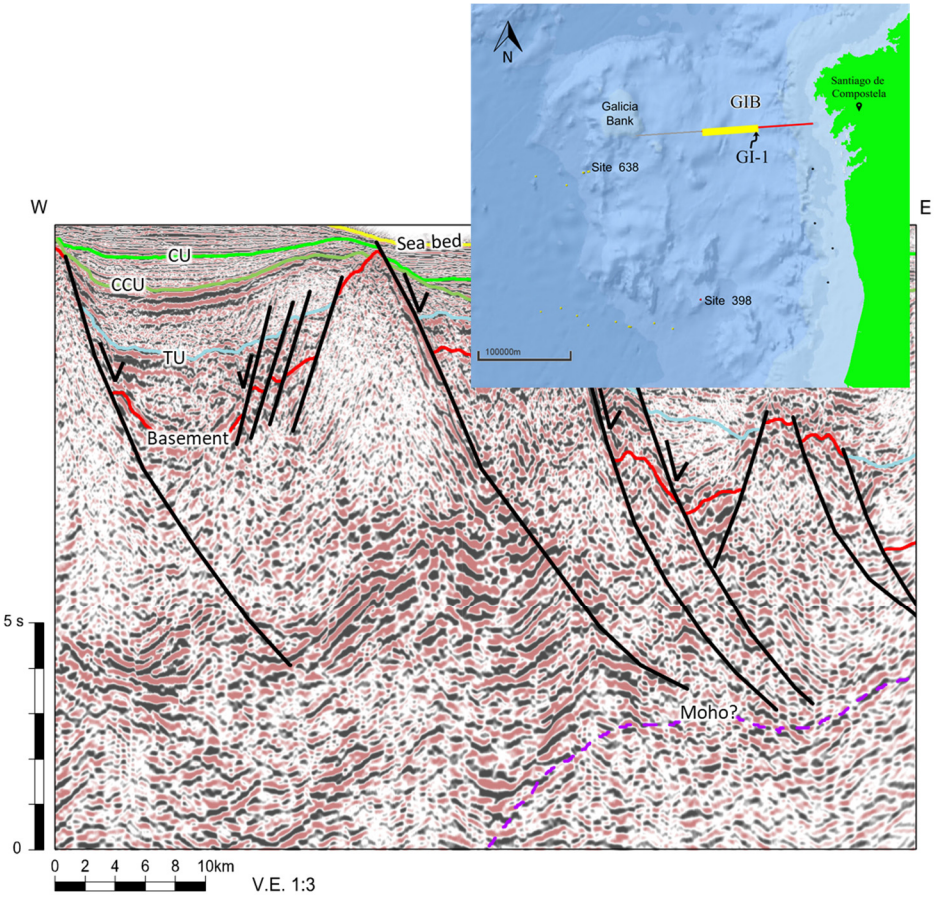

Figure 3.22 Seismic section over GI-1 showing the Basement Unit. Yellow line on map: location of section. CU: Cenozoic Unconformity. CCU: Cenomanian Unconformity. TU: Tithonian Unconformity. Moho derived from Pérez-Gussinyé et al. (2003).

3.4 Interpretation summary

Interpretation of seismo-stratigraphic units across the East Orphan, Porcupine, and Galicia Interior basins shows general similarities in terms of the seismic character, with potential MTDs interpreted in the Cenozoic unit, a relatively thin Upper Cretaceous unit, a thick Lower Cretaceous unit, and a complex syn-rift unit, dominated by Jurassic sediments. The faulting style is similar within the three basins, nevertheless, a denser fault network is interpreted in the East Orphan Basin. Inversion structures and rollovers are present in all of the basins.

In the next chapter, the restoration of the interpreted horizons will be detailed to provide insights about the evolution and crustal structure of the basins through time.

CHAPTER 4. STRUCTURAL RESTORATION

Before starting the structural restoration, the selected seismic lines were depth-converted using the average interval velocities obtained from the stacking velocities of the Orphan lines. The same average velocities were used to depth-convert the Porcupine Basin lines since the average interval velocities agree with the velocities previously modelled by Readman et al. (2005) and O'Reilly et al. (2006).

Using the depth-converted data obtained from the seismic interpretation (Figure 4.1), the selected seismic lines are restored, taking into account thermal subsidence, the main folds and faults, and sediment compaction of each layer. This restoration process begins with the removal of the water layer followed by the removal of the effects of thermal subsidence, folding, faulting, and compaction, as required, for each specific unit until the last remaining interval corresponds to the Basement; in other words, the section is restored to its approximate original pre-rift configuration.

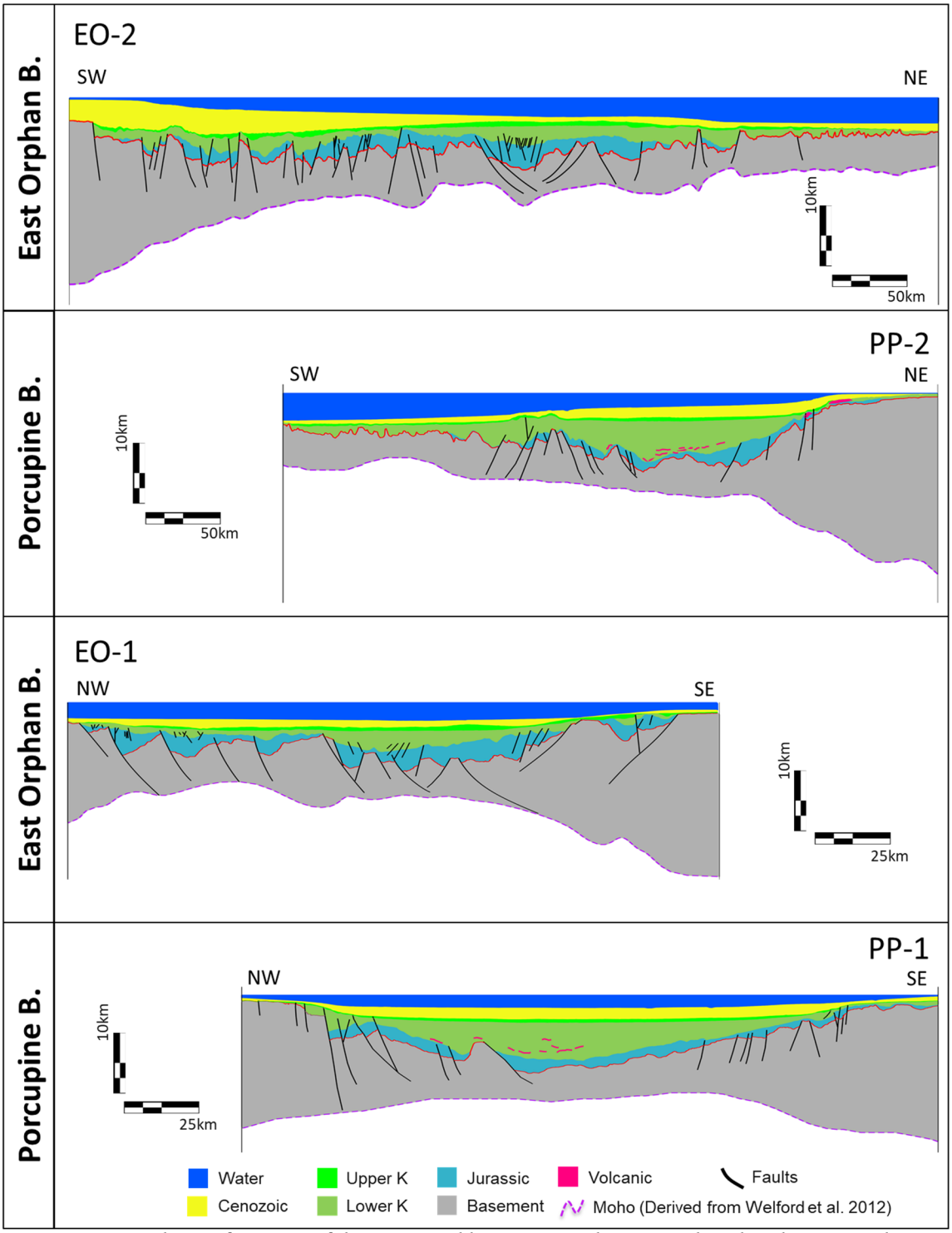

Figure 4.1 Present day configuration of the interpreted lines, EO-2 and PP-2 are plotted at the same scales, EO-1 and PP-1 are plotted at the same scales. See Figures 3.1 and 3.9 for line locations.

4.1 Cenozoic

4.1.1 Decompaction

The first step in the restoration process is decompacting the Cenozoic unit by removing the water layer. To compensate for the loss of volume due to burial depth for the East Orphan and Porcupine basins, the 2D Decompaction workflow in Move™ was applied. This workflow allows for the removal of the overlying units, correcting the porosity loss of the lower units by using the porosity-depth function (Equation 2.4) proposed by Sclater & Christie (1980). These functions are based on the type of lithology present in each layer. The lithological composition used for each unit is shown in Table 4.1.

Table 4.1 Generic lithological composition of each seismo-stratigraphic unit

	Sandstone (%)	**Shale (%)**	**Limestone (%)**	**Porosity at the surface**	**Depth Coefficient**	**Compaction Curve**
Water	0	0	0	1	NA	NA
Cenozoic	0	80	20	0.59	0.49	Sclater-Christie
U. Cretaceous	80	10	10	0.50	0.31	Sclater-Christie
L. Cretaceous	20	80	0	0.60	0.46	Sclater-Christie
Jurassic	60	30	10	0.52	0.36	Sclater-Christie
Basement	NA	NA	NA	0.10	0.55	Sclater-Christie

The decompaction workflow also takes into account the isostatic response for the unloading of sediments. Airy isostasy was used for both the East Orphan and Porcupine basins.

After removing the water layer, the Cenozoic unit experienced an increase in thickness (~430 m on average). The Cenozoic unit showed greater thickening in areas with a thicker

water column, as is expected since a higher water column means greater pressure affecting the Cenozoic sedimentary layer (Figure 4.2).

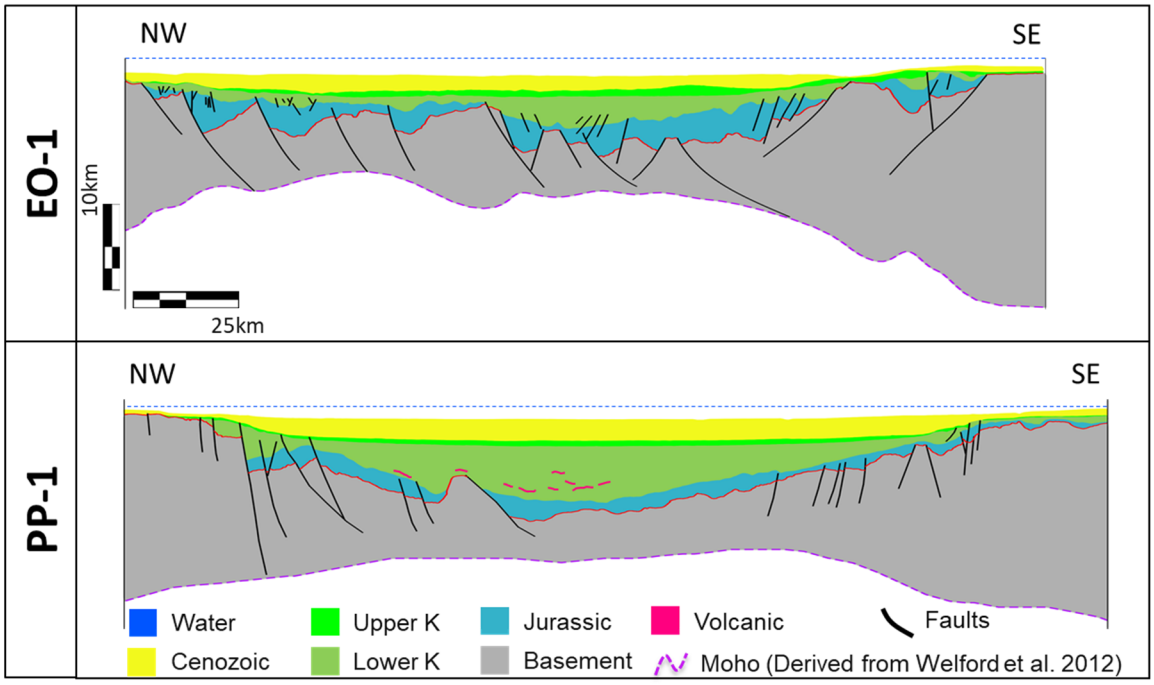

Figure 4.2 Sections showing the decompaction of the Cenozoic unit from removal of the water layer. Both sections are plotted at the same scales. See Figures 3.1 and 3.9 for line locations.

4.1.2 Thermal subsidence

The Cenozoic unit is interpreted as a post-rift unit meaning that the thermal subsidence effects must be removed following decompaction. The thickness of the unstretched continental crust is usually 25–30 km thick and is interpreted as relatively unstretched continental crust (Morewood et al., 2005; Shannon et al., 1999; Welford et al., 2012). Therefore, 30 km is used as the initial thickness of the crust and 125 km as the initial thickness of the lithosphere. The parameters used to remove the effects of thermal subsidence are shown in Table 4.2 and Table 4.3. The Triassic rifting episode was not included since no Triassic sediments were interpreted within either basin. The same

parameters and rifting events were used for both basins. In this thesis, rather than using a simple constant stretching factor, β, for each line, a variable β from Welford et al. (2012) (Figure 4.3) was used to capture the highly variable stretching along both the East Orphan and Porcupine megatransects.

Table 4.2 Parameters used to estimate thermal subsidence.

Thickness of lithosphere	125000m	Morewood et al., 2005 Shannon et al., 1999 Welford et al., 2012
Initial thickness of continental crust	30000m	
Mantle density	3300 $^{kg}/_{m^3}$	Gouiza et al., 2015 McKenzie, 1978
Continental density	2800 $^{kg}/_{m^3}$	
Sediment density	2500 $^{kg}/_{m^3}$	
Seawater density	1020 $^{kg}/_{m^3}$	
Thermal expansion coeff. of the mantle and crust	0.000034 $^{1}/_{°C}$	
Temperature of the asthenosphere	1333.0 °C	
Thermal conductivity	1.95 $^{W}/_{(m \cdot K)}$	
Specific heat capacity	0.234 $^{kcal}/_{(kg \cdot K)}$	
Thermal diffusivity	0.0000008 $^{m^2}/_{s}$	
Lithosphere thermal time constant (Tau)	63 Ma	
Extension factor of the lithosphere (β)	Variable	Welford et al., 2012

Table 4.3 Rifting episodes for the East Orphan and Porcupine basins used to estimate thermal subsidence (based on Gouiza et al., 2017; Shannon et al., 2007; Shannon & Naylor, 1998; Sibuet et al., 2007; Skogseid et al., 2004).

	Rifting Age (Ma)	**Duration (Ma)**
Lower Cretaceous (K)	125	24.5
Upper Jurassic (J)	163.5	18.5

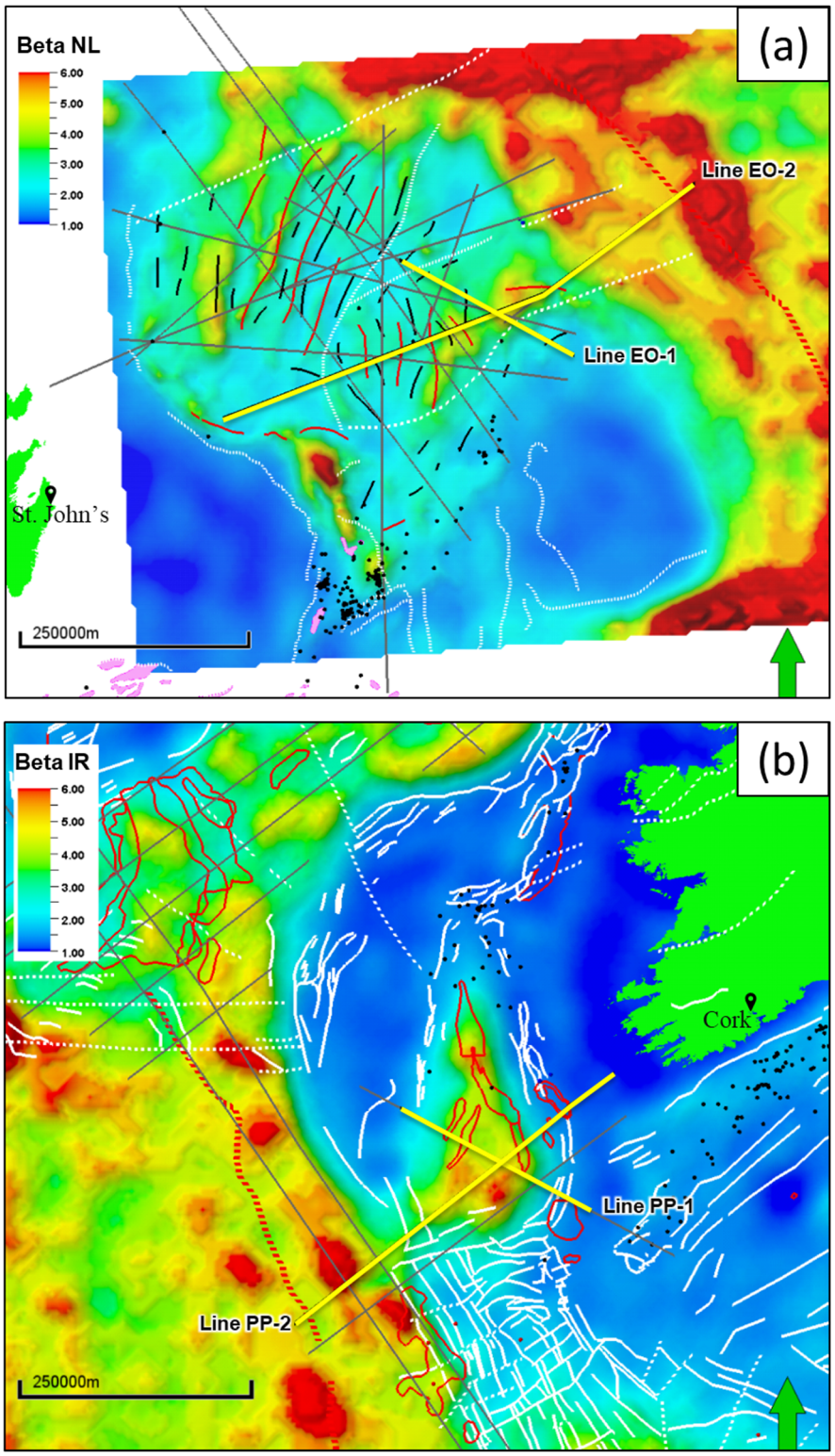

Figure 4.3 Extension factor of the crust (β) from Welford et al. (2012). (a) Orphan Basin with the structural elements adapted from Edwards, Jauer, Moir, & Wielens (2003), Srivastava et al. (1990), and Sibuet et al. (2007). (b) Porcupine Basin with the structural elements from Naylor et al. (2002). See Figure 2.10 for legend.

An example of the sections after removing the effects of thermal subsidence for the Cenozoic unit are shown in Figure 4.4.

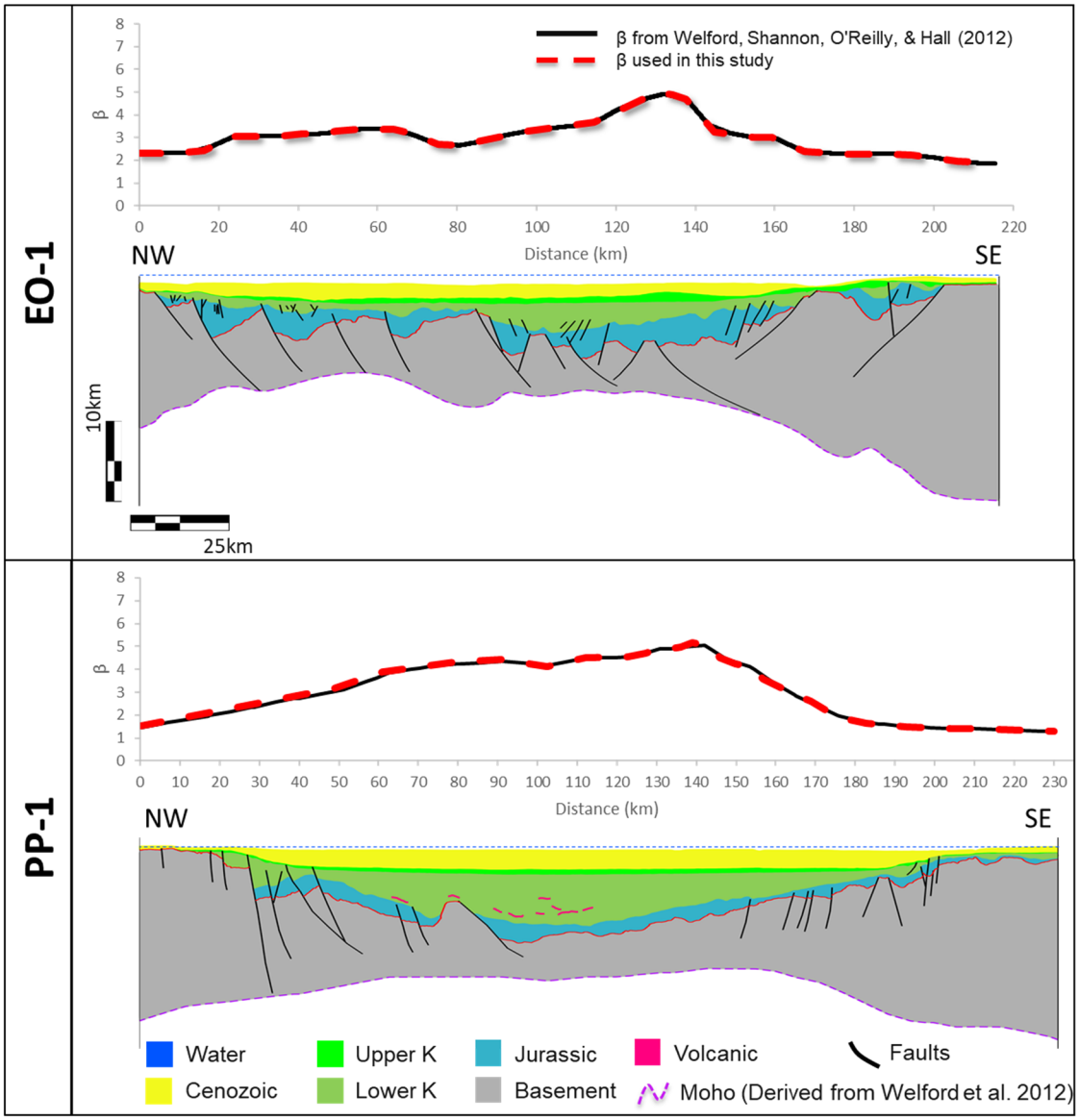

Figure 4.4 Sections showing the β values used to remove the effects of thermal subsidence for the Cenozoic unit.

The thermal subsidence tool in Move™ reveals that the continental crust rebounded by ~980 m in the East Orphan Basin and ~940 m in the Porcupine Basin for the Cenozoic unit.

4.2 Upper Cretaceous

4.2.1 Decompaction

To decompact the Upper Cretaceous unit, the Cenozoic unit is removed using the porosity-depth function proposed by Sclater & Christie (1980) and the lithological composition shown in Table 4.1.

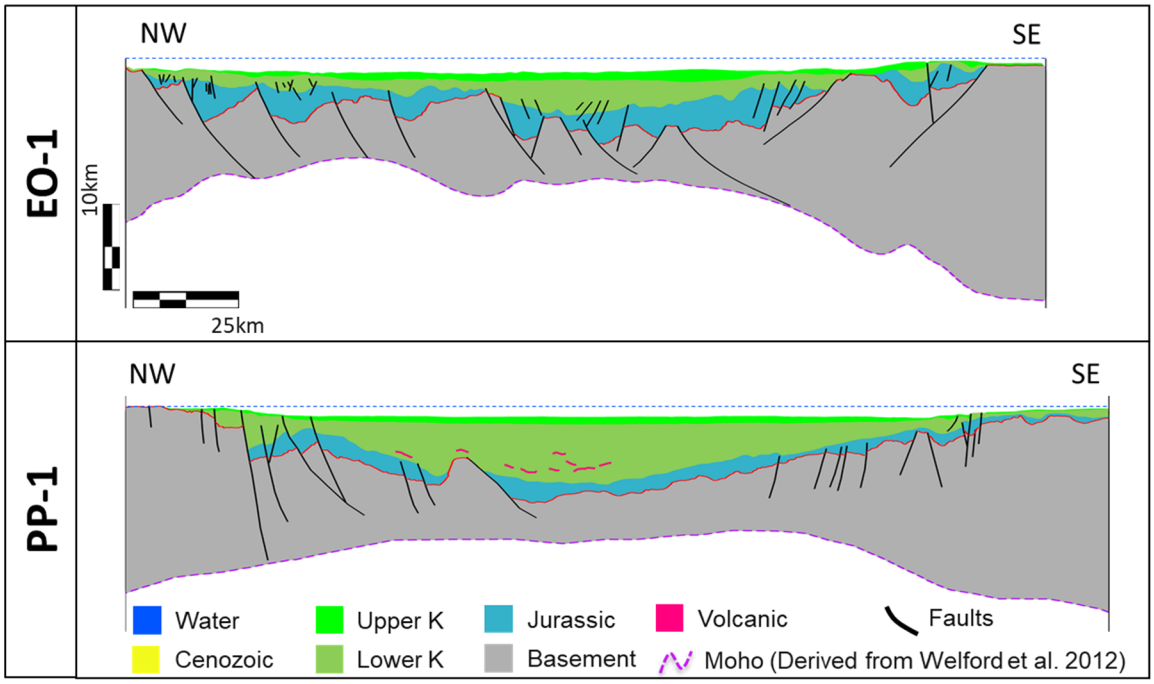

Figure 4.5 Sections showing the decompaction of the Upper Cretaceous unit from removal of the Cenozoic. Both sections are plotted at the same scales. See Figures 3.1 and 3.9 for line locations.

The decompaction of the Upper Cretaceous unit results in an increase in thickness (~250 m on average), mostly associated with areas where the thickest Cenozoic package was located. An example of the decompacted Upper Cretaceous unit is shown in Figure 4.5. The isostatic response to unloading sediments (Airy isostasy) was also taken into account during decompaction.

4.2.2 Thermal subsidence

Similar to the Cenozoic unit, the Upper Cretaceous is a post-rift unit, and therefore the effects of thermal subsidence must be removed. The parameters and rifting events used are shown in Table 4.2 and Table 4.3, respectively. The same distribution of β from Welford et al. (2012) used for the Cenozoic unit (Figure 4.4) was used for the Upper Cretaceous.

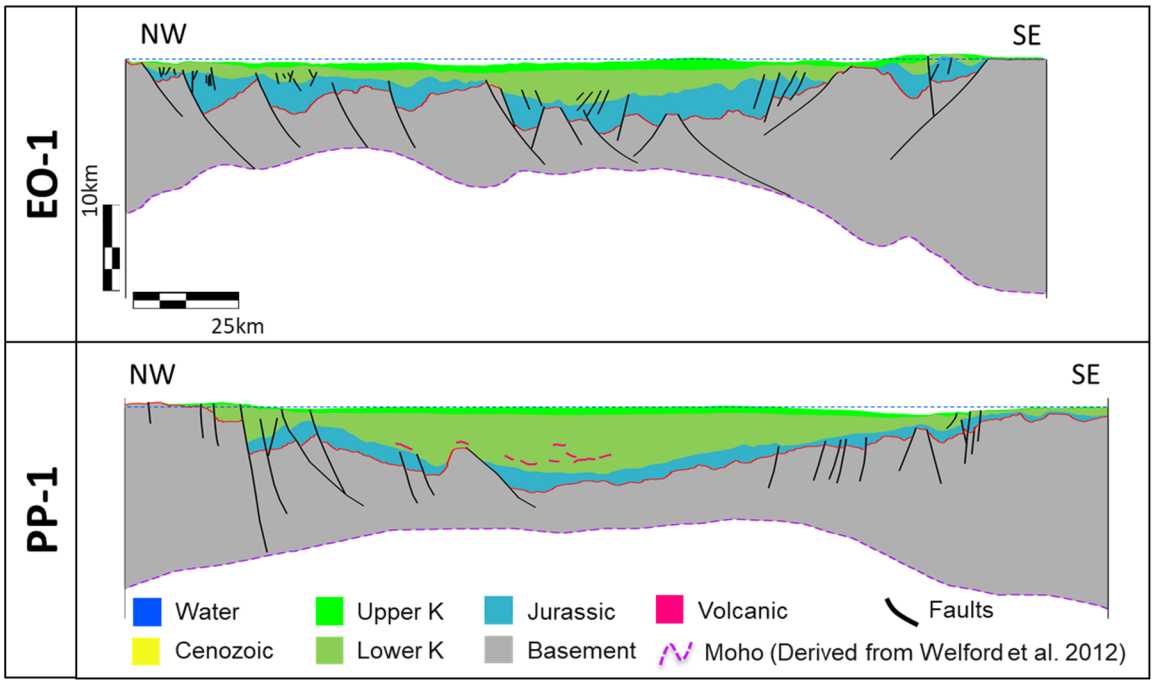

Figure 4.6 Sections after removing the effects of thermal subsidence for the Upper Cretaceous unit. Both sections are plotted at the same scales. See Figures 3.1 and 3.9 for line locations.

After removing the effect of thermal subsidence, the Upper Cretaceous unit rebounded by approximately 1100 m and 1150 m in the East Orphan and Porcupine basins, respectively. The differences mainly reflect the β factor variations used for each basin. Higher values of β are found in the Porcupine Basin (see Figure 4.3).

4.2.3 Unfolding

An additional step was applied to unfold the Upper Cretaceous unit due to the presence of a localised inversion structure affecting this unit in the south-eastern part of the Porcupine Basin. The Simple shear method within the 2D Unfolding module was used. This step mainly affects the area beneath the unfolded section since the inversion does not uniformly affect the entire Porcupine Basin but rather only a localised area of the basin (Figure 4.7).

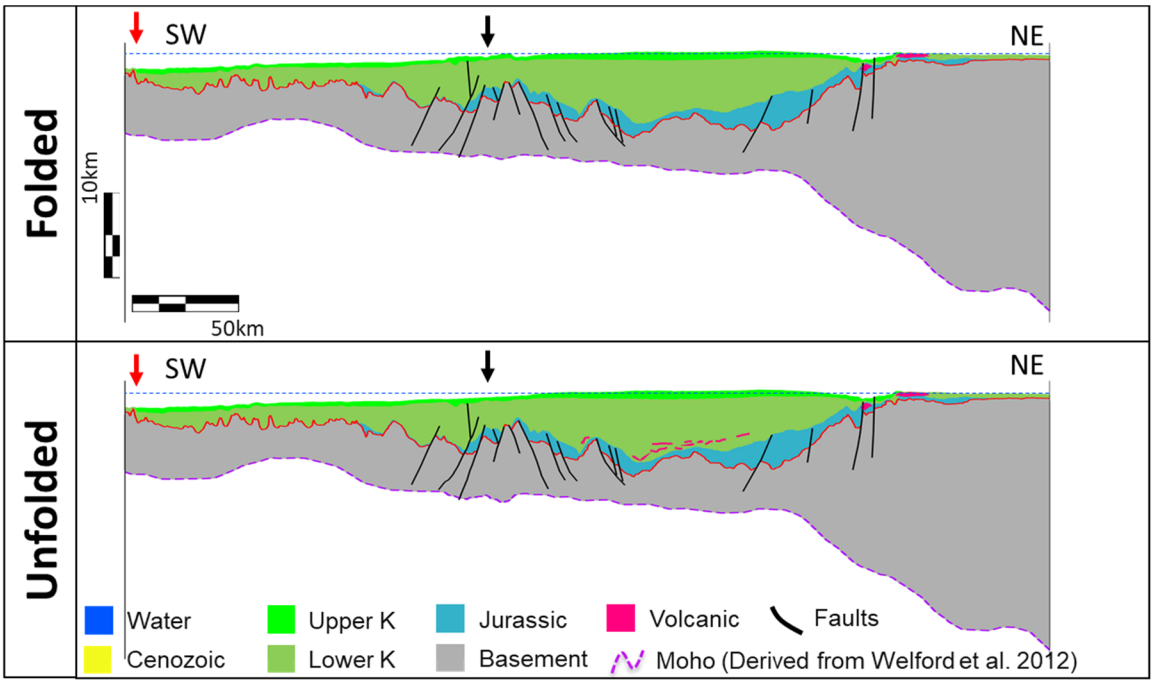

Figure 4.7 Line PP-2 showing the unfolded Upper Cretaceous unit. Upper section: folded. Lower section: unfolded. Black arrows: unfolded segment. Red arrows: magnetic anomaly 34 from Srivastava et al. (1990). *See Figure 3.9 for line location.*

Even though inversion structures were identified in the East Orphan Basin during the seismic interpretation, these structures are not present on the lines chosen for the restoration.

4.3 Lower Cretaceous

4.3.1 Decompaction

The Lower Cretaceous unit was decompacted by removing the Upper Cretaceous unit (see the parameters used in Table 4.1). The increase in thickness due to decompaction is more significant (400-700 m) where the thickness of the overlying layer, the Upper Cretaceous, was greater (Figure 4.8).

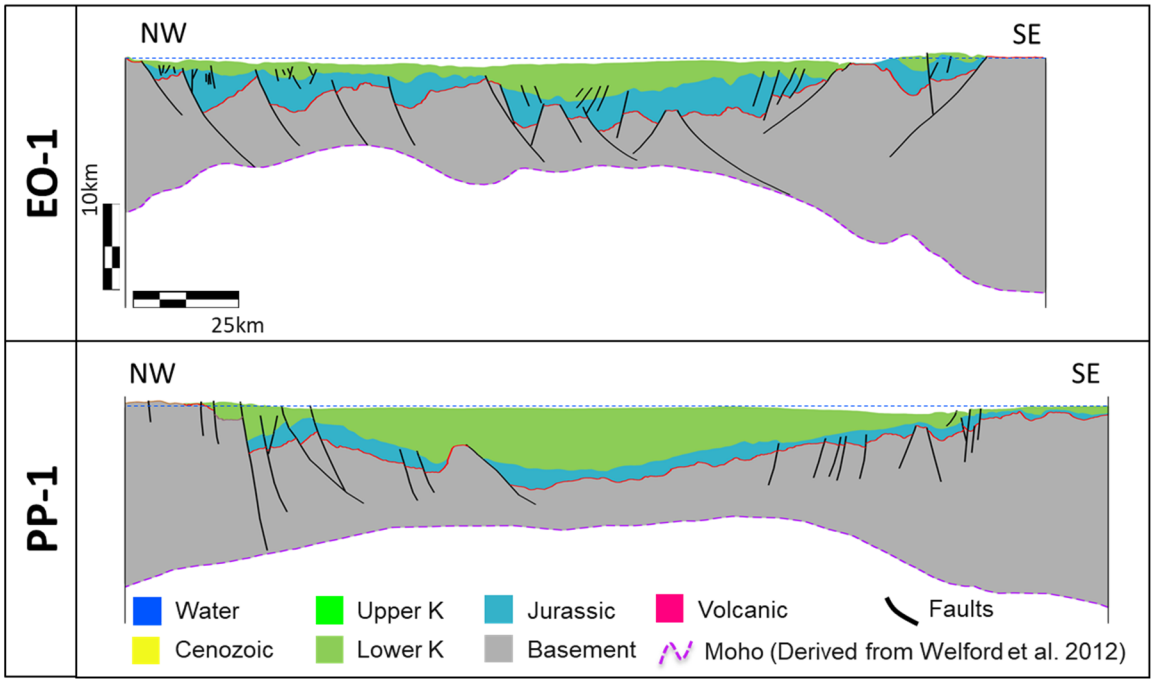

Figure 4.8 Sections showing the decompaction of the Lower Cretaceous unit from removal of the Upper Cretaceous. Both sections are plotted at the same scales. See Figures 3.1 and 3.9 for line locations.

4.3.2 Fault restoration

The Lower Cretaceous unit is a syn-rift layer, meaning that deposition occurred during rifting since syn-sedimentary layers characterised by growth faults are present over both the East Orphan and Porcupine basins. Therefore, the faults affecting this layer must be restored to their approximate pre-rifting geometry. To carry out the fault restoration, the

2D Move-on-Fault workflow of Move™ was applied using the Simple Shear algorithm and an antithetic shear angle of ±60° (see section 2.2.5.4 for details). The Simple Shear algorithm in Move™ maintains the area between beds.

The Lower Cretaceous unit is not significantly affected by faults, indicating either a less accentuated or more distributed rift period, with potentially slow extension rates (hyperextension?) in some parts of the basins. After restoring all of the Lower Cretaceous faults, the Upper Cretaceous unit was unfolded to a zero datum (Figure 4.9). This step was applied to better visualise the depocentres of the basins during the Lower Cretaceous (~100.5-145 Ma) and because of the lack of paleobathymetric estimates available for both basins. Flattening the Lower Cretaceous unit does not significantly impact the restoration process since no petroleum system effects are predicted from these restorations. The paleowater depths proposed by BeicipFranlab, Nalcor Energy Oil and Gas, & Government of Newfoundland and Labrador (2018) for this period show an average water depth of ~200 m. Based on the restored sections, the main depocenters during the Lower Cretaceous are located where the highest values of β are found in both basins (see Figures 4.3a and 4.3b).

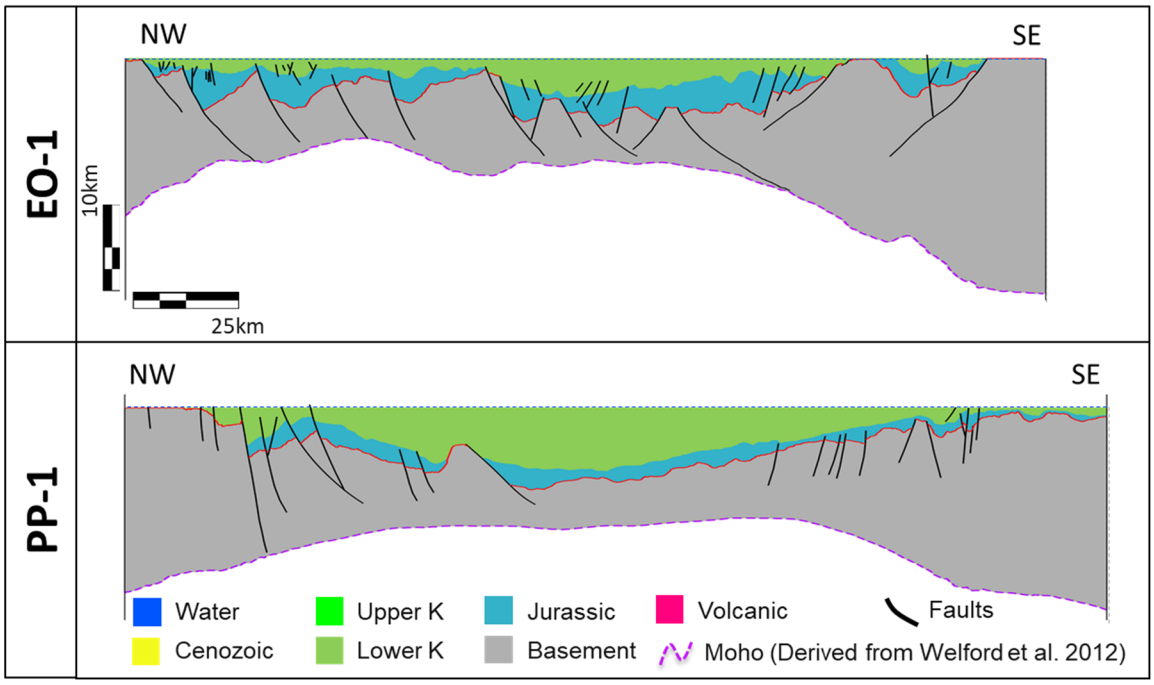

Figure 4.9 Sections showing the fault restoration of the Lower Cretaceous unit. Both sections are plotted at the same scales. See Figures 3.1 and 3.9 for line locations.

4.4 Jurassic

4.4.1 Decompaction

Since the Lower Cretaceous unit is a syn-rift unit, deposited during a rifting period, no thermal subsidence effects have to be removed. The Jurassic unit was decompacted by removing the overlying Lower Cretaceous unit. Similar to the rest of the layers, the main effects of decompaction are seen over the areas with thicker overlying sediments. The Jurassic unit is generally continuous except at the crests of certain uplifted blocks, possibly indicating subaerial exposure (erosion?/non-deposition?) in these areas (Figure 4.10).

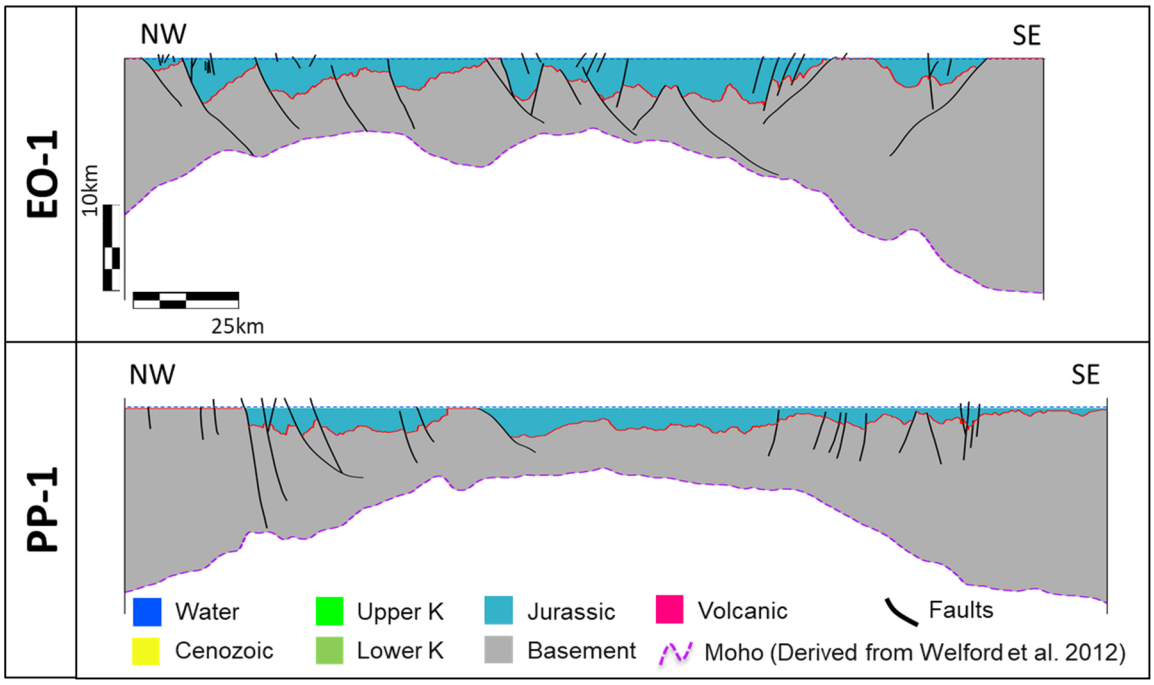

Figure 4.10 Sections showing the decompaction of the Jurassic unit from removal of the Lower Cretaceous. Both sections are plotted at the same scales. See Figures 3.1 and 3.9 for line locations.

4.4.2 Fault restoration

Fault offsets were restored for the Jurassic unit. In contrast with the Lower Cretaceous unit, the Jurassic unit is highly dissected with basement involved faults. Growth faults are particularly common in both the East Orphan and Porcupine basins. After fault restoration, the Jurassic unit was unfolded. The unit was normalized to a zero-datum due to the lack of paleobathymetric estimates and to better visualise the depocentres of the basins during the Jurassic (~145-201 Ma). Based on results shown in the restored sections, the main depocentres from the Jurassic show higher sediment thickness variability than Lower Cretaceous depocentres. A number of small depocentres (pockets) associated with half-grabens are observed, rather than the more clearly defined depocentre from the Lower Cretaceous (Figure 4.11). The amount of extension due to the restoration of the faults that

affected the Jurassic unit is around 10.6 km and 6.2 km for lines EO-1 and PP-1, respectively. Whereas for the lines EO-2 and PP-2, the extension is ~13 km and ~5.3 km respectively.

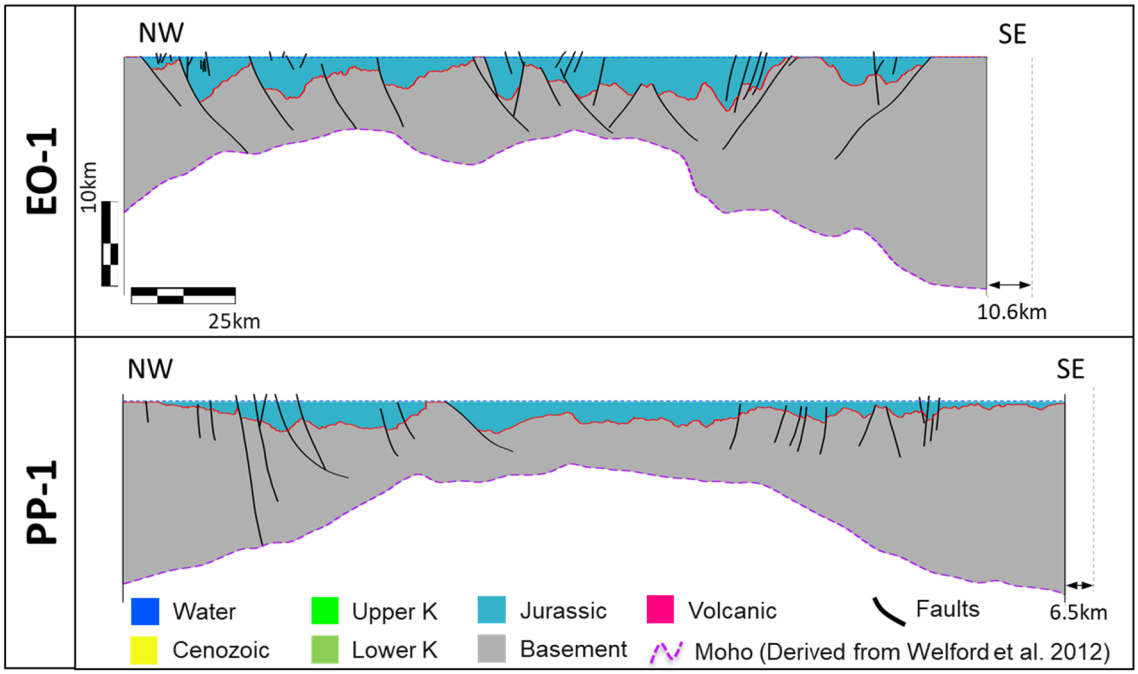

Figure 4.11 Sections showing the fault restoration of the Jurassic unit. Both sections are plotted at the same scales. See Figures 3.1 and 3.9 for line locations.

4.5 Basement

4.5.1 Decompaction

The thinning of the crust depends on several factors (rheology, temperature, composition, pre-existing structures, etc.) and is usually modelled using a non-linear viscoelastic material (Lavier & Manatschal, 2006; Naliboff et al., 2017). Because of the lack of constraints to define the correct porosity-depth curve for the crust, a very low initial porosity and depth coefficients were assumed (Table 4.1). The difference between not using a decompaction curve (assuming no changes due to removing the upper layers) and the coefficients chosen,

is on the order of 50 m. The decompaction of the Jurassic unit does not significantly affect the Basement (crust).

4.5.2 Fault restoration

The Basement unit exhibits a significant number of faults, with some of them reaching depths close to the Moho. After fault restoration, the Basement unit was unfolded. The unit was restored to zero datum due to the lack of paleobathymetric estimates and to better visualise the crustal structure of the basins prior to the Jurassic (older than 252 Ma). Based on results of restoration, the extension during this period amounts to 23.8 km and 9.1 km for lines EO-1 and PP-1, respectively (Figure 4.12). Whereas for lines EO-2 and PP-2, the extension is 20.6 km and 13.6 km, respectively.

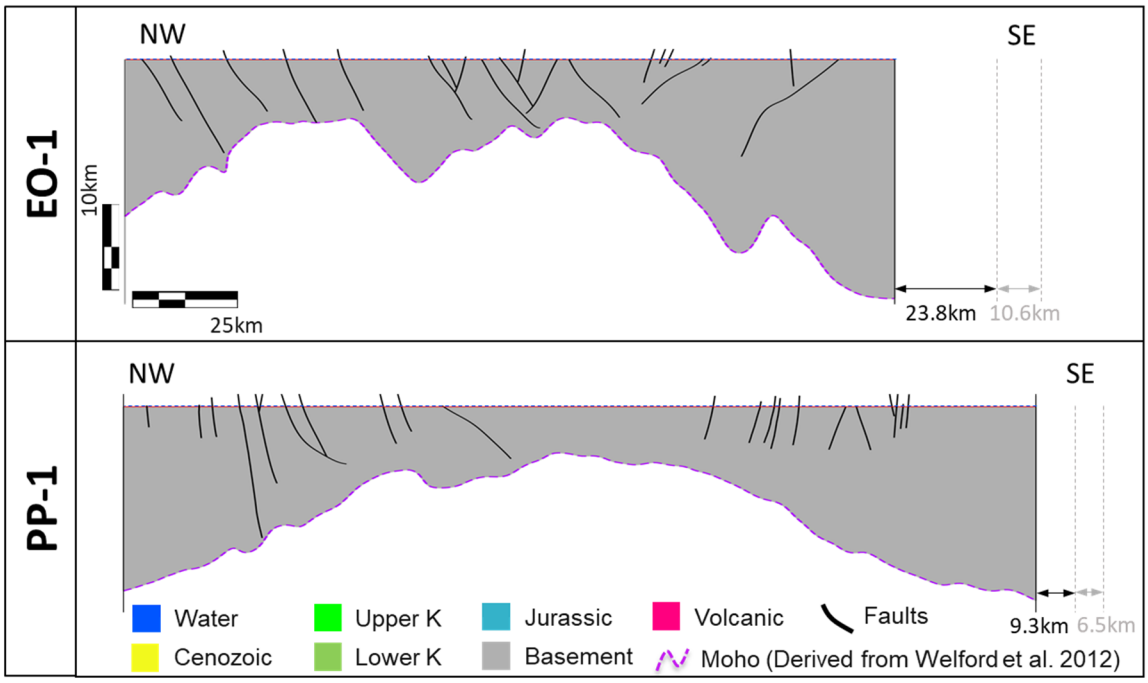

Figure 4.12 Sections showing the decompaction of the Basement/crustal unit from removal of the Jurassic. Both sections are plotted at the same scale. See Figures 3.1 and 3.9 for line locations.

4.6 Restoration summary

The structural restoration of the selected lines in the East Orphan and Porcupine basins shows that evolution, sedimentary cover thickness, and crustal structure of the basins differ significantly. The East Orphan Basin shows higher variability and asymmetry in its crustal structure than the symmetrical and elongated Porcupine Basin, with a thicker sedimentary cover found in the Porcupine Basin. Faulting also reflects these differences with higher variability in dipping directions in the East Orphan Basin compared with the Porcupine Basin.

In the next chapter, the restored sections are relocated through time in Move™ by using the kinematic evolution model of Nirrengarten et al. (2018) in GPlates for reference.

CHAPTER 5. KINEMATIC EVOLUTION MODELS

Restored sections of Orphan and Porcupine basins were compared with the kinematic evolution model from Nirrengarten et al. (2018) using GPlates to obtain a better understanding of the evolution of these complex but highly prospective basins. GPlates enables both visualisation and manipulation of plate-tectonic reconstructions and associated data through geological time. The Nirrengarten et al. (2018) kinematic evolution model is chosen over others, such as Seton et al. (2012), Matthews et al. (2016), and Müller et al. (2016), because it is the only model that explicitly considers the rotation of the Flemish Cap and the Porcupine High. It does this by including micro-blocks for the Flemish Cap, Orphan Knoll, and the East and West Orphan basins on the Newfoundland margin and for the Porcupine High, Rockall and Hatton highs, and the Rockall and Porcupine basins on the Irish margin.

The locations of seismic transects EO-1, EO-2, PP-1, PP-2, and GI-1 were imported into GPlates, attaching EO-1 and EO-2 to the Orphan Knoll plate (Plate ID 1002), PP-1 and PP-2 to the Porcupine High plate (Plate ID 3001), and GI-1 to the Iberian Peninsula (Plate ID 304) in the Nirrengarten et al. (2018) kinematic model. As the plates move through time in each of the models, the locations of the seismic transects are anchored to the plates, therefore, follow the same pole of rotation as the plate. The main drawback of the kinematic model is that it does not take into account the internal deformation of the tectonic plates, which is a crucial factor when studying hyperextended basins such as the East Orphan and Porcupine basins. Nonetheless, the kinematic model of Nirrengarten et al. (2018) is considered a good approximation in the absence of deformable kinematic models.

Shapefiles of the restored lines were exported from GPlates and imported into Move™. The lines can now be geographically positioned in geologic time. The Cenozoic line was tied to its present-day position, the Late Cretaceous to the 66 Ma reconstructed position, the Early Cretaceous to the 100.5 Ma reconstructed position, the Jurassic to the 145 Ma reconstructed position, and the Basement to the 200 Ma reconstructed position.

5.1 Cenozoic

The present-day configuration of the lines shows the V-shape geometry of the Porcupine Basin and the U-shape configuration of the West and East Orphan basins. A more tabular geometry, however, is exhibited by the Rockall Basin, widening toward its southern limit, near the Charlie-Gibbs Fracture Zone (CGFZ) (Figure 5.1).

5.2 Late Cretaceous

The Late Cretaceous (~66 Ma) reconstructed location of the restored lines is shown in Figure 5.2. At this time, the Labrador Sea was already forming at a more advanced stage of development compared to the Reykjanes Ridge that was in an emerging stage. The rotation of the Flemish Cap out of the Orphan Basin and the Porcupine High out of the Porcupine Basin had already occurred. Both East Orphan and Porcupine basins are already isolated with no direct connection between them.

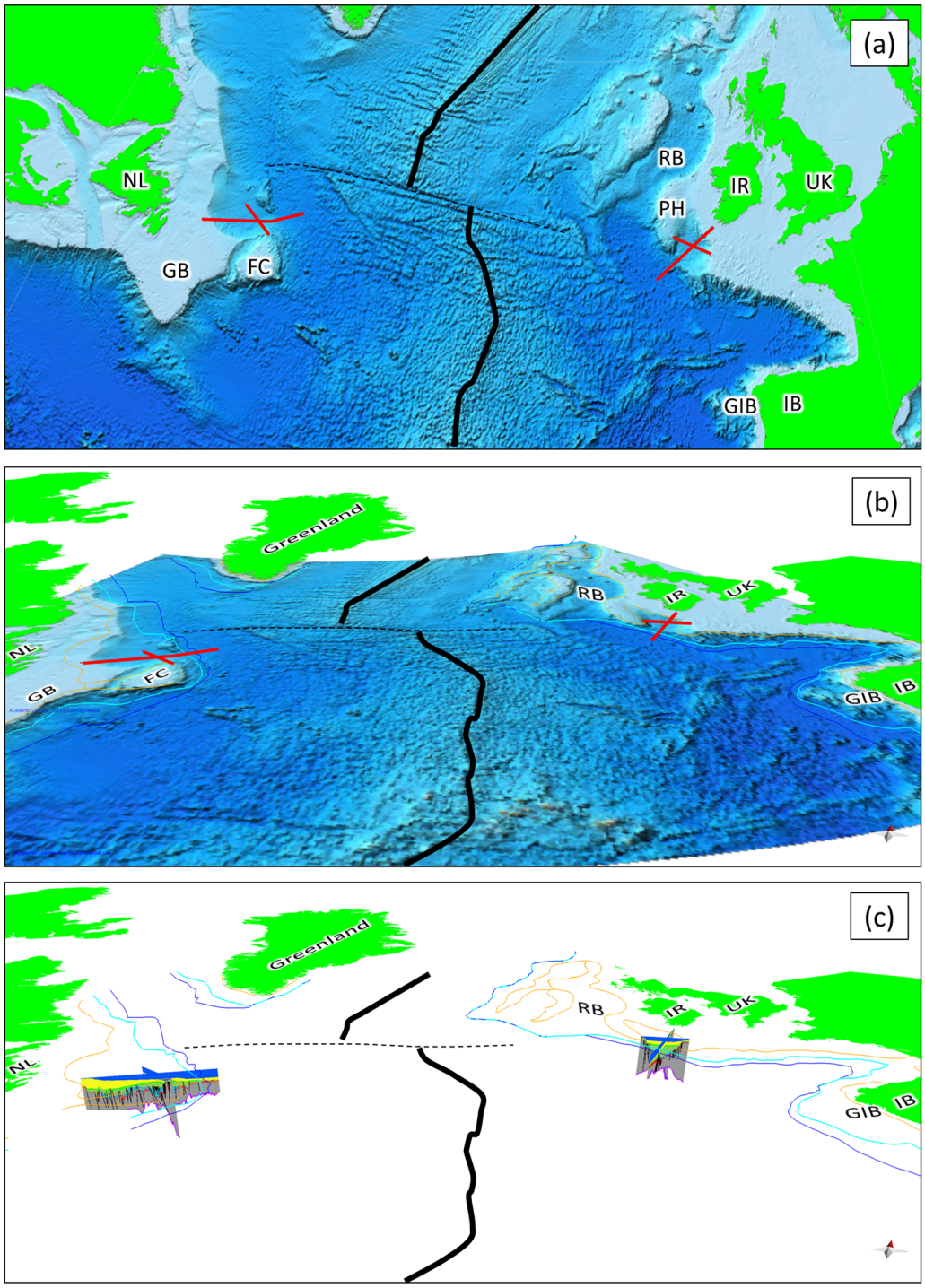

Figure 5.1 Present day location of the interpreted lines in (a) map view with bathymetry, in (b) perspective view with bathymetry, and in (c) perspective view with reconstructed sections. NL: Newfoundland, FC: Flemish Cap, GB, Grand Banks, IR: Ireland, UK: United Kingdom, RB: Rockall Basin, GIB: Galicia Interior Basin, IB: Iberian Peninsula. Black solid line/polygon: rift location. Black dashed line: transfer zone. Orange line: necking line. Dark blue line: landward limit of oceanic crust. Light blue line: edge of continental crust. All the polyline boundaries are extracted from Nirrengarten et al. (2018).

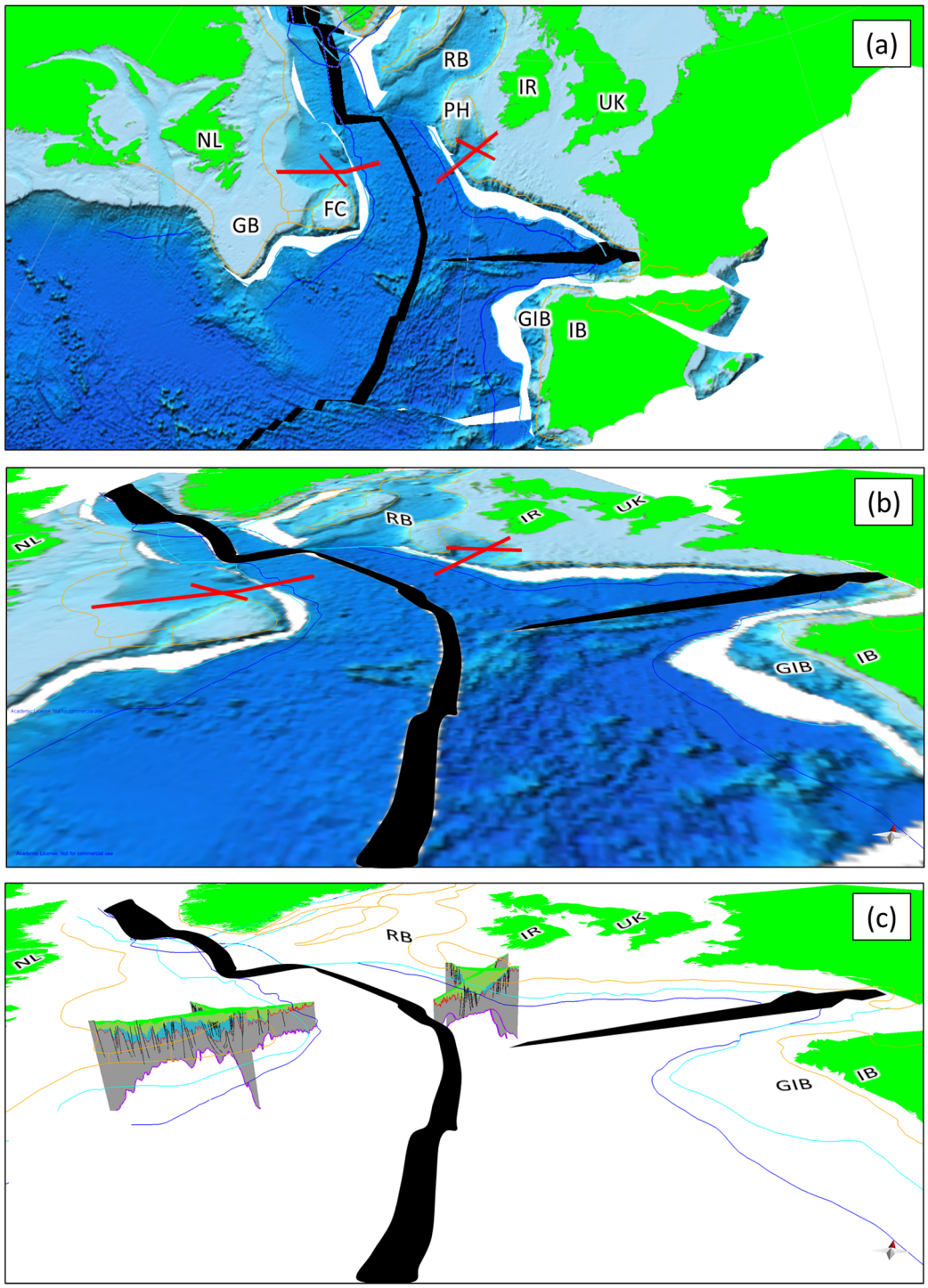

Figure 5.2 Late Cretaceous (~66 Ma) location of the restored lines in (a) map view with bathymetry, in (b) perspective view with bathymetry, and in (c) perspective view with reconstructed sections. NL: Newfoundland, FC: Flemish Cap, GB: Grand Banks, IR: Ireland, UK: United Kingdom, RB: Rockall Basin, GIB: Galicia Interior Basin, IB: Iberian Peninsula. Black solid line/polygon: rift location. Black dashed line: transfer zone. Orange line: necking line. Dark blue line: landward limit of oceanic crust. Light blue line: edge of continental crust. All the polyline boundaries are extracted from Nirrengarten et al. (2018).

5.3 Early Cretaceous

At this time (~100 Ma), the West Orphan Basin and the Rockall Basin seem to be, at least partially, connected. The Labrador Sea rifting is at an incipient stage, and the development of the Reykjanes Ridge has not yet started. Again, the more important rotation of the Flemish Cap out of the Orphan Basin and the Porcupine High out of the Porcupine Basin had already occurred at this time.

5.4 Jurassic

At the end of the Jurassic (~145 Ma), according to the kinematic evolution model of Nirrengarten et al. (2018), the West Orphan Basin was still closed or in the process of creation (Figure 5.4). In other words, most of the extension, opening of the West and East Orphan basins, and subsequent rotation of the Flemish Cap occurred during the Early Cretaceous (145-100.5 Ma). However, the East Orphan was partially formed at this time meaning that its formation is associated with more than one rifting period. Similar to the East Orphan Basin, the Porcupine Basin had started to form at this time, which created a continuous and aligned geometry with the Galicia Interior Basin (GIB).

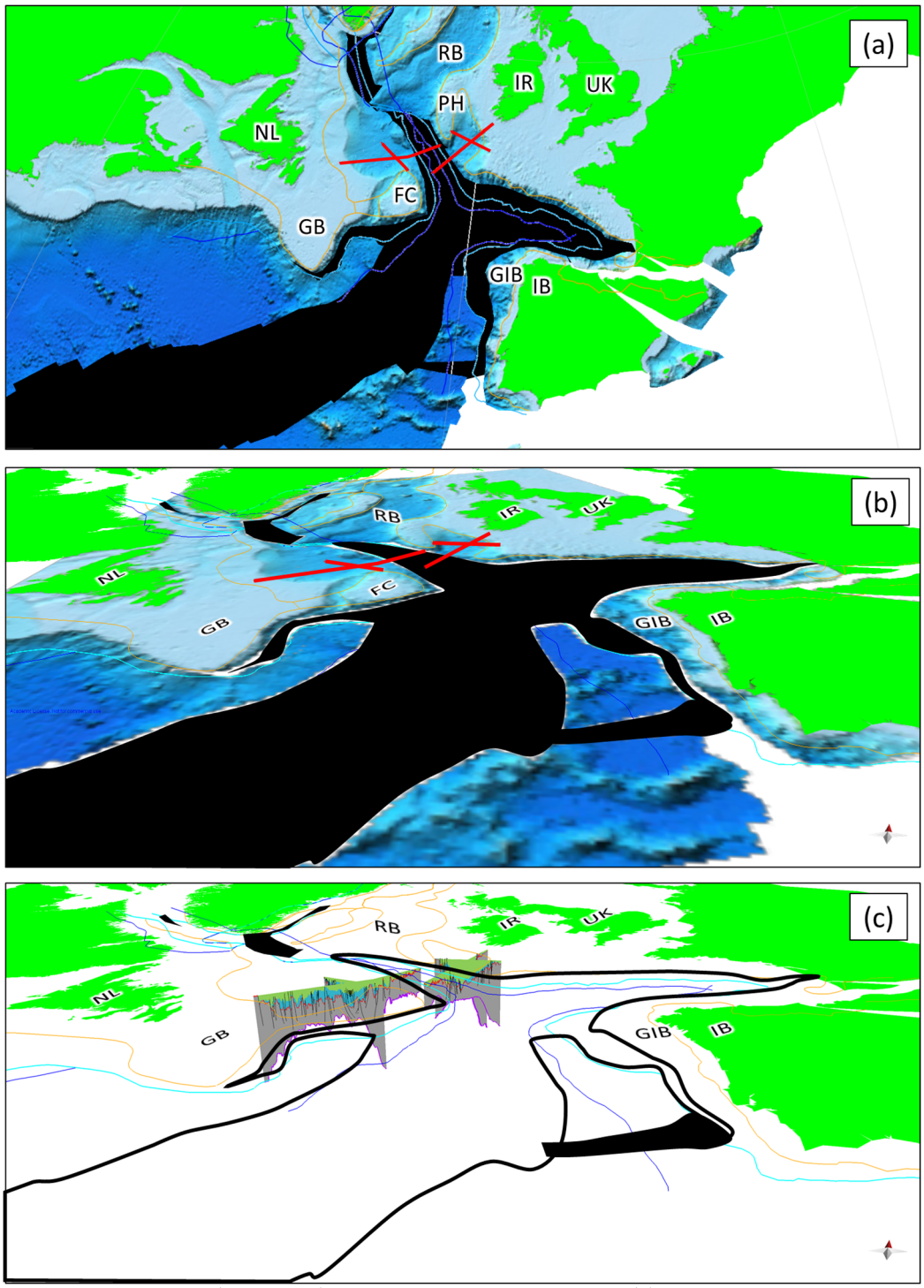

Figure 5.3 Early Cretaceous (~100.5 Ma) location of the restored lines in (a) map view with bathymetry, in (b) perspective view with bathymetry, and in (c) perspective view with reconstructed sections. NL: Newfoundland, FC: Flemish Cap, GB, Grand Banks, IR: Ireland, UK: United Kingdom, RB: Rockall Basin, GIB: Galicia Interior Basin, IB: Iberian Peninsula. Black solid line/polygon: rift location. Black dashed line: transfer zone. Orange line: necking line. Dark blue line: landward limit of oceanic crust. Light blue line: edge of continental crust. All the polyline boundaries are extracted from Nirrengarten et al. (2018).

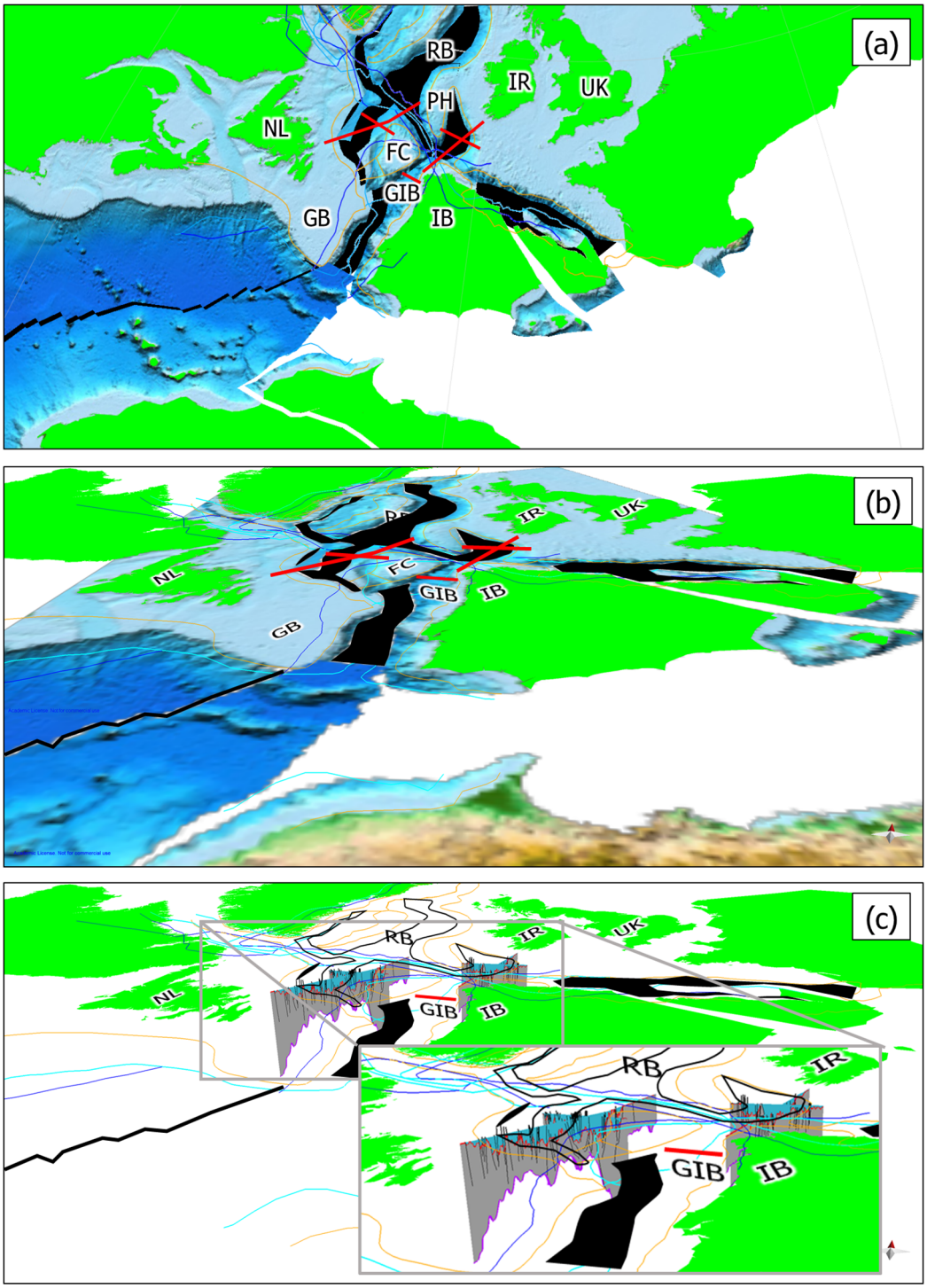

Figure 5.4 Jurassic (~145 Ma) location of the restored lines in (a) map view with bathymetry, in (b) perspective view with bathymetry, and in (c) perspective view with reconstructed sections. NL: Newfoundland, FC: Flemish Cap, GB, Grand Banks, IR: Ireland, UK: United Kingdom, RB: Rockall Basin, GIB: Galicia Interior Basin, IB: Iberian Peninsula. Black solid line/polygon: rift location. Black dashed line: transfer zone. Orange line: necking line. Dark blue line: landward limit of oceanic crust. Light blue line: edge of continental crust. All the polyline boundaries are extracted from Nirrengarten et al. (2018).

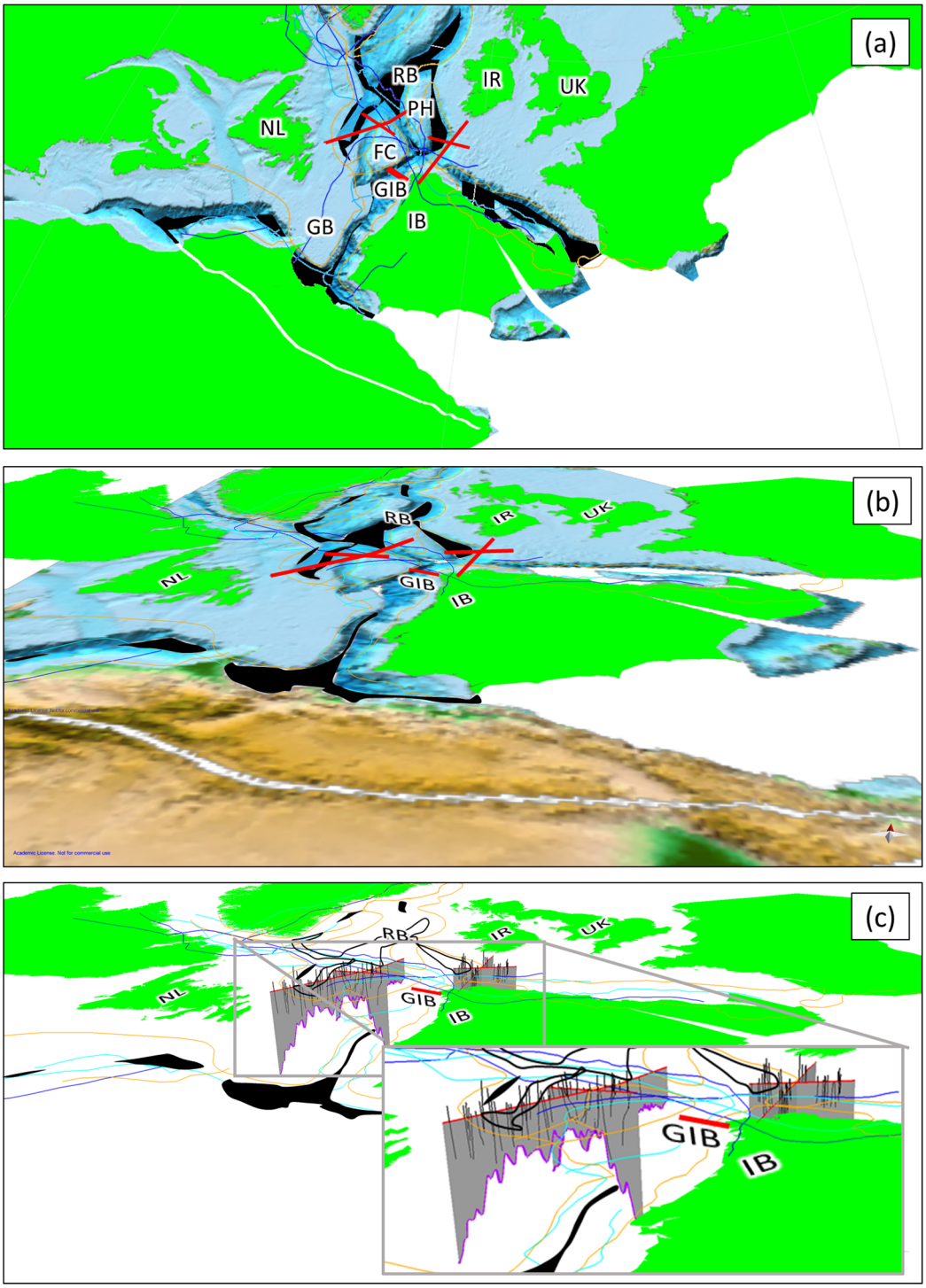

Figure 5.5 Base Jurassic (~200 Ma) location of the restored lines in (a) map view with bathymetry, in (b) perspective view with bathymetry, and in (c) perspective view with reconstructed sections. NL: Newfoundland, FC: Flemish Cap, GB, Grand Banks, IR: Ireland, UK: United Kingdom, RB: Rockall Basin, GIB: Galicia Interior Basin, IB: Iberian Peninsula. Black solid line/polygon: rift location. Black dashed line: transfer zone. Orange line: necking line. Dark blue line: landward limit of oceanic crust. Light blue line: edge of continental crust. All the polyline boundaries are extracted from Nirrengarten et al. (2018).

5.5 Basement

At the beginning of the Jurassic (~200 Ma), the East Orphan Basin was in an early stage of development with a narrower configuration than the one it exhibits today. Meanwhile, the Rockall Basin remained wider than the East Orphan Basin. The Flemish Pass, Jeanne d'Arc, East Orphan, and Rockall basins may have formed as a continuous system at this time. Porcupine Basin was also at a young stage of basin development, showing a possible connection with the GIB (Figure 5.5).

5.6 Kinematic modelling summary

The kinematic evolution model of Nirrengarten et al. (2018) shows that the ancient connection between the East Orphan Basin and the Porcupine Basin is questionable. Additionally, it shows a potential alignment between the Porcupine and the Galicia Interior basins.

The next chapter involves integration and discussion of the findings shown in the previous chapters.

CHAPTER 6. INTERPRETATION AND DISCUSSION

This chapter comprises the integration, interpretation, analysis, comparison, and discussion of all of the results generated in the previous chapters. The megasequences corresponding to the defined seismo-stratigraphic units are analysed followed by definition and discussion of the structural domains present along the interpreted lines. The amount of stretching estimated for both basins and the implications are then discussed. The consequences of using non-deformable kinematic evolution models will also be addressed before discussing the relationship between the East Orphan and Porcupine basins, and eventually the Galicia Interior Basin.

6.1 Tectonostratigraphic Megasequences

Based on the characteristics for each seismo-stratigraphic unit described in Chapter 3, three tectonostratigraphic megasequences are interpreted:

6.1.1 Pre-rift crust

Due to the poorer quality of the seismic data with depth, no pre-rift sediments are resolved. However, the thickness of the crust is estimated using the interpreted acoustic basement and the Moho proxy. Therefore, this megasequence is represented by the crust. It is limited at its top by the acoustic basement and its base by the Moho proxy. The average thickness of the crust in both basins is 10 km and 12 km in the East Orphan and Porcupine basins, respectively. Crustal thickness is as thin as 3.8 km in the East Orphan Basin and 3.2 km in the Porcupine Basin. Both values coincide with highly stretched crust (β~5). Both basins contain two main crustal sections where the thickness of the crust decreases considerably.

The East Orphan Basin, however, shows more local regions of thin crust that coincide with the location of the two main depocentres, while Porcupine Basin exhibits one main area of thin crust.

The restored pre-rift crustal section corresponds to the crustal architecture prior to rifting, assuming that all of the extension was due to brittle deformation. The faulting style of the crust beneath both basins is similar, with normal faults dipping away from the flanks of the basins. Greater faulting complexity within the East Orphan Basin indicates either variability during the periods of extension (in magnitude and direction) or variation in the nature (pre-existing structures) and composition (rheology) of the crust (more brittle deformation in some areas of the East Orphan Basin compared to the Porcupine Basin).

The extension estimated from the restoration of the crust varies from 23.8 km (EO-1) in the East Orphan Basin to 9.3 km (PP-1) in the Porcupine Basin. This observation indicates that the most important extension occurred during the Jurassic, significantly affecting the East Orphan Basin.

6.1.2 Syn-rift

The syn-rift megasequence consists of the Lower Cretaceous and Jurassic units. The base of this megasequence (~200 Ma) coincides with the top of the acoustic basement. The megasequence differs between the East Orphan and Porcupine basins. The East Orphan Basin has an asymmetric geometry with several sub-basins (pockets) defined by rotated fault blocks. The thickness of the megasequence ranges from 3800 m to 3700 m along lines EO-1 and EO-2. These characteristics may reflect variable rheology of the crust, the existence of pre-existing structures within the basin, and/or overprinted intermittent

oblique rifting periods. The Porcupine Basin, in contrast, shows a more symmetric geometry with a thicker pre-rift megasequence. The thickness ranges from 4500 m to 4200 m along lines PP-1 and PP-2. These characteristics suggest more continuous deposition of sediments as well as fewer interrupted rifting events.

The restored sections for this megasequence reveal at least two main depocentres in the East Orphan Basin. The main depocentre coincides with an area on the eastern flank of the basin with β values higher than 3.5 (hyperextension?), as determined by Welford et al. (2012). Whereas on the western flank, several sub-basins (pockets) are formed by tilted fault blocks.

In the Porcupine Basin, the characteristics are different than in the East Orphan Basin. One well-defined depocentre within the central part of the basin is identified along the lines PP-1 and PP-2. This depocentre also coincides with the zone of highest β values (>3.5) defined by Welford et al. (2012). Sills are interpreted here (e.g., Naylor et al., 2002), intruding the Lower Cretaceous unit. These sills are located just above the Porcupine Median Volcanic Ridge and the Porcupine Volcanic Ridge System. Therefore, they may be interpreted as being fed by magmatic systems that created these ridges.

The general structure of each basin also differs from the East Orphan Basin. In the East Orphan Basin, basement-related faults, rotated basement blocks, and syn-depositional tectonic structures are distributed throughout the basin. In the Porcupine Basin, the basement-related faults are more common on the basin flanks, rotated basement blocks are mostly associated with the Lugh High (Figure 1.12) at the southern limit of the basin, and the syn-depositional tectonic structures are less pronounced. The horizontal extension

associated with the restoration of the syn-rift megasequence is approximately 10.6 km (line EO-1) within the East Orphan Basin and 6.2 km (line PP-1) in the Porcupine Basin. This difference in the amount of horizontal extension suggests that the Early Cretaceous extension was more severe in the East Orphan Basin than the one experienced by the Porcupine Basin. Based on the thickness variability of each independent unit, the structural style, and the amount of extension, it is interpreted that connectivity between the East Orphan and the Porcupine basins during deposition of the syn-rift megasequence is not evident.

6.1.3 Post-rift

The post-rift megasequence is represented by the Cenozoic and Upper Cretaceous units. The base of this megasequence (~100.5 Ma) marks the beginning of the break up between Europe and North America (Seton et al., 2012). During the deposition of this megasequence, the conditions evolved from active extension to passive, at the end of the Early Cretaceous (~100.5 Ma). After the cessation of the main rifting period during the Early Cretaceous (~145-100.5 Ma), a quieter passive environment, in terms of extension, was established in the Cenozoic (~66 Ma). Thick sedimentary sequences were deposited during this time. In the East Orphan Basin, the average thickness of this megasequence is between 1300 m along line EO-1 and 2700 m along line EO-2. Whereas in the Porcupine Basin, the average thickness is between 1500 m and 1800 m along lines PP-2 and PP-1. The structural architecture of the basins is similar. The East Orphan and the Porcupine basins exhibit a symmetric geometry, with thicker intervals observed for the post-rift deposits of the East Orphan Basin. This difference in thickness may suggest two scenarios: (1) more sedimentary

sources available to fill the basin, or (2) similar amounts of sediment availability but a localised accommodation space to be filled in the East Orphan Basin. The second scenario seems to be more reasonable since the Porcupine Basin has a wider area (~70,000 km^2) than the East Orphan Basin (~33,000 km^2).

6.2 Crustal Architecture

The East Orphan Basin and the Porcupine Basin have previously been defined as basins with hyperextended crust and partially serpentinised mantle (Lundin & Doré, 2011; Welford et al., 2010, 2012). Consequently, three domains and several subdomains are used to characterize their crustal architecture (see Figures 6.1 and 6.2) based on the morphological criteria first proposed by Péron-Pinvidic et al. (2013) and later complemented by Sutra et al. (2013), Chenin et al. (2015), and Chenin et al. (2017).

The different rift domains were interpreted along the same lines that were used for the structural restoration (Figure 6.1). Maps of these crustal domains were constructed for West Orphan, East Orphan, Rockall, and Porcupine basins using the depth-to-basement and Moho proxy from Welford et al. (2012), interpreted crustal domains from Lundin & Doré (2011) and Welford et al. (2010), and observations generated from this study (Figure 6.2).

Along the Newfoundland margin (Figure 6.2a), the proximal domain corresponds to the Bonavista Platform and discrete parts of the Flemish Cap and is characterised by a crustal thickness from 20 km to more than 30 km and β factors lower than 1.5. Overall, the Flemish Cap is interpreted to be a continental ribbon, as defined by Péron-Pinvidic & Manatschal (2010), with a crustal thickness of around 20 km and a β factor ranging from 1 to 1.5 containing some localised less-stretched areas with thicker crust. This variability in crustal

thickness and β factor within the Flemish Cap suggests that it should be modelled as a deformable continental ribbon rather than the classic rigid ribbon part of a larger rigid plate (e.g., Barnett-Moore, Müller, Williams, Skogseid, & Seton, 2018; Matthews et al., 2016; Nirrengarten et al., 2018; Seton et al., 2012).

The necking subdomain is distributed across both the East and West Orphan sub-basins with a crustal thickness between 10 to 20 km and β factors of 1.5 to 3.2. A further subdivision of the necking subdomain is used in this thesis to better delineate the deformation zones between the less stretched distal domain and the highly stretched hyperextended subdomain. These polygons can be used as deformable zones in future deformable kinematic evolution models (e.g., Peace, Welford, Ball, & Nirrengarten, 2018).

The 1st-degree necking subdomain is characterised by a crustal thickness of 15-20 km and a β factor of 1.5 to 2. This degree of stretching is mild with no evident faulting present. The 2nd-degree necking subdomain exhibits a crustal thickness of 12-15 km and a β factor of 2 to 2.5. Polyphase faulting becomes important within this subdomain (Reston, 2007) and most seismically detectable faults are planar.

The 3rd-degree necking subdomain corresponds to a crustal thickness of 10-12 km and β factors of 2.5 to 3.2. Planar faulting is still significant and listric faulting becomes more important. Based on this subdivision, the Orphan Knoll falls into the unique category of a continental ribbon with a relatively thin crust (<20km) that has been internally deformed.

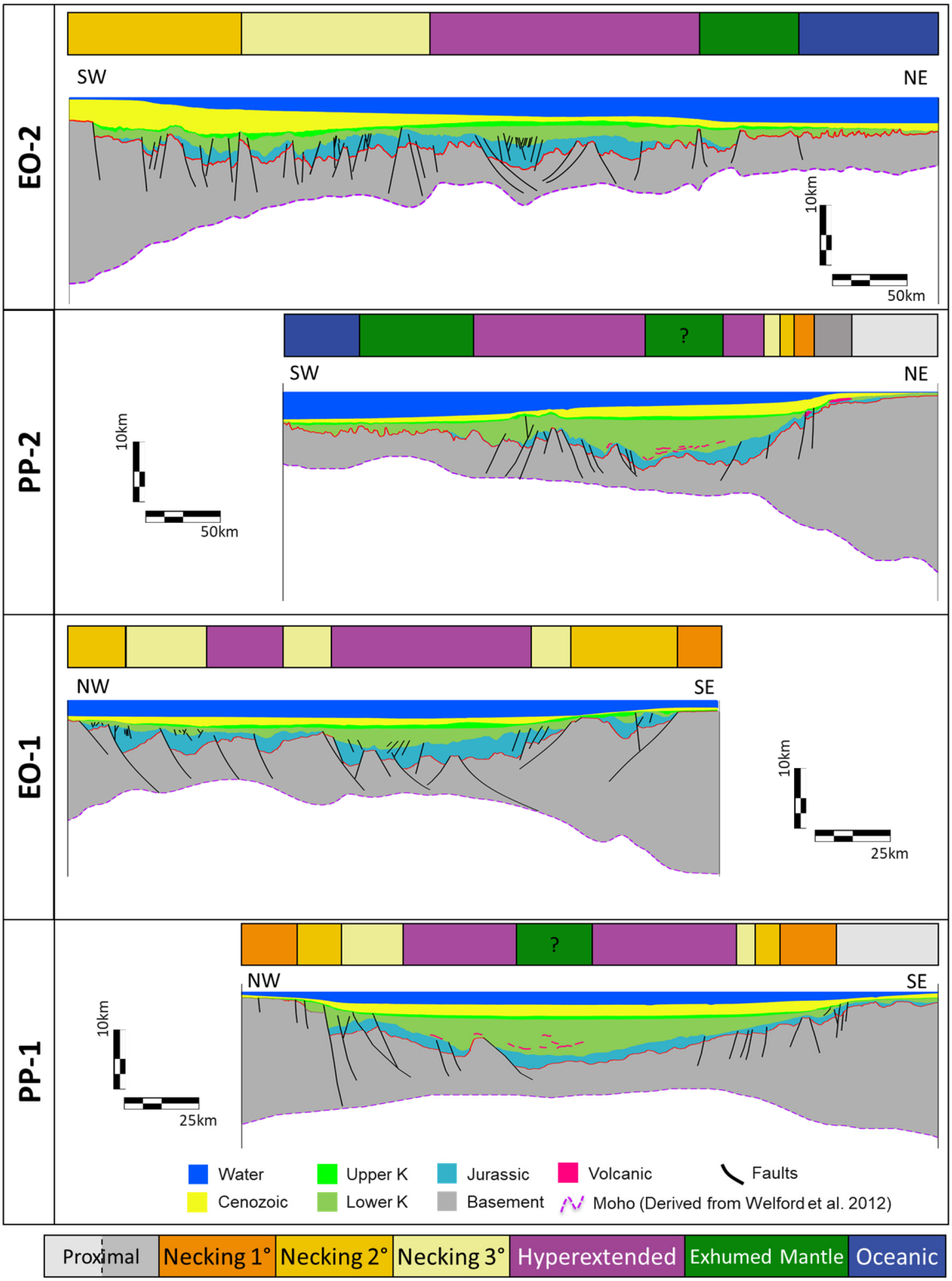

Figure 6.1 Geological sections with the interpreted crustal architecture. See Figure 4.3 for line locations.

Two main hyperextended zones are interpreted within depocentres of the West and East Orphan sub-basins (Figure 6.2a). A third hyperextended zone is interpreted in the northern part of the Jeanne d'Arc Basin. At least part of the White Rose field falls inside this hyperextended subdomain. With a highly thin crust (down to 4 km thick) and a β factor higher than 3.2 (Pérez-Gussinyé & Reston, 2001), this subdomain exhibits mostly listric faults affecting the Basement unit and planar faults affecting the overlying younger sedimentary units (see EO-1 and EO-2 in Figure 6.1). In the West Orphan Basin, the hyperextended subdomain includes a section of the Charlie-Gibbs Fracture Zone (CGFZ) in which volcanic intrusions (seamounts?) have been interpreted (BeicipFranlab, Nalcor Energy Oil and Gas, & Government of Newfoundland and Labrador, 2016; C. E. Keen, Dafoe, & Dickie, 2014). The exhumation subdomain on the Newfoundland margin is located just inboard of the oceanic domain to the east of the Orphan Knoll, where IODP wells U1302 and U1303 were drilled.

Along the Irish margin (Figure 6.2b), the proximal domain is present within some areas of the Porcupine High and the Rockall High. Similar to characteristics observed along the Newfoundland margin, it exhibits a crustal thickness from 20 km to more than 30 km and β factors lower than 1.5. Both the Porcupine High and the Rockall High are interpreted as continental ribbons (Péron-Pinvidic & Manatschal, 2010) with crustal thicknesses greater than 20 km and β factors of 1.2-1.5, surrounded by zones of lower β factors (Figure 6.2b).

The 1st-degree necking subdomain surrounds the proximal domain within Porcupine and Rockall basins and has a crustal thickness between 15 to 20 km and β factors of 1.5 to 2. Only shallow basement-involved planar faults are observed in this subdomain.

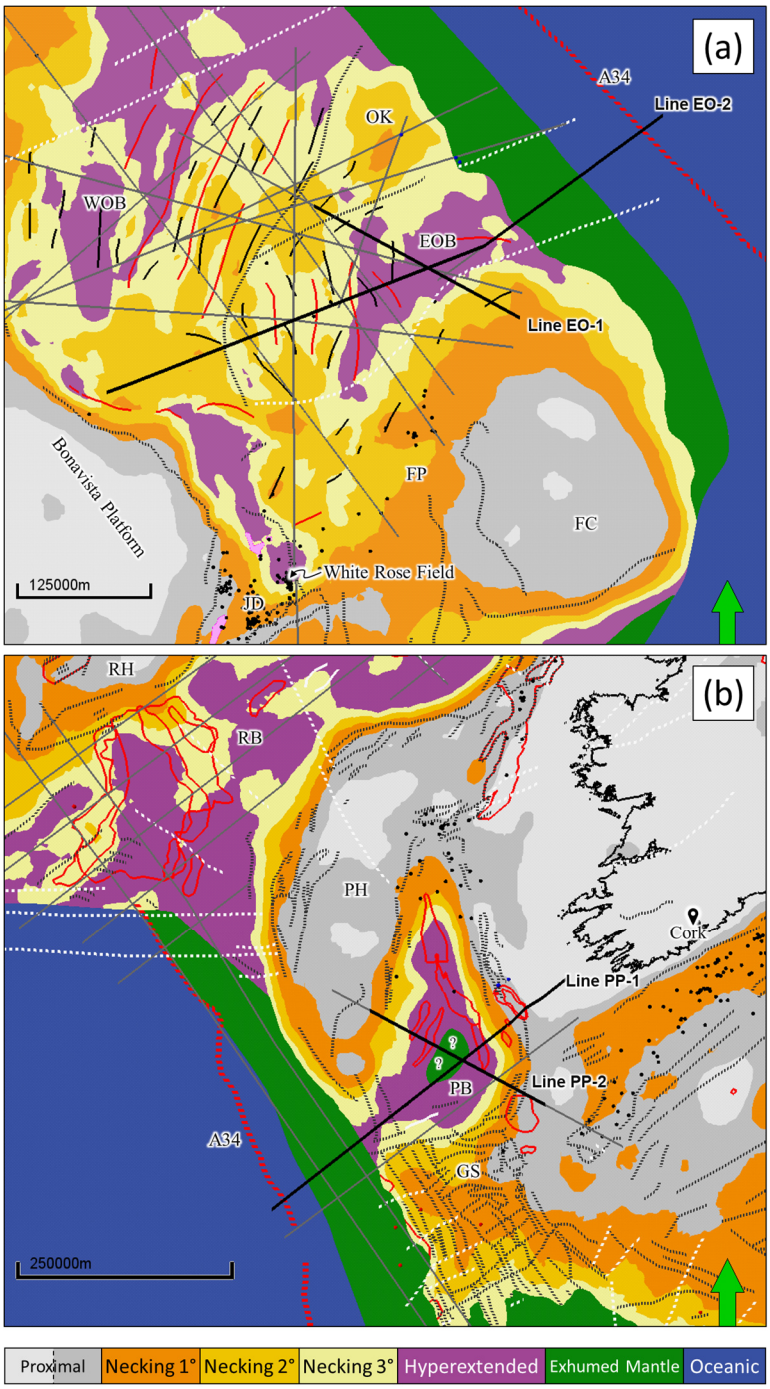

Figure 6.2 Map of the rift domains preserved in the (a) East Orphan and West Orphan basins and (b) the Porcupine Basin. Based on the work of Welford et al. (2010), Lundin & Doré (2011), Welford et al. (2012), and observations from this thesis work along the interpreted seismic lines. Structural elements adapted from Edwards, Jauer, Moir, & Wielens (2003), Srivastava et al. (1990), Sibuet et al. (2007), and Naylor et al. (2002). Dotted black lines: normal faults/basin edge. Dashed white lines: transfer faults. Continuous black lines: antiform structures. Solid red lines: synform structures. Solid red polygons: igneous bodies. Dotted red line: magnetic anomaly 34 from Srivastava et al. (1990). Black dots: wells. Gray lines: available seismic lines. Continuous thick black lines: seismic transects restored in this thesis. Pink polygons: salt.

The 2nd-degree necking subdomain encompassing the Goban Spur Basin has a crustal thickness between 10 and 15 km and β factors of 2 to 3.2. Basement-involved listric faults are found in this subdomain with some of them reaching depths close to the Moho. The 3rd-degree necking subdomain surrounds the hyperextended areas within the Porcupine and Rockall basins. It represents a crustal thickness between 10 and 12 km and β factors of 2.5 to 3.2. Most faults are interpreted to be listric although some are planar faults.

Two main hyperextended zones corresponding to the main depocentres are also interpreted within the Rockall and Porcupine basins. In the southern part of the Rockall Basin, volcanic intrusions have also been interpreted (Naylor et al., 2002). The exhumation domain is interpreted to correspond to part of the seaward limit of the Rockall Basin, extending towards the south, and west of the Porcupine Basin (Figure 6.2b). Based on the presence of volcanic intrusions (Naylor et al., 2002) and highly thin crust (down to 6 km thick) with possible serpentinised mantle (O'Reilly et al., 2006), an area of potential exhumed mantle in the central part of the Porcupine Basin is also interpreted.

6.3 Conjugate or contemporaneous basins?

The evolution of the Atlantic margins of Newfoundland and Ireland have been the subject of study for many years (Burk & Drake, 1974; Anthony G. Doré et al., 1999; Kristoffersen, 1978; Lundin, 2002; Skogseid, 2010; Srivastava et al., 1990; Srivastava & Verhoef, 1992; Srivastava, Verhoef, & Macnab, 1988; Welford et al., 2010, 2012, Ziegler, 1982, 1988). Some paleoreconstructions of the North Atlantic Ocean (e.g., Knott, Burchell, Jolley, & Fraser, 1993; Skogseid, 2010) show the East Orphan and Porcupine basins forming a continuous

basin despite fundamental differences in their evolution, structural style, sedimentary thickness, and amount of volcanic intrusions.

After restoration of the geological cross-sections of the East Orphan and Porcupine basins (Figures 6.3 and 6.4) into their respective spatial and stratigraphic positions at the time of formation, it is possible to compare the two basins. The overall results for both basins are summarised in Table 6.1. Thermal subsidence amounts are similar for both basins since the parameters used are the same, with the exception of the β factors that varied within each basin.

Sedimentary thicknesses are different for the two basins, with a thicker sedimentary sequence deposited in the Porcupine Basin during the Cenozoic, and similar thicknesses in both basins during the Upper Cretaceous. The most important difference, in terms of thicknesses, is observed for the Lower Cretaceous unit of the Porcupine Basin that is ~1400 m thicker than the same unit in the East Orphan Basin. For the Jurassic unit, the opposite is observed as the East Orphan Basin exhibits a thicker sedimentary layer than the Porcupine Basin.

Table 6.1 Summary of average parameters estimated from the restored sections. Totals are listed in the final row. Yellow: Cenozoic, light green: Upper Cretaceous, dark green: Lower Cretaceous, blue: Jurassic, gray: Basement.

Thermal Subsidence (m)				**Thickness (m)**				**Extension (km)**			
EOB		**PB**		**EOB**		**PB**		**EOB**		**PB**	
EO-1	EO-2	PP-1	PP-2	EO-1	EO-2	PP-1	PP-2	EO-1	EO-2	PP-1	PP-2
970	986	938	946	1307	2707	1813	1515	-	-	-	-
1182	1138	1180	1122	641	722	558	599	-	-	-	-
-	-	-	-	1657	2077	3300	3109	10.6	13.6	6.5	4.7
-	-	-	-	2450	1868	1552	1421	23.8	29.2	9.3	12.8
-	-	-	-	11415	8590	12080	10065	-	-	-	-
2052	**2125**	**2060**	**2126**	-	-	-	-	**34.5**	**43.3**	**15.8**	**17.6**

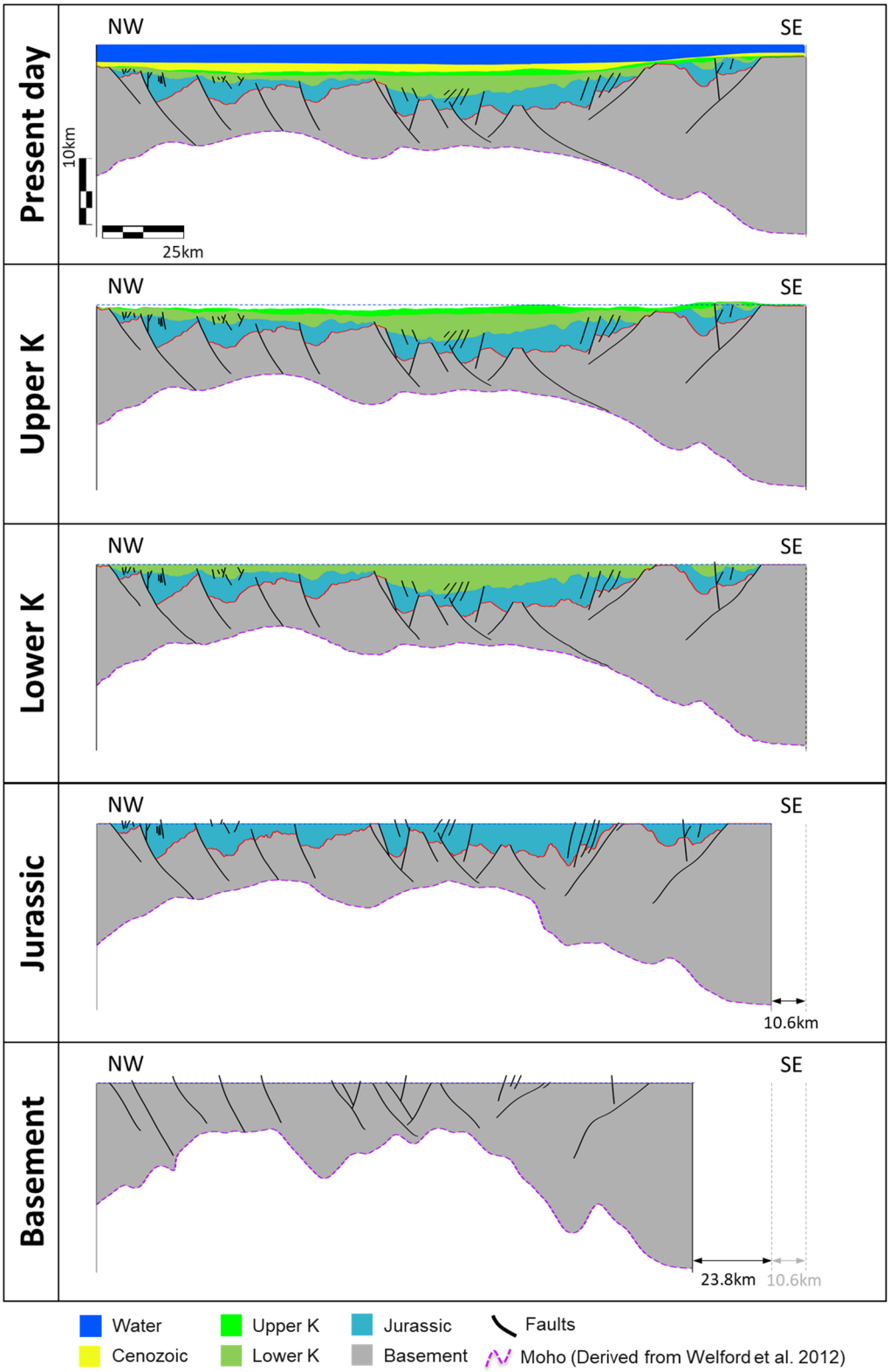

Figure 6.3 Structural restoration of line EO-1 across the East Orphan Basin.

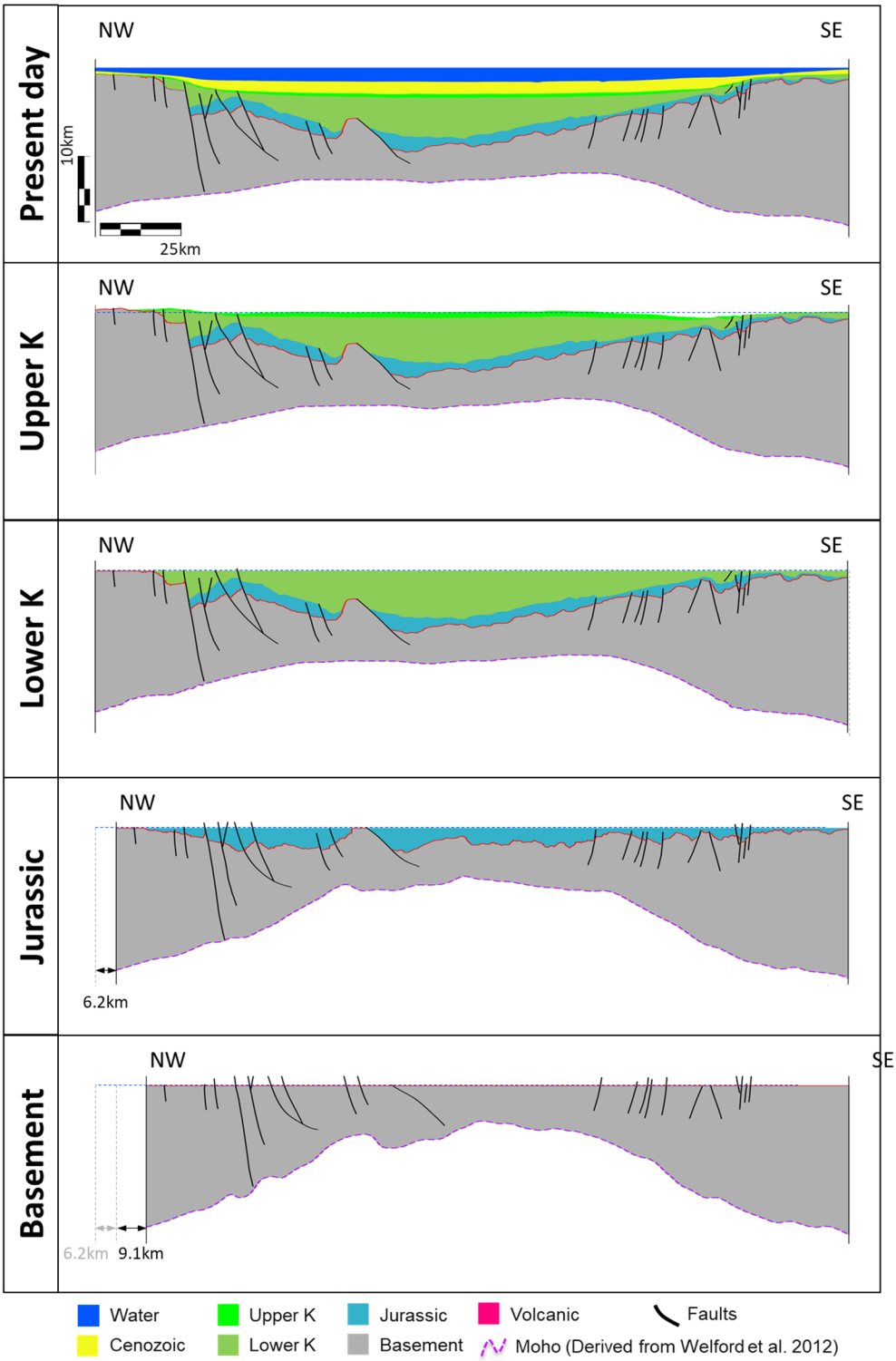

Figure 6.4 Structural restoration of line PP-1 across the Porcupine Basin.

Due to the greater thickness of sediments in Porcupine Basin, it is considered to be a nourished basin. In terms of crustal thickness, the average is greater for the Porcupine Basin but both basins contain areas with highly thinned crust of less than 6 km (O'Reilly et al., 2006; Welford et al., 2012).

Table 6.2 Amount of extension extracted from Nirrengarten et al. (2018) kinematic evolution model. See Table 6.1 for legend of colours

Extension (km)			
EO-1		PP-1	
Nirregarten et al. (2018)	This thesis	Nirregarten et al. (2018)	This thesis
-	-	-	-
-	-	-	-
14.3	10.6	7	6.5
73	23.8	75	9.3
-	-	-	-
87.1	**34.5**	**82**	**15.8**

The amounts of extension also differ for both basins with more extension (~34.5 km) observed for the East Orphan Basin (along the line EO-1) than the Porcupine Basin (15.8 km along the line PP-1). The amounts of extension calculated with the Nirrengarten et al. (2018) kinematic evolution model (Table 6.2) are significantly higher. These amounts were estimated in GPlates by creating points at the end of each line, anchoring these points to their respective plate Id, and measuring the distance between the points as the model changed through time. These differences may be a consequence of several factors: (1) highly variable composition/rheology of the crust beneath both basins, (2) variable and high extension factor of the lithosphere (β>2) with seismically undetectable (polyphase faulting) listric subhorizontal faulting and depth-dependent stretching occurring in varying degrees across either basin, and (3) highly oblique extension that could have contributed to the formation of both basins (e.g., rotation of the Flemish Cap and Porcupine High out of the

Orphan and Porcupine basins, respectively). The latter scenario would generate 3D stress and strain fields (Brune, Willliams, & Müller, 2018) that would vary depending on the direction of measurement. Thus, the extension estimated in this thesis would need to be used as a vector component to estimate the right amount of extension in a required direction.

Based on the characteristics summarised above, the potential linkage between the East Orphan and the Porcupine basins seems implausible. Therefore, the East Orphan and Porcupine basins should be considered as contemporaneous basins located on conjugate margins rather than conjugate basins.

6.4 Galicia Interior Basin: A continuation of the Porcupine Basin?

The kinematic evolution models of Nirrengarten et al. (2018) and Matthews et al. (2016) place the Porcupine Basin relatively aligned and continuous with the Galicia Interior Basin (Figure 6.5). Due to this potential connectivity, the seismic line GIB-1, located along the Galicia Interior Basin (Figure 6.6), was digitised from Pérez-Gussinyé, Ranero, Reston, & Sawyer (2003) and interpreted for comparison with line PP-1 from the Porcupine Basin. The age of each sedimentary unit within the Galicia Interior Basin is based on the information published by Murillas et al. (1990) and Pérez-Gussinyé et al. (2003), and the interpretation followed the same methodology applied to the Orphan and Porcupine seismic lines (Figure 6.7).

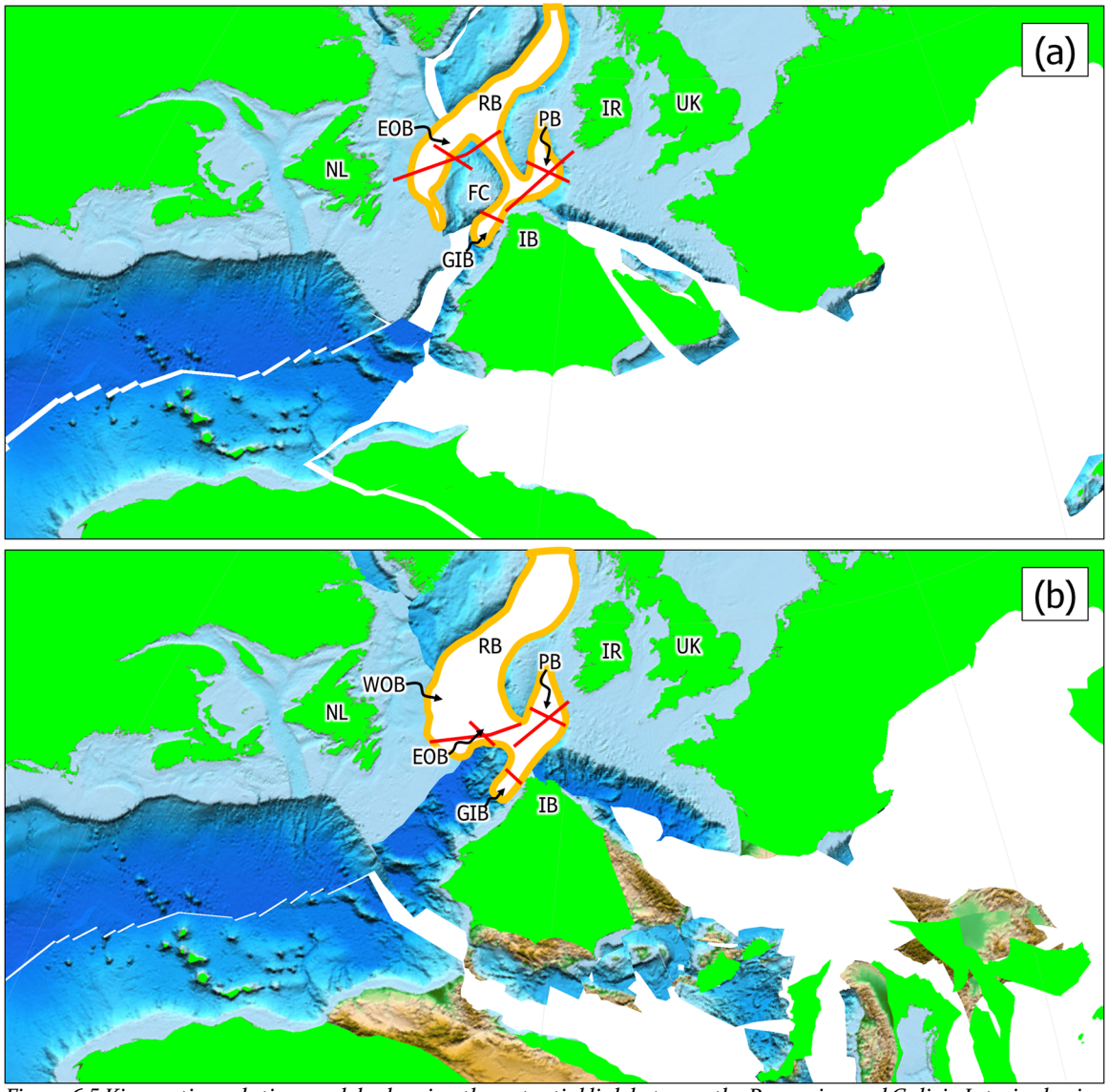

Figure 6.5 Kinematic evolution models showing the potential link between the Porcupine and Galicia Interior basins at the end of the Jurassic (~145 Ma). (a) Nirrengarten et al. (2018). (b) Matthews et al. (2016). WOB: West Orphan Basin. EOB: East Orphan Basin. RB: Rockall Basin. PB: Porcupine Basin. GIB: Galicia Interior Basin. FC: Flemish Cap. IB: Iberia Peninsula. Orange lines: basin boundaries. Red continuous lines: seismic lines shown in this thesis.

Line GIB-1 across the Galicia Interior Basin, shows a similar basin and crustal structure to the one interpreted for line PP-1 across the Porcupine Basin. Both basins show relatively symmetric geometry and a well-defined depocentre located in their central part. The average crustal thickness along line GIB-1 is 13.3 km with a highly thinned crust (~4 km) in

the central part of the basin and larger crustal thickness (15-20 km) on the edges of the basin. (Pérez-Gussinyé et al., 2003).

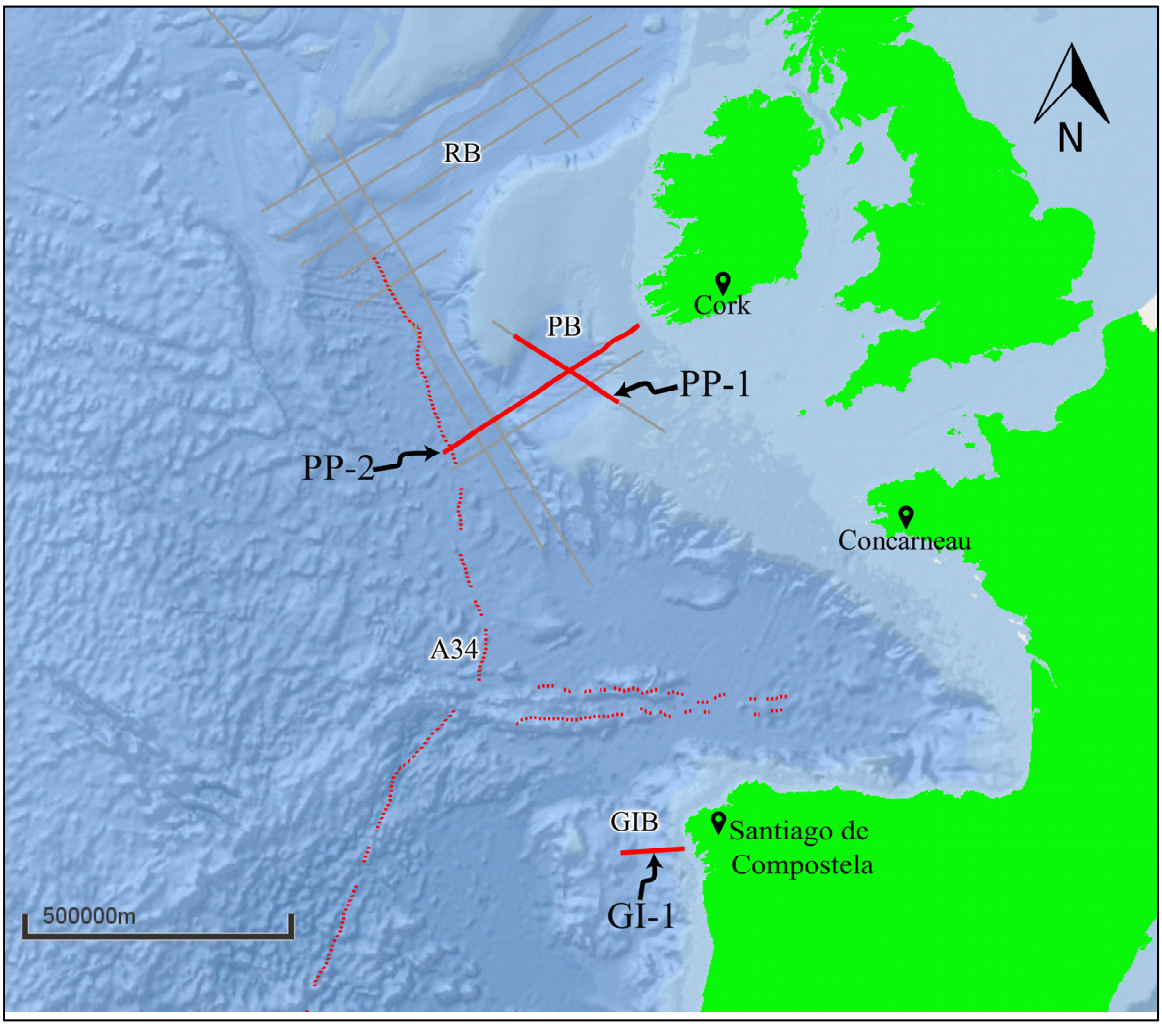

Figure 6.6 Map showing the location of the Galicia Interior Basin (GIB). PB: Porcupine Basin; RB: Rockall Basin; GIB: Galicia Interior Basin; A34: magnetic anomaly 34 from Srivastava et al. (1990); grey and red solid lines represent 2D seismic lines, with red ones corresponding to the main focus of this MSc project.

Along line GI-1, the sedimentary thickness is noticeably different, with thinner sedimentary layers for the Cenozoic and Lower Cretaceous units but thicker layers for the Lower Cretaceous and Jurassic units. The variation in sedimentary thickness could be associated with different basin widths, with more accommodation space available in the Porcupine Basin, and different sediment sources.

Based on the kinematic evolution models of Nirrengarten et al. (2018), Peace et al. (2018), and Matthews et al. (2016), the Galicia Interior Basin and the Porcupine Basin formed a continuous basin during the Jurassic period. However, the only apparent similarity between the basins is their general structure. If the Galicia Interior Basin and the Porcupine Basin formed a continuous elongated basin during the Jurassic, the direction and amount of extension, timing of rifting, micro-plates involved and their internal deformation, are key elements to take into account in any attempt to build a kinematic evolution model that reproduces the relationship between the basins and the triple point around which they all evolved simultaneously.

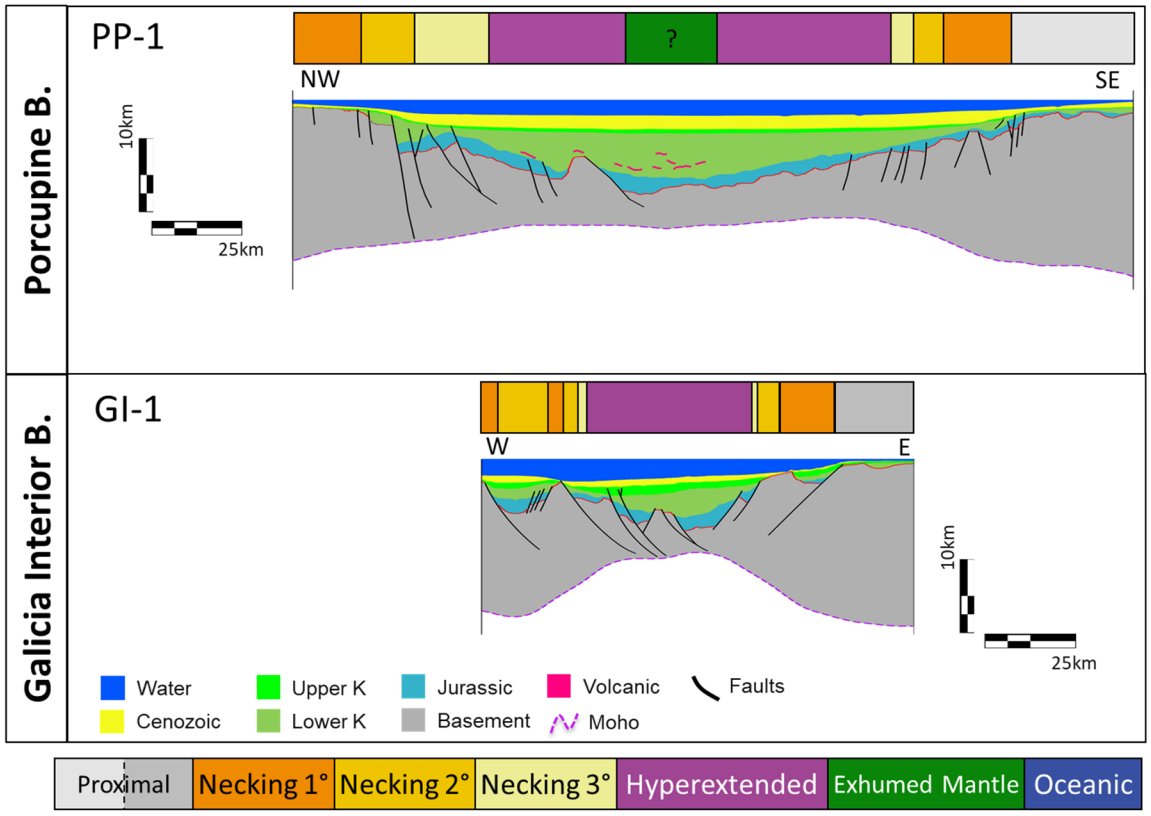

Figure 6.7 Geological sections with interpreted crustal architecture. Moho in line PP-1 is derived from Welford et al. (2012) and in line GI-1 is derived from Pérez-Gussinyé et al. (2003). See Figure 6.6 for line locations.

CHAPTER 7. CONCLUSIONS

7.1 Conclusions

Interpretations of PSTM seismic reflection profiles of East Orphan, West Orphan, Porcupine, and Galicia Interior basins, as well as structural restoration of the selected lines, were integrated with crustal-scale geophysical datasets and kinematic evolution models to carry out an integrated comparison of the East Orphan, Porcupine, and Galicia Interior basins. Key findings include the following:

(1) The East Orphan Basin exhibits a complex distribution of sediments with several depocentres in sub-basins (pockets). By comparison, the Porcupine Basin forms a more symmetric basin with only one depocentre at the centre of the basin.

(2) Localised inversion structures were identified along the East Orphan (Early Cretaceous?) and Porcupine (Late Cretaceous-Paleocene?) basins potentially indicating localised zones of compression in a regional oblique extensional regime.

(3) Hyperextended crust that coincides with the location of the main depocentres is identified along the East Orphan, Porcupine, and Galicia Interior basins and indicates similar rifting events within each of the basins.

(4) Based on the similar estimated ages of the interpreted seismo-stratigraphic units, the rifting events that affected the East Orphan, Porcupine, and Galicia Interior basins are interpreted to be synchronous.

(5) Variations in crustal characteristics and thicknesses of the sedimentary cover may indicate that highly oblique intermittent rifting events affected the East Orphan Basin whereas the Porcupine Basin could potentially have been affected by fewer interrupted rifting events.

(6) Different amounts of extension in the East Orphan and Porcupine basins and the evolution models of Nirrengarten et al. (2018) and Matthews et al. (2016) indicate that the connection between the East Orphan and the Porcupine basins is unlikely, but rather an early connection between the East Orphan Basin and the Rockall Basin is possible.

(7) It is proposed that a continuous basin was formed by the Porcupine and Galicia Interior basins during the Early to Late Jurassic. This scenario links the Flemish Cap with the Porcupine High and the Orphan Knoll with the Rockall High.

7.2 Recommendations for future work

Several studies could potentially improve the results of this thesis project:

- If more seismic data were available for the West Orphan, East Orphan, Rockall, Porcupine, and Galicia Interior basins, additional seismic interpretation could be performed and lines subsequently restored, to better constrain the extension vectors for each basin at each period of time.

- Include future released well data to better tie the seismic interpretation with the chronostratigraphic tops in all of the basins studied in this thesis.

- Build a 3D restoration for each basin by integrating all of the current and future available data to get a better understanding of the structural evolution of the basins and better predict potential hydrocarbon traps.

- 3D gravity inversion over the Galicia Margin would complement the interpretation of the crustal domains carried out in this thesis and subsequently support future kinematic evolution models.

- A kinematic evolution model that takes into account the internal deformation of the crustal domains defined in this thesis would provide a better estimate and understanding of the amount of extension and structures present along and surrounding the Newfoundland and Irish conjugate margins.

- Modelling of the restored lines shown in this thesis, taking into account the non-linear viscoelastic behaviour of the crust to improve the estimated amount of extension.

REFERENCES

Airy, G. B. (1855). On the Computation of the Effect of the Attraction of Mountain-Masses, as Disturbing the Apparent Astronomical Latitude of Stations in Geodetic Surveys. *Philosophical Transactions of the Royal Society of London*, *145*, 101–104. Retrieved from http://www.jstor.org/stable/108511

Allen, P. A., & Allen, J. R. (2005). *Basin Analysis: Principles and Applications* (2nd ed.). Blackwell Science Ltd.

Amante, C., & Eakins, B. W. (2009). ETOPO1 1 Arc-Minute Global Relief Model: Procedures, Data Sources and Analysis. In *NOAA Technical Memorandum NESDIS NGDC-24* (p. 19). Boulder, Colorado, United States of America: National Centers for Environmental Information, NESDIS, NOAA, U.S. Department of Commerce. https://doi.org/10.7289/V5C8276M

Arenas, R., Martínez-Catalán, J. R., & Díaz García, F. (2004). Zona de Galicia-Trás-os-Montes. In J. A. Vera (Ed.), *Geologia de España* (pp. 133–165). Madrid, España: Sociedad Geológica de España-Instituto Geológico y Minero de España.

Barnett-Moore, N., Müller, R. D., Williams, S., Skogseid, J., & Seton, M. (2018). A reconstruction of the North Atlantic since the earliest Jurassic. *Basin Research*, *30*, 160–185. https://doi.org/10.1111/bre.12214

BeicipFranlab, Nalcor Energy Oil and Gas, & Government of Newfoundland and Labrador. (2016). *Offshore Newfoundland & Labrador Resource Assessment Orphan Basin Area NL16-CFB01*. St. John's, NL, Canada: Nalcor Energy Oil and Gas.

BeicipFranlab, Nalcor Energy Oil and Gas, & Government of Newfoundland and Labrador. (2018). *Offshore Newfoundland & Labrador Resource Assessment Orphan Basin Area NL18-CFB01*. St. John's, NL, Canada: Nalcor Energy Oil and Gas. Retrieved from http://exploration.nalcorenergy.com/wp-content/uploads/2018/09/Area-A-2018-Orphan-Flemish-Resource-Assessment-Public-Atlas-Final.pdf

Boillot, G., Auxietre, J.-L., Dunand, J.-P., Dupeuble, P.-A., & Mauffret, A. (1979). The northwestern Iberian margin: A Cretaceous passive margin deformed during Eocene. In M. Talwani, W. Hay, & W. B. F. Ryan (Eds.), *Deep Drilling Results in the Atlantic Ocean: Continental Margins and Paleoenvironment* (Vol. 3, pp. 138–153). American Geophysical Union. https://doi.org/10.1029/ME003p0138

Boillot, G., Mougenot, D., Girardeau, J., & Winterer, E. L. (1989). Rifting Processes on the West Galicia Margin, Spain. In A. J. Tankard & H. R. Balkwill (Eds.), *Extensional Tectonics and Stratigraphy of the North Atlantic Margins* (Vol. 46, pp. 363–377). American Association of Petroleum Geologists. Retrieved from http://search.datapages.com/data/specpubs/structu1/data/a156/a156/0001/0350/0363.htm

Boillot, G., Winterer, E. L., Boillot, G., Winterer, E. L., Meyer, A. W., Applegate, J., … Williamson, M. A. (1988). *Proceedings of the Ocean Drilling Program - Scientific Results: Galicia Margin*. (E. K. Mazzullo, Ed.) (Vol. 103). Ocean Drilling Program. https://doi.org/10.2973/odp.proc.sr.103.1988

Boillot, G., Winterer, E. L., Meyer, A. W., Applegate, J., Baltuck, M., Bergen, J. A., … Williamson, M. A. (1987). Site 638. In R. M. Littleton (Ed.), *Proceedings of the Ocean Drilling Program: Initial Reports* (Vol. 103, Pt. A). Ocean Drilling Program. https://doi.org/10.2973/odp.proc.ir.103.109.1987

Bonvalot, S., Balmino, G., Briais, A., Kuhn, M., Peyrefitte, A., Vales, N., … Sarrailh, M. (2012). *World Gravity Map*. (Commission for the Geological Map of the World, Ed.). Paris, France: BGI-CGMW-CNES-IRD. Retrieved from http://bgi.omp.obs-mip.fr/activities/Projects/world_gravity_map_wgm

Bradley, D. C. (2008). Passive margins through earth history. *Earth-Science Reviews*, *91*(1–4), 1–26. https://doi.org/10.1016/j.earscirev.2008.08.001

Brune, S., Willliams, S. E., & Müller, R. D. (2018). Oblique rifting: the rule, not the exception. *Solid Earth Discussions*, *9*(5), 1187–2018. https://doi.org/10.5194/se-2018-63

Burk, C. A., & Drake, C. L. (Eds.). (1974). *The geology of continental margins*. Springer-Science+Business Media, LLC. https://doi.org/10.1007/978-3-662-01141-6

C-NLOPB. (2009). Schedule of Wells: Newfoundland and Labrador Offshore Area. Retrieved October 23, 2018, from https://www.cnlopb.ca/wells-3/

Calvès, G., Torvela, T., Huuse, M., & Dinkleman, M. G. (2012). New evidence for the origin of the Porcupine Median Volcanic Ridge: Early Cretaceous volcanism in the Porcupine Basin, Atlantic margin of Ireland. *Geochemistry, Geophysics, Geosystems*, *13*(6), 1–18. https://doi.org/10.1029/2011GC003852

Capdevila, R., & Mougenot, D. (1988). Pre-Mesozoic Basement of the Western Iberian Continental Margin and Its Place in the Variscan Belt. In E. K. Mazzullo (Ed.), *Proceedings of the Ocean Drilling Program - Scientific Results: Galicia Margin* (Vol. 103, pp. 733–740). Ocean Drilling Program. https://doi.org/10.2973/odp.proc.sr.103.116.1988

Chenin, P., Manatschal, G., Lavier, L. L., & Erratt, D. (2015). Assessing the impact of orogenic inheritance on the architecture, timing and magmatic budget of the North Atlantic rift system: a mapping approach. *Journal of the Geological Society*, *172*(6), 711–720. https://doi.org/10.1144/jgs2014-139

Chenin, P., Manatschal, G., Picazo, S., Müntener, O., Karner, G., Johnson, C., & Ulrich, M. (2017). Influence of the architecture of magma-poor hyperextended rifted margins on orogens produced by the closure of narrow versus wide oceans. *Geosphere*, *13*(2), 559–576. https://doi.org/10.1130/GES01363.1

Chian, D., Reid, I. D., & Jackson, H. R. (2001). Crustal structure beneath Orphan Basin and implications for nonvolcanic continental rifting. *Journal of Geophysical Research*, *106*(B6), 10,923-10,940. https://doi.org/10.1029/2000JB900422

Croker, P. F., & Shannon, P. M. (1987). The evolution and hydrocarbon prospectivity of the Porcupine Basin, offshore Ireland. In J. Brooks & K. W. Glennie (Eds.), *Petroleum Geology of North-West Europe* (Vol. 2, pp. 633–642). Grahan & Trotman Ltd.

Croker, P. F., & Shannon, P. M. (1995). The petroleum geology of Ireland's offshore basins: introduction. In P. F. Croker & P. M. Shannon (Eds.), *The Petroleum Geology of Ireland's Offshore Basins* (Vol. 93, pp. 1–8). Geological Society of London. https://doi.org/10.1144/GSL.SP.1995.093.01.01

Cross, T. A., & Lessenger, M. A. (1988). Seismic Stratigraphy. *Annual Review of Earth and Planetary Sciences*, *16*(1), 319–354. https://doi.org/10.1146/annurev.ea.16.050188.001535

Daly, J. S. (2009). Precambrian. In C. H. Holland & I. Sanders (Eds.), *The Geology of Ireland* (2nd ed., pp. 7–42). Edinburgh, United Kingdom: Dunedin Academic Press.

Department of Communications, C. A. & E. of I. (2010). Integrated Petroleum Affairs System (IPAS). Retrieved October 22, 2018, from http://gis.dcenr.gov.ie/internetIPAS/servlet/internet/IPAS2IOffshoreWellsSearch

Department of Mines and Energy. (2000). *Sedimentary Basins and Hydrocarbon Potential of Newfoundland and Labrador* (No. 2000-01). St. John's, Canada: Government of Newfoundland and Labrador. Retrieved from https://www.nr.gov.nl.ca/mines&en/publications/sedimentarybasins.pdf

Dix, C. H. (1955). Seismic Velocities from surface measurements. *Geophysics*, *20*(1), 68–86. https://doi.org/10.1190/1.1438126

Doré, A. G., & Lundin, E. R. (2015). Hyperextended continental margins — Knowns and unknowns. *Geology*, *43*(1), 95–96. https://doi.org/10.1016/0040

Doré, A. G., Lundin, E. R., Jensen, L. N., Birkeland, Ø., Eliassen, P. E., & Fichler, C. (1999). Principal tectonic events in the evolution of the northwest European Atlantic margin. In A. J. Fleet & S. A. R. Boldy (Eds.), *Petroleum Geology of Northwest Europe: Proceedings of the 5th Petroleum Geology Conference* (pp. 41–61). London, England: Geological Society. https://doi.org/10.1144/0050041

Dorschel, B., Wheeler, A. J., Monteys, X., & Verbruggen, K. (2010). *Atlas of the Deep-Water Seabed: Ireland*. Springer Netherlands. https://doi.org/10.1007/978-90-481-9376-9

Edwards, T., Jauer, C. D., Moir, P., & Wielens, J. B. . (Eds.). (2003). Tectonic elements, Grand Banks of Newfoundland (East Coast Basin Atlas Series). Open File 1795: Geological Survey of Canada. https://doi.org/10.4095/214599

Enachescu, M. (1987). Tectonic and Structural Framework of the Northeast Newfoundland Continental Margin. In C. Beaumont & A. J. Tankard (Eds.), *Sedimentary Basins and Basin-Forming Mechanisms* (pp. 117–146). Calgary, Canada: Canadian Society of Petroleum Geologists.

Enachescu, M., Kearsey, S., Hardy, V., Sibuet, J.-C., Hogg, J., Srivastava, S. P., … Ferguson, R. (2005). Evolution and Petroleum Potential of Orphan Basin, Offshore

Newfoundland, and its Relation to the Movement and Rotation of Flemish Cap Based on Plate Kinematics of the North Atlantic. In P. J. Post, N. C. Rosen, D. L. Olson, S. L. Palmes, K. T. Lyons, & G. B. Newton (Eds.), *Petroleum Systems of Divergent Continental Margin Basin, 25th Annual GCSSEPM Foundation—Bob F. Perkins Research Conference December 4–7* (pp. 75–131). Houston, Texas, USA. https://doi.org/10.5724/gcs.05.25.0075

Enachescu, M., Kearsey, S., Hogg, J., Einarsson, P., Nader, S., & Smee, J. (2004). Orphan Basin, offshore Newfoundland, Canada: Structural and Tectonic Framework, Petroleum Systems and Exploration Potential. *SEG International Exposition and 74th Annual Meeting, Expanded Abstracts*, *23*(October), 382–385.

Enachescu, M., Meyer, S., & Hogg, J. (2004a). East Orphan Basin, offshore Newfoundland and Labrador: Structural Setting and Evolution with Seismic and Potential Fields Arguments. *Canadian Society of Exploration Geophysicists (CSEG) Annual Convention, Expanded Abstracts*. Retrieved from http://cseg.ca/assets/files/resources/abstracts/2004/114S0216-Enachescu_M_East_Orphan Basin.pdf

Enachescu, M., Meyer, S., & Hogg, J. (2004b). The East Orphan Basin, Offshore Newfoundland and Labrador : a Deepwater Super Extended Rift with Hydrocarbon Potential. In *Canadian Society of Petroleum Geologists (CSPG) Annual Convention, Expanded Abstracts*. Canadian Society of Petroleum Geologists. Retrieved from http://www.cspg.org/documents/Conventions/Archives/Annual/2004/230S0208.pdf

Farias, P., Gallastegui, G., González Lodeiro, F., Marquínez, J., Martín Parra, L. M., Martínez-Catalán, J. R., … Rodríguez Fernández, L. R. (1987). Aportaciones al conocimiento de la litoestratigrafía y estructura de Galicia Central. In *IX Reunião sobre a Geologia do Oeste Peninsular* (pp. 411–431). Porto, Portugal: Universidade do Porto. Retrieved from https://www.researchgate.net/publication/215580332_Aportaciones_al_conocimiento_de_la_litoestratigrafa_y_estructura_de_Galicia_Central

Fossen, H. (2010). *Structural Geology* (1st ed.). Cambridge, United Kingdom: Cambridge University Press.

Fowler, C. M. R. (2005). *The Solid Earth: An Introduction to Global Geophysics* (2nd ed.). Cambridge University Press. Retrieved from http://www.cambridge.org/ca/academic/subjects/earth-and-environmental-science/solid-earth-geophysics/solid-earth-introduction-global-geophysics-2nd-edition?format=AR

Gagnevin, D., Haughton, P. D. W., Whiting, L., & Saqab, M. M. (2017). Geological and geophysical evidence for a mafic igneous origin of the Porcupine Arch, offshore Ireland. *Journal of the Geological Society*. https://doi.org/10.1144/jgs2017-041

Gardner, G. H. F., Gardner, L. W., & Gregory, A. R. (1974). Formation velocity and density—The diagnostic basics for stratigraphic traps. *Geophysics*, *39*(6), 770–780.

https://doi.org/10.1190/1.1440465

Gibbs, A. D. (1984). Structural evolution of extensional basin margins. *Journal of the Geological Society*, *141*(4), 609–620. https://doi.org/10.1144/gsjgs.141.4.0609

Gouiza, M., Hall, J., & Bertotti, G. (2015). Rifting and pre-rift lithosphere variability in the Orphan Basin, Newfoundland margin, Eastern Canada. *Basin Research*, *27*(4), 367–386. https://doi.org/10.1111/bre.12078

Gouiza, M., Hall, J., & Welford, J. K. (2017). Tectono-stratigraphic evolution and crustal architecture of the Orphan Basin during North Atlantic rifting. *International Journal of Earth Sciences*, *106*(3), 917–937. https://doi.org/10.1007/s00531-016-1341-0

Greenroyd, C. J., Peirce, C., Rodger, M., Watts, A. B., & Hobbs, R. W. (2007). Crustal structure of the French Guiana margin, West Equatorial Atlantic. *Geophysical Journal International*, *169*(3), 964–987. https://doi.org/10.1111/j.1365-246X.2007.03372.x

Groupe Galice. (1979). The Continental Margin off Galicia and Portugal: Acoustical Stratigraphy, Dredge Stratigraphy, and Structural Evolution. In F. H. Laughter & E. M. Fagerberg (Eds.), *Initial Reports of the Deep Sea Drilling Project* (Vol. 47, Pt. 2, pp. 633–662). U.S. Government Printing Office. https://doi.org/10.2973/dsdp.proc.47-2.133.1979

Hall, J., Marillier, F., & Dehler, S. A. (1998). Geophysical studies of the structure of the Appalachaian Orogen in the Atlantic borderlands of Canada. *Canadian Journal of Earth Sciences*, *35*(11), 1205–1221. https://doi.org/10.1139/e98-075

Harland, W. B., & Gayer, R. A. (1972). The Arctic Caledonides and earlier Oceans. *Geological Magazine*, *109*(4), 289–314. https://doi.org/10.1017/S0016756800037717

Johnson, H., Ritchie, J. D., Gatliff, R. W., Williamson, J. P., Cavill, J., & Bulat, J. (2001). Aspects of the structure of the Porcupine and Porcupine Seabight basins as revealed from gravity modelling of regional seismic transects. In P. M. Shannon, P. D. W. Haughton, & D. V. Corcoran (Eds.), *The Petroleum Exploration of Ireland's Offshore Basins* (Vol. 188, pp. 265–274). Geological Society of London. https://doi.org/10.1144/GSL.SP.2001.188.01.15

Keen, C. E., & Beaumont, C. (1990). Geodynamics of rifted continental margins. In M. J. Keen & G. L. Williams (Eds.), *Geology of the Continental Margin of Eastern Canada* (pp. 393–472). Ottawa, Canada: Geological Survey of Canada. https://doi.org/10.4095/132690

Keen, C. E., Dafoe, L. T., & Dickie, K. (2014). A volcanic province near the Western termination of the Charlie-Gibbs Fracture Zone at the rifted margin, offshore northeast Newfoundland. *Tectonics*, *33*(6), 1133–1153. https://doi.org/10.1002/2014TC003547

Keen, C. E., Stockmal, G. S., Welsink, H. J., Quinlan, G., & Mudford, B. (1987). Deep crustal structure and evolution of the rifted margin northeast of Newfoundland: results from LITHOPROBE East. *Canadian Journal of Earth Sciences*, *24*(8), 1537–1549. https://doi.org/10.1139/e87-150

Keen, M. J., & Piper, D. J. W. (1990). Geological and Historical Perspective. In M. J. Keen & G. L. Williams (Eds.), *Geology of the Continental Margin of Eastern Canada* (pp. 7–24). Ottawa, Canada: Geological Survey of Canada. https://doi.org/10.4095/132690

Klitgord, K. D., & Schouten, H. (1986). Plate kinematics of the central Atlantic. In P. R. Vogt & B. E. Tucholke (Eds.), *The Western North Atlantic Region* (pp. 351–378). Geological Society of America. https://doi.org/10.1130/DNAG-GNA-M.351

Knott, S. D., Burchell, M. T., Jolley, E. J., & Fraser, A. J. (1993). Mesozoic to Cenozoic plate reconstructions of the North Atlantic and hydrocarbon plays of the Atlantic margins. In J. R. Parker (Ed.), *Petroleum Geology of Northwest Europe: Proceedings of the 4th Conference* (pp. 953–974). London, United Kingdom: Geological Society. https://doi.org/10.1144/0040953

Krawczyk, C. M., Reston, T. J., Beslier, M.-O., & Boillot, G. (1996). Evidence for detachment tectonics on the Iberia Abyssal Plain rifted margin. In R. B. Whitmarsh, D. S. Sawyer, A. Klaus, & D. G. Masson (Eds.), *Proceedings of the Ocean Drilling Program - Scientific Results: Iberia Abyssal Plain* (Vol. 149, pp. 603–615). Ocean Drilling Program. https://doi.org/10.2973/odp.proc.sr.149.244.1996

Kristoffersen, Y. (1978). Sea-floor spreading and the early opening of the North Atlantic. *Earth and Planetary Science Letters*, *38*(2), 273–290. https://doi.org/10.1016/0012-821X(78)90101-2

Lau, K. W. H., Watremez, L., Louden, K. E., & Nedimović, M. R. (2015). Structure of thinned continental crust across the Orphan Basin from a dense wide-angle seismic profile and gravity data. *Geophysical Journal International*, *202*(3), 1969–1992. https://doi.org/10.1093/gji/ggv261

Lavier, L. L., & Manatschal, G. (2006). A mechanism to thin the continental lithosphere at magma-poor margins. *Nature*, *440*(March), 324–328. https://doi.org/10.1038/nature04608

Lundin, E. R. (2002). North Atlantic – Arctic : Overview of sea-floor spreading and rifting history. In E. . Eide (Ed.), *BATLAS – Mid Norway plate reconstructions atlas with global and Atlantic perspectives* (pp. 40–47). Geological Survey of Norway.

Lundin, E. R., & Doré, A. G. (2011). Hyperextension, serpentinization, and weakening: A new paradigm for rifted margin compressional deformation. *Geology*, *39*(4), 347–350. https://doi.org/10.1130/G31499.1

MacDonald, H., Allan, P. M., & Lovell, J. P. B. (1987). Geology of oil accumulation in Block 26/28, Porcupine Basin, Off shore Ireland. In J. Brooks & K. W. Glennie (Eds.), *Petroleum Geology of North-West Europe* (Vol. 2, pp. 643–651). Grahan & Trotman Ltd.

Manatschal, G. (2004). New models for evolution of magma-poor rifted margins based on a review of data and concepts from West Iberia and the Alps. *International Journal of Earth Sciences*, *93*(3), 432–466. https://doi.org/10.1007/s00531-004-0394-7

Mann, P., Gahagan, L., & Gordon, M. B. (2003). Tectonic setting of the world's giant oil

fields. In M. T. Halbouty (Ed.), *AAPG Memoir: Giant oil and gas fields of the decade 1990–1999* (Vol. 78, pp. 15–105). American Association of Petroleum Geologists.

Martínez-Catalán, J. R. (1990). A non-cylindrical model for the northwest Iberian allochthonous terranes and their equivalents in the Hercynian belt of Western Europe. *Tectonophysics*, *179*(3–4), 253–272. https://doi.org/10.1016/0040-1951(90)90293-H

Masson, D. G., & Miles, P. R. (1986). Development of Mesozoic sedimentary basins around the margins of the North Atlantic. *AAPG Bulletin*, *70*(6), 721–729. Retrieved from http://archives.datapages.com/data/bulletns/1986-87/data/pg/0070/0006/0700/0721.htm

Matte, P. (2001). The Variscan collage and orogeny (480-290 Ma) and the tectonic definition of the Armorica microplate: A review. *Terra Nova*, *13*(2), 122–128. https://doi.org/10.1046/j.1365-3121.2001.00327.x

Matthews, K. J., Maloney, K. T., Zahirovic, S., Williams, S. E., Seton, M., & Müller, R. D. (2016). Global plate boundary evolution and kinematics since the late Paleozoic. *Global and Planetary Change*, *146*, 226–250. https://doi.org/10.1016/j.gloplacha.2016.10.002

Mauffret, A., Boillot, G., Auxietre, J. L., & Dunand, J. P. (1978). Évolution structurale de la marge continentale au Nord-Ouest de la péninsule ibérique. *Bulletin de La Société Géologique de France*, *S7–XX*(4), 375–388. https://doi.org/10.2113/gssgfbull.S7-XX.4.375

McAlpine, K. D. (1990). Mesozoic stratigraphy, sedimentary evolution, and petroleum potential of the Jeanne d'Arc Basin, Grand Banks of Newfoundland. *Paper - Geological Survey of Canada*, *89–17*, 50. https://doi.org/10.4095/130934

McKenzie, D. (1978). Some remarks on the development of sedimentary basins. *Earth and Planetary Science Letters*, *40*(1), 25–32. https://doi.org/10.1016/0012-821X(78)90071-7

Mena, A., Francés, G., Pérez-Arlucea, M., Hanebuth, T. J. J., Bender, V. B., & Nombela, M. A. (2018). Evolution of the Galicia Interior Basin over the last 60 ka: Sedimentary processes and palaeoceanographic implications. *Journal of Quaternary Science*. https://doi.org/10.1002/jqs.3032

Mitchum, R. M., Vail, P. R., & Sangree, J. B. (1977). Seismic Stratigraphy and Global Changes of Sea Level, Part 6: Stratigraphic Interpretation of Seismic Reflection Patterns in Depositional Sequences. In C. E. Payton (Ed.), *Seismic Stratigraphy — Applications to Hydrocarbon Exploration* (Vol. M26, pp. 117–133). American Association of Petroleum Geologists. Retrieved from http://archives.datapages.com/data/specpubs/seismic1/data/a165/a165/0001/0100/0117.htm

Montadert, L., de Charpal, O., Roberts, D., Guennoc, P., & Sibuet, J.-C. (1979). Northeast Atlantic passive continental margins: Rifting and subsidence processes. In M. Talwani, W. Hay, & W. B. F. Ryan (Eds.), *Deep Drilling Results in the Atlantic Ocean: Continental Margin and Paleoenvironment* (Vol. 3, pp. 154–186). American Geophysical Union. https://doi.org/10.1029/ME003p0154

Montadert, L., Winnock, E., Deltiel, J. R., & Grau, G. (1974). Continental Margins of Galicia-Portugal and Bay of Biscay. In C. A. Burk & C. L. Drake (Eds.), *The Geology of Continental Margins* (pp. 323–342). Springer-Verlag. https://doi.org/10.1007/978-3-662-01141-6

Montenat, C., Guery, F., & Berthou, P. Y. (1988). Mesozoic Evolution of the Lusitanian Basin: Comparison with the Adjacent Margin. In E. K. Mazzullo (Ed.), *Proceedings of the Ocean Drilling Program - Scientific Results: Galicia Margin* (Vol. 103, pp. 757–775). Ocean Drilling Program. https://doi.org/10.2973/odp.proc.sr.103.117.1988

Morewood, N. C., Mackenzie, G. D., Shannon, P. M., O'Reilly, B. M., Readman, P. W., & Makris, J. (2005). The crustal structure and regional development of the Irish Atlantic margin region. In A. G. Doré & B. A. Vining (Eds.), *Petroleum Geology: North-West Europe and Global Perspectives—Proceedings of the 6th Petroleum Geology Conference* (pp. 1023–1033). London, United Kingdom: Geological Society of London.

Müller, R. D., Seton, M., Zahirovic, S., Williams, S. E., Matthews, K. J., Wright, N. M., … Cannon, J. (2016). Ocean Basin Evolution and Global-Scale Plate Reorganization Events Since Pangea Breakup. *Annual Review of Earth and Planetary Sciences*, *44*(1), 107–138. https://doi.org/10.1146/annurev-earth-060115-012211

Murillas, J., Mougenot, D., Boulot, G., Comas, M. C., Banda, E., & Mauffret, A. (1990). Structure and evolution of the Galicia Interior Basin (Atlantic western Iberian continental margin). *Tectonophysics*, *184*(3–4). https://doi.org/10.1016/0040-1951(90)90445-E

Murphy, F. C., Anderson, T. ., Daly, J. S., Gallagher, V., Graham, J. R., Johnston, J. D., … Wrafter, J. P. (1991). An Appraisal of Caledonian Suspect Terranes in Ireland. *Irish Journal of Earth Sciences*, *11*(1), 11–41. Retrieved from http://www.jstor.org/stable/30002331

Murphy, J. B., Keppie, J. D., Nance, R. D., & Dostal, J. (2010). Comparative evolution of the Iapetus and Rheic Oceans: A North America perspective. *Gondwana Research*, *17*(2–3), 482–499. https://doi.org/10.1016/j.gr.2009.08.009

Naliboff, J. B., Buiter, S. J. H., Péron-Pinvidic, G., Osmundsen, P. T., & Tetreault, J. (2017). Complex fault interaction controls continental rifting. *Nature Communications*, *8*(1). https://doi.org/10.1038/s41467-017-00904-x

Natural Resources Canada. (2017). Basin Database. Retrieved from http://basin.gdr.nrcan.gc.ca

Naylor, D., & Shannon, P. M. (2005). The structural framework of the Irish Atlantic Margin. In A. G. Doré & B. A. Vining (Eds.), *Petroleum Geology: North-West Europe and Global Perspectives* (pp. 1009–1021). London, United Kingdom: Geological Society of London. https://doi.org/10.1144/0061009

Naylor, D., & Shannon, P. M. (2009). Geology of offshore Ireland. In C. H. Holland & I. Sanders (Eds.), *The Geology of Ireland* (2nd ed., pp. 405–460). Edinburgh, United

Kingdom: Dunedin Academic Press.

Naylor, D., & Shannon, P. M. (2011). *Petroleum Geology of Ireland*. Edinburgh, United Kingdom: Dunedin Academic Press.

Naylor, D., Shannon, P. M., & Murphy, N. (2002). Porcupine-Goban region - a standard structural nomenclature system. Dublin, Ireland: Petroleum Affairs Division.

Nester, D. C., & Padgett, M. J. (1993). Geophysical Methods: Seismic Interpretation. In D. Morton-Thompson & A. M. Woods (Eds.), *AAPG Methods in Exploration Series: Development Geology Reference Manual* (Vol. 10, pp. 379–380). American Association of Petroleum Geologists. Retrieved from http://archives.datapages.com/data/specpubs/methodo1/data/a095/a095/0001/0350/0379.htm

Nirrengarten, M., Manatschal, G., Tugend, J., Kusznir, N. J., & Sauter, D. (2018). Kinematic evolution of the southern North Atlantic: implications for the formation of hyper-extended rift systems. *Tectonics*, *37*(1), 1–30. https://doi.org/10.1002/2017TC004495

Norton, M. G. (2002). *Tectonic Evolution of the Porcupine Basin* (No. P00/8). (Porcupine Studies Group (PSG), Ed.). Republic of Ireland: Petroleum Affairs Division (PAD)-Petroleum Infrastructure Programme (PIP).

O'Reilly, B. M., Hauser, F., Ravaut, C., Shannon, P. M., & Readman, P. W. (2006). Crustal thinning, mantle exhumation and serpentinization in the Porcupine Basin, offshore Ireland: evidence from wide-angle seismic data. *Journal of the Geological Society*, *163*(5), 775–787. https://doi.org/10.1144/0016-76492005-079

O'Sullivan, J. M., Jones, S. M., & Hardy, R. J. (2010a). Comparative analysis of the Porcupine Median Volcanic Ridge with modern day Pacific Ocean seamounts – further evidence of an amagmatic Mesozoic basin history for the South Porcupine Basin, offshore Ireland. In *II Central and North Atlantic conjugate margins conference* (Vol. V, pp. 216–219). Lisbon, Portugal: Método Directo. Retrieved from http://metododirecto.pt/CM2010/index.php/vol/article/view/128/56

O'Sullivan, J. M., Jones, S. M., & Hardy, R. J. (2010b). Geological Modelling of the Porcupine Median Ridge : Implications for the Hydrocarbon Prospectivity of North Atlantic Hyper-Extensional Basin and Margin Systems. *Search and Discovery*, *#10253*. Retrieved from http://www.searchanddiscovery.com/documents/2010/10253osullivan/ndx_osullivan.pdf

Peace, A. L., Welford, J. K., Ball, P. J., & Nirrengarten, M. (2018). Deformable plate tectonic models of the southern North Atlantic: Insights into rift- related deformation and magmatism. *Manuscript Sumbitted for Publication*.

Peacock, D. C. P., Knipe, R. J., & Sanderson, D. J. (2000). Glossary of normal faults. *Journal of Structural Geology*, *22*(3), 291–305. https://doi.org/10.1016/S0191-8141(00)80102-9

Pérez-Gussinyé, M., Ranero, C. R., Reston, T. J., & Sawyer, D. S. (2003). Mechanisms of

extension at nonvolcanic margins: Evidence from the Galicia interior basin, west of Iberia. *Journal of Geophysical Research: Solid Earth*, *108*(B5), 1–19. https://doi.org/10.1029/2001JB000901

Pérez-Gussinyé, M., & Reston, T. J. (2001). Rheological evolution during extension at nonvolcanic rifted margins: Onset of serpentinization and development of detachments leading to continental breakup. *Journal of Geophysical Research: Solid Earth*, *106*(B3), 3961–3975. https://doi.org/10.1029/2000JB900325

Péron-Pinvidic, G., & Manatschal, G. (2010). From microcontinents to extensional allochthons: witnesses of how continents rift and break apart? *Petroleum Geoscience*, *16*(3), 189–197. https://doi.org/10.1144/1354-079309-903

Péron-Pinvidic, G., Manatschal, G., & Osmundsen, P. T. (2013). Structural comparison of archetypal Atlantic rifted margins: A review of observations and concepts. *Marine and Petroleum Geology*, *43*, 21–47. https://doi.org/10.1016/j.marpetgeo.2013.02.002

Ramsay, J. G., & Huber, M. I. (1987). *The Techniques of Modern Structural Geology: Folds and Fractures* (Vol. 2). London: Academic Press.

Readman, P. W., O'Reilly, B. M., Shannon, P. M., & Naylor, D. (2005). The deep structure of the Porcupine Basin, offshore Ireland, from gravity and magnetic studies. In A. Doré & B. A. Vining (Eds.), *Petroleum Geology: North-West Europe and Global Perspectives—Proceedings of the 6th Petroleum Geology Conference* (pp. 1047–1056). London, United Kingdom: Geological Society of London.

Reston, T. J. (2007). Extension discrepancy of North Atlantic nonvolcanic rifted margins: Depth-dependent stretching or unrecognized faulting? *Geology*, *35*(4), 367–370. https://doi.org/10.1130/G23213A.1

Reston, T. J., Gaw, V., Pennell, J., Kläschen, D., Stubenrauch, A., & Walker, I. (2004). Extreme crustal thinning in the south Porcupine Basin and the nature of the Porcupine Median High: implications for the formation of non-volcanic rifted margins. *Journal of the Geological Society*, *161*(5), 783–798. https://doi.org/10.1144/0016-764903-036

Reston, T. J., Pennell, J., Stubenrauch, A., Walker, I., & Pérez-Gussinyé, M. (2001). Detachment faulting, mantle serpentinization, and serpentinite-mud, volcanism beneath the Porcupine Basin, southwest of Ireland. *Geology*, *29*(7), 587–590. https://doi.org/10.1130/0091-7613(2001)029<0587:DFMSAS>2.0.CO;2

Robeson, D., Burnett, R. D., & Clayton, G. (1988). The Upper Palaeozoic Geology of the Porcupine, Erris and Donegal Basins, Offshore Ireland. *Irish Journal of Earth Sciences*, *9*(2), 153–175. Retrieved from http://www.jstor.org/stable/30002482

Schlumberger. (2018). Wavelet extraction. Retrieved September 10, 2018, from https://www.glossary.oilfield.slb.com/en/Terms/w/wavelet_extraction.aspx

Sclater, J. G., & Christie, P. A. F. (1980). Continental stretching: An explanation of the Post-Mid-Cretaceous subsidence of the central North Sea Basin. *Journal of Geophysical Research: Solid Earth*, *85*(B7), 3711–3739. https://doi.org/10.1029/JB085iB07p03711

Seton, M., Müller, R. D., Zahirovic, S., Gaina, C., Torsvik, T. H., Shephard, G. E., … Chandler, M. (2012). Global continental and ocean basin reconstructions since 200Ma. *Earth-Science Reviews*, *113*(3–4), 212–270. https://doi.org/10.1016/j.earscirev.2012.03.002

Shannon, P. M. (2016). Old challenges, new developments and new plays in Irish offshore exploration. In M. Bowman & B. Levell (Eds.), *Petroleum Geology of NW Europe: 50 Years of Learning – Proceedings of the 8th Petroleum Geology Conference*. London, United Kingdom: Geological Society of London. https://doi.org/10.1144/PGC8.12

Shannon, P. M., Corcoran, D. V., & Haughton, P. D. W. (2001). The petroleum exploration of Ireland's offshore basins: introduction. In P. M. Shannon, P. D. W. Haughton, & D. V. Corcoran (Eds.), *The Petroleum Exploration of Ireland's Offshore Basins* (Vol. 188, pp. 1–8). Geological Society of London. https://doi.org/10.1144/GSL.SP.2001.188.01.01

Shannon, P. M., Jacob, A. W. B., O'Reilly, B. M., Hauser, F., Readman, P. W., & Makris, J. (1999). Structural setting, geological development and basin modelling in the Rockall Trough. In A. J. Fleet & S. A. R. Boldy (Eds.), *Petroleum Geology of Northwest Europe: Proceedings of the 5th Petroleum Geology Conference* (pp. 421–431). London, England: Geological Society. https://doi.org/10.1144/0050421

Shannon, P. M., McDonnell, A., & Bailey, W. R. (2007). The evolution of the Porcupine and Rockall basins, offshore Ireland: The geological template for carbonate mound development. *International Journal of Earth Sciences*, *96*(1), 21–35. https://doi.org/10.1007/s00531-006-0081-y

Shannon, P. M., & Naylor, D. (1998). An assessment of Irish offshore basins and petroleum plays. *Journal of Petroleum Geology*, *21*(2), 125–152. https://doi.org/10.1111/j.1747-5457.1998.tb00651.x

Sheriff, R. E., & Geldart, L. P. (1995). *Exploration Seismology* (2nd ed.). United States of America: Cambridge University Press.

Sibuet, J.-C., & Collette, B. J. (1991). Triple junctions of Bay of Biscay and North Atlantic: new constraints on the kinematic evolution. *Geology*, *19*(5), 522–525. https://doi.org/10.1130/0091-7613(1991)019<0522:TJOBOB>2.3.CO;2

Sibuet, J.-C., Ryan, W. B. F., Arthur, M. A., Barnes, R. O., Habib, D., Iaccarino, S., … Williams, C. A. (1979). Site 398. In F. H. Laughter & E. M. Fagerberg (Eds.), *Initial Reports of the Deep Sea Drilling Project* (Vol. 47 Pt. 2, pp. 25–233). U.S. Government Printing Office. https://doi.org/10.2973/dsdp.proc.47-2.102.1979

Sibuet, J.-C., Srivastava, S. P., Enachescu, M., & Karner, G. D. (2007). Early Cretaceous motion of Flemish Cap with respect to North America: implications on the formation of Orphan Basin and SE Flemish Cap Galicia Bank conjugate margins. In G. D. Karner, G. Manatschal, & L. M. Pinheiro (Eds.), *Imaging, Mapping and Modelling Continental Lithosphere Extension and Breakup* (Vol. 282, pp. 63–76). London, England: Geological Society. https://doi.org/10.1144/SP282.4

Sinclair, I. K., Shannon, P. M., Williams, B. P. J., Harker, S. D., & Moore, J. G. (1994). Tectonic

control on sedimentary evolution of three North Atlantic borderland Mesozoic basins. *Basin Research*, *6*(4), 193–217. https://doi.org/10.1111/j.1365-2117.1994.tb00085.x

Skogseid, J. (2010). The Orphan Basin – a key to understanding the kinematic linkage between North and NE Atlantic Mesozoic rifting. In R. P. Dos Reis & N. Pimentel (Eds.), *II Central and North Atlantic Conjugate Margins Conference* (Vol. II, pp. 13–23). Lisbon, Portugal: Open Journal Systems 2.3.8.0. Retrieved from http://metododirecto.pt/CM2010/index.php/vol/article/view/239/36

Skogseid, J., Barnwell, A., Aarseth, E. S., Alsgaard, P. C., Briseid, H. C., & Zwach, C. (2004). Orphan Basin: Multiple Failed' Rifting During Early Opening of the North Atlantic. *Eos Transactions of the American Geophysical Union*. Joint Assembly Supplement, Abstract T41B-03: American Geophysical Union. Retrieved from http://abstractsearch.agu.org/meetings/2004/SM/T41B-03.html

Smee, J., Nader, S., Einarsson, P., Hached, R., & Enachescu, M. (2003). Orphan Basin, Offshore Newfoundland: New seismic data and hydrocarbon plays for a dormant Frontier Basin. In *Joint CSPG/CSEG National Convention, Conference* (p. 7). Retrieved from http://www.cspg.org/documents/Conventions/Archives/Annual/2003/498S0211.pdf

Srivastava, S. P., Roest, W. R., Kovacs, L. C., Oakey, G. N., Lévesque, S., Verhoef, J., & Macnab, R. (1990). Motion of Iberia since the Late Jurassic: Results from detailed aeromagnetic measurements in the Newfoundland Basin. *Tectonophysics*, *184*(3–4), 229–260. https://doi.org/10.1016/0040-1951(90)90442-B

Srivastava, S. P., & Verhoef, J. (1992). Evolution of Mesozoic sedimentary basins around the North Central Atlantic: a preliminary plate kinematic solution. In J. Parnell (Ed.), *Basins on the Atlantic Seaboard: Petroleum Geology, Sedimentology and Basin Evolution* (Vol. 62, pp. 397–420). London, England: Geological Society. https://doi.org/10.1144/GSL.SP.1992.062.01.30

Srivastava, S. P., Verhoef, J., & Macnab, R. (1988). Results from a detailed aeromagnetic survey across the northeast Newfoundland margin, Part II: Early opening of the North Atlantic between the British Isles and Newfoundland. *Marine and Petroleum Geology*, *5*(4), 324–337. https://doi.org/10.1016/0264-8172(88)90026-8

Stolfová, K., & Shannon, P. M. (2009). Permo-Triassic development from Ireland to Norway: basin architecture and regional controls. *Geological Journal*, *44*(November), 652–676. https://doi.org/10.1002/gj.1187

Sutra, E., & Manatschal, G. (2012). How does the continental crust thin in a hyperextended rifted margin? Insights from the Iberia margin. *Geology*, *40*(2), 139–142. https://doi.org/10.1130/G32786.1

Sutra, E., Manatschal, G., Mohn, G., & Unternehr, P. (2013). Quantification and restoration of extensional deformation along the Western Iberia and Newfoundland rifted margins. *Geochemistry, Geophysics, Geosystems*, *14*(8), 2575–2597. https://doi.org/10.1002/ggge.20135

Tate, M. P., & Dobson, M. R. (1988). Syn- and post-rift igneous activity in the Porcupine Seabight Basin and adjacent continental margin W of Ireland. In A. C. Morton & L. M. Parson (Eds.), *Early Tertiary Volcanism and the Opening of the NE Atlantic* (Vol. 39, pp. 309–334). London: Geological Society of London. https://doi.org/10.1144/GSL.SP.1988.039.01.28

Turcotte, D. L., & Schubert, G. (1982). *Geodynamics – applications of continuum physics to geological problems* (1st ed.). New York: Wiley.

van der Pluijm, B. A., & Marshak, S. (2004). *Earth Structure*. (L. A. W. Wiegman, Ed.) (2nd ed.). United States of America: W. W. Norton & Company, Inc.

Watremez, L., Prada, M., Minshull, T. A., O'Reilly, B. M., Chen, C., Reston, T. J., … Lebedev, S. (2016). Deep structure of the Porcupine Basin from wide-angle seismic data. In *Petroleum Geology Conference series* (Vol. 8, pp. 199–209). London, United Kingdom: Geological Society. https://doi.org/10.1144/PGC8.26

Watts, A. B. (2001). *Isostasy and flexure of the lithosphere*. Cambridge, United Kingdom: Cambridge University Press.

Welford, J. K., Cameron, D., Carter, J., & Wright, R. (2015). Evidence for hyper-extended continental crust in the East Orphan Basin from seismic reflection data and potential field forward modelling and inversion. *CSEG Recorder*, *40*(8), 16–20.

Welford, J. K., & Hall, J. (2007). Crustal structure of the Newfoundland rifted continental margin from constrained 3-D gravity inversion. *Geophysical Journal International*, *171*(2), 890–908. https://doi.org/10.1111/j.1365-246X.2007.03549.x

Welford, J. K., Hall, J., Sibuet, J.-C., & Srivastava, S. P. (2010). Structure across the northeastern margin of Flemish Cap, offshore Newfoundland from Erable multichannel seismic reflection profiles: Evidence for a transtensional rifting environment. *Geophysical Journal International*, *183*(2), 572–586. https://doi.org/10.1111/j.1365-246X.2010.04779.x

Welford, J. K., Shannon, P. M., O'Reilly, B. M., & Hall, J. (2012). Comparison of lithosphere structure across the Orphan Basin–Flemish Cap and Irish Atlantic conjugate continental margins from constrained 3D gravity inversions. *Journal of the Geological Society*, *169*(4), 405–420. https://doi.org/10.1144/0016-76492011-114

Wernicke, B. (1985). Uniform-sense normal simple shear of the continental lithosphere. *Canadian Journal of Earth Sciences*, *22*(1), 108–125. https://doi.org/10.1139/e85-009

White, R. S., & McKenzie, D. (1989). Magmatism at rift zones: the generation of volcanic continental margins and flood basalts. *Journal of Geophysical Research*, *94*(B6), 7685–7729. https://doi.org/10.1029/JB094iB06p07685

Williams, H. (1979). Appalachian Orogen in Canada. *Canadian Journal of Earth Sciences*, *16*(3), 792–807. https://doi.org/10.1139/e79-070

Williams, H. (Ed.). (1995). *Geology of the Appalachian–Caledonian Orogen in Canada and*

Greenland. *Geology of Canada* (Vol. 6). Ottawa, Canada: Geological Survey of Canada. https://doi.org/10.4095/205242

Williams, H., Dehler, S. A., Grant, A. C., & Oakey, G. N. (1999). Tectonics of Atlantic Canada. *Geoscience Canada*, *26*(2), 51–70. Retrieved from https://journals.lib.unb.ca/index.php/GC/article/view/4003/4517

Woodward, N. B., Boyer, S. E., & Suppe, J. (1989). *Balanced Geological Cross-Sections: An Essential Technique in Geological Research and Exploration* (Short Course in Geology). (M. L. Crawford & E. Padovani, Eds.) (Vol. 6). Washington, D. C.: American Geophysical Union. https://doi.org/10.1029/SC006

Yilmaz, Ö. (2008). *Seismic Data Analysis: Processing, Inversion, and Interpretation of Seismic Data*. (S. M. Doherty, Ed.) (Vol. I). Tulsa, Oklahoma, United States of America: Society of Exploration Geophysicists. https://doi.org/doi:10.1190/1.9781560801580

Ziegler, P. A. (1982). *Geological Atlas of Western and Central Europe* (1st ed.). The Hague, The Netherlands: Shell Internationale Petroleum Maatschappij B.V.

Ziegler, P. A. (1988). *Evolution of the Arctic-North Atlantic and the Western Tethys* (Vol. 43). American Association of Petroleum Geologists. Retrieved from http://archives.datapages.com/data/alt-browse/aapg-special-volumes/m43.htm

APPENDICES

Appendix A

Glossary of terms

This glossary is a compilation of Peacock et al. (2000), van der Pluijm & Marshak (2004), Fossen (2010), and Gibbs (1984). See Figures A.1 and A.2.

Graben: Long and relatively narrow area of subsidence mostly bounded by sub-parallel normal fault zones that dip towards the area of subsidence. Grabens are commonly bounded by horsts.

Horst: Elongate area of uplift mostly bounded by sub-parallel normal fault zones that dip away from the area of uplift. Horsts are commonly bounded by grabens or half-grabens.

Half graben: Asymmetric area of subsidence controlled by hanging wall subsidence above a single controlling (basin-bounding) fault. A half-graben typically contains a hanging wall sedimentary wedge that thickens towards the fault, with older beds having steeper dips than younger beds.

Conjugate Faults: relationship between two intersecting sets of faults that each formed under the same stress field.

Listric normal fault: a fault that shows a decrease in dip downwards. Listric normal faults may pass downwards into a detachment or a décollement.

Décollement: A bedding- or layer-parallel fault or shear zone, above which the rocks may be deformed. The process of décollement may be described as the detachment of the upper cover from its substratum.

Detachment: Fault along a basal surface, along which overlying strata are detached. Detachment is commonly used for a regionally extensive, gently dipping normal fault; they are commonly associated with extension in metamorphic core complexes and can displace crystalline rocks. Although the term is often used synonymously with décollement, Ramsay & Huber (1987) suggest that detachments are low-angle faults that are nearly, but not exactly, parallel to any one horizon.

Bookshelf faults: A system of sub-parallel faults that involve the progressive rotation of beds and faults as displacement occurs.

Transfer zone: an area of deformation and bed rotation between two normal faults that overstep in map view.

Relay ramp: An area of reoriented bedding between two normal faults that overstep in map view and that have the same dip direction.

Rider: equivalent to emergent imbricate wedges in thrust tectonic terminology. Defined by Gibbs (1984) to describe the geometry of the wedges riding in sequence on the sole fault.

Rollover: The fold structure defined by the steepening of otherwise horizontal hanging-wall layers toward a normal fault. Normally related to a downward-flattening (listric) fault (it could be either a rollover anticline or a rollover syncline, depending on the geometry of the underlying fault).

Extensional duplex: Duplex forming along an extensional fault, where individual riders are separated by extensional faults and bound by a roof fault and a floor fault.

Synthetic fault: A fault dipping in the same direction as an adjacent main fault.

Antithetic fault: a fault dipping in the opposite direction to an adjacent master fault or dominating fault set.

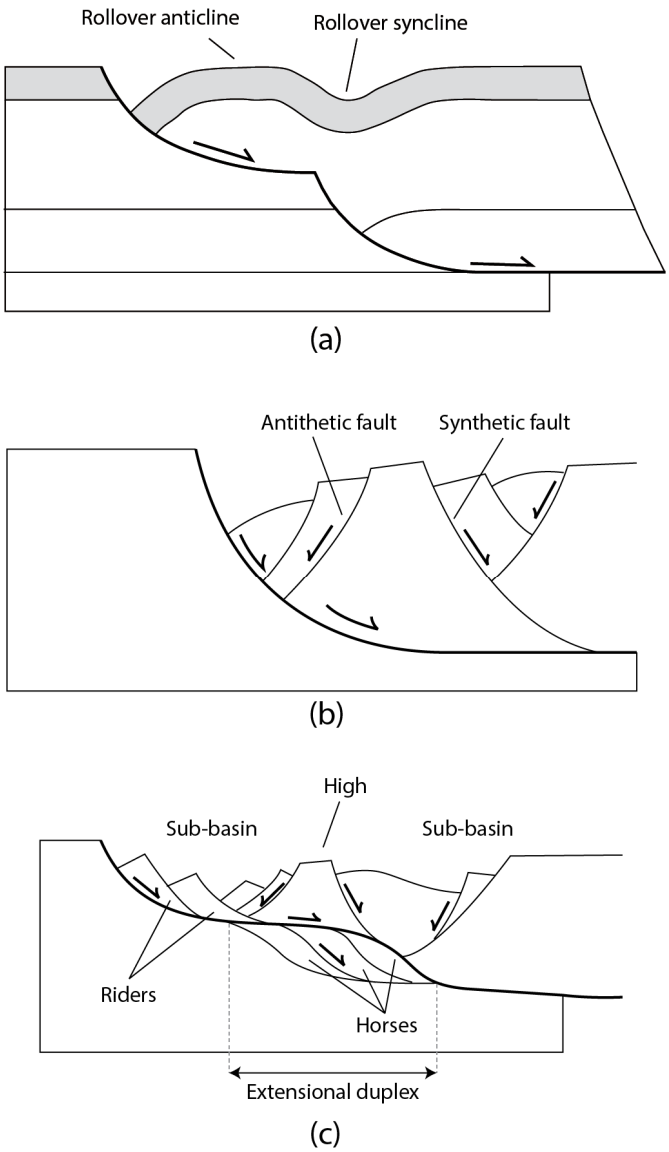

Figure A.1 (a) Rollover anticline and rollover syncline. (b) Antithetic faults and synthetic faults. (c) Extensional duplex. Adapted from (Gibbs, 1984) *and van der Pluijm & Marshak (2004).*

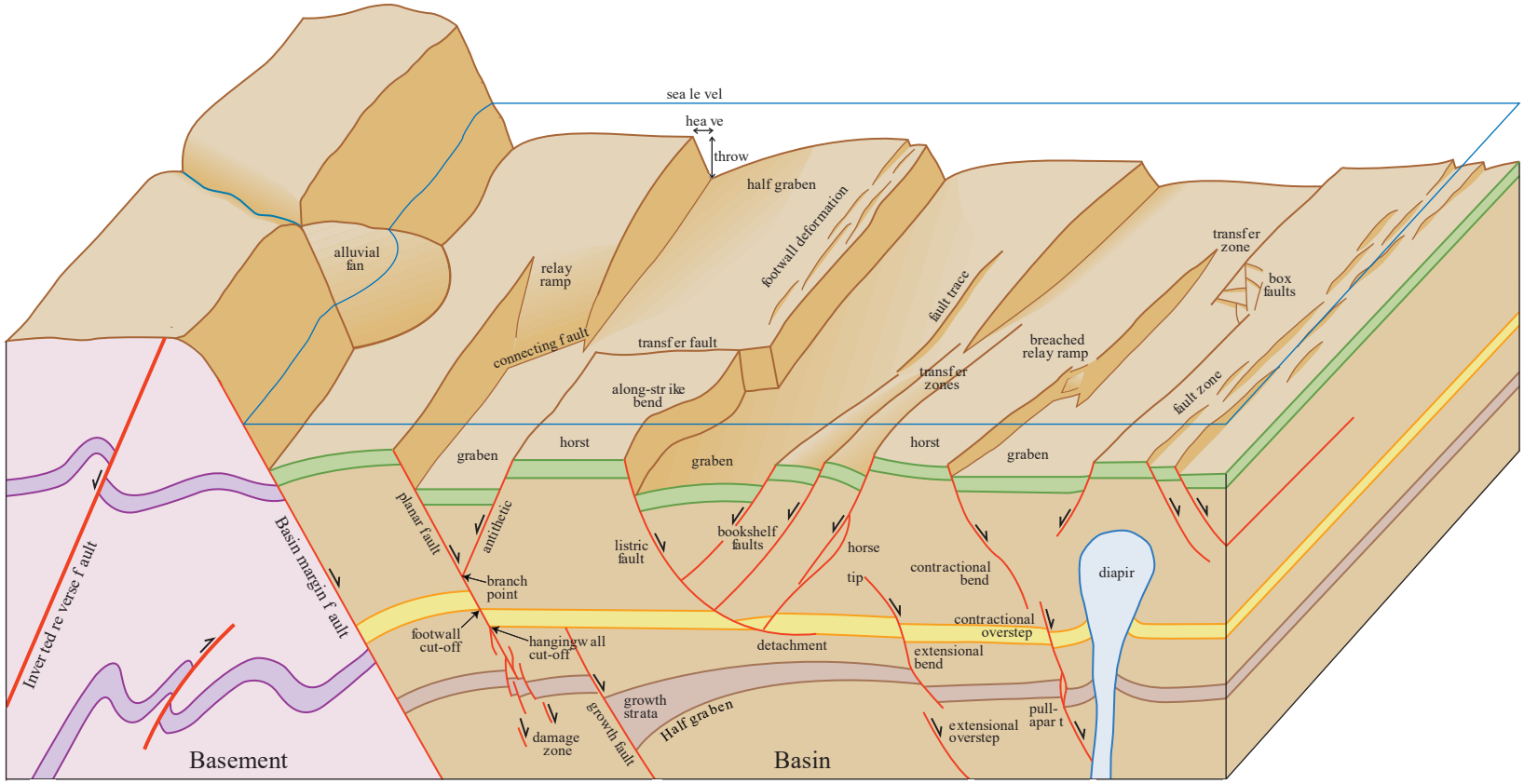

Figure A.2 Schematic block diagram showing the main geometric features of normal faults (after Peacock et al., 2000).

Duplex: Tectonic unit consisting of a series of horses that are arranged in a piggy-back fashion between a sole and a roof thrust. Also used for similar structures in extensional and strike-slip settings (extensional and strike-slip duplexes).

Horse: tectonic sheet bounded by thrust faults on each side and occurring in trains in duplex structures. S-shaped geometry common.

Appendix B

Porcupine-Goban region - Structural Elements

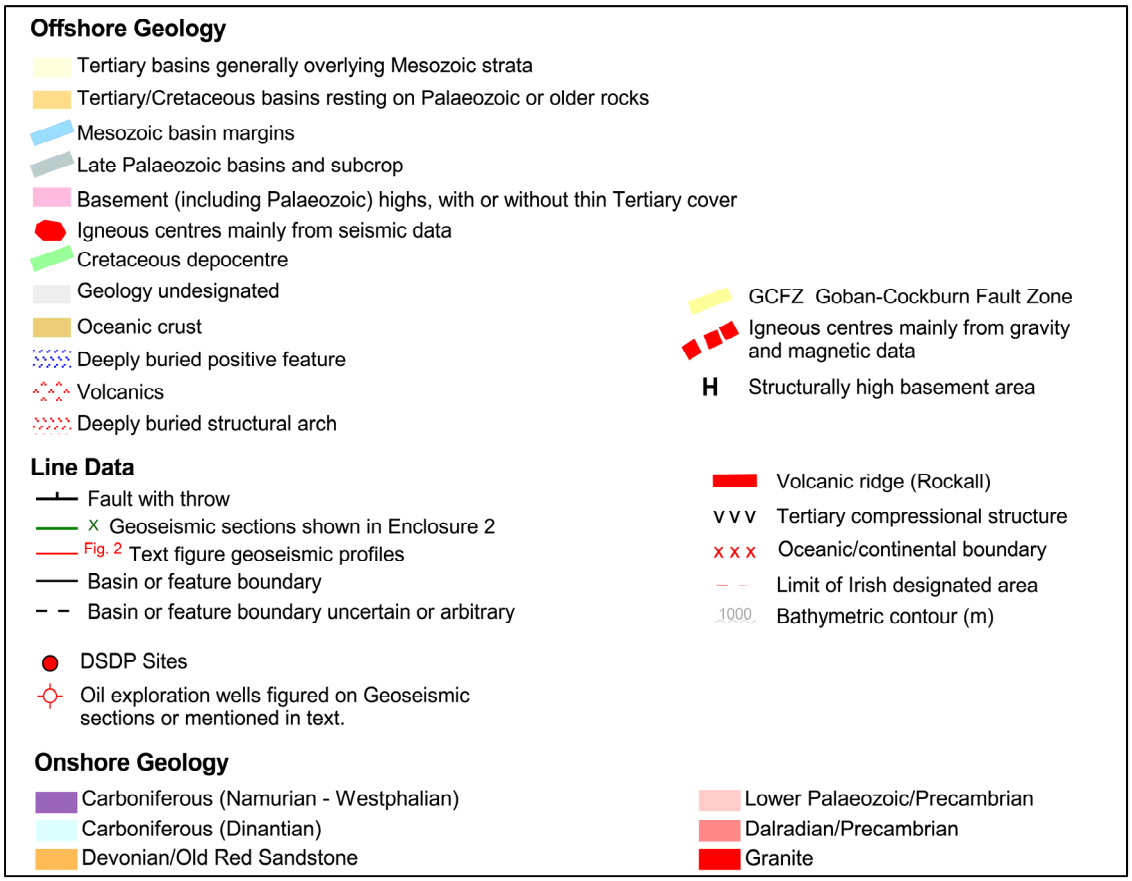

Figure B.1 Structural elements map legend of the Porcupine-Goban region (Naylor et al., 2002).